INVESTIGATION OF ENVIRONMENTAL IMPACTS OF BENEFICIAL REUSE OF BAUXITE RESIDUE IN COAL-REFUSE AREA BASED ON A HYDRO-THERMAL-GEOCHEMICAL MODEL

by

Yi Xu

BS, Hohai University, 2006

Submitted to the Graduate Faculty of

Swanson School of Engineering in partial fulfillment

of the requirements for the degree of

Doctor of Philosophy

University of Pittsburgh

2013

UNIVERSITY OF PITTSBURGH

SWANSON SCHOOL OF ENGINEERING

This dissertation was presented

by

Yi Xu

It was defended on

October 17, 2013

and approved by

James Peterson, Ph.D. Associate Professor, Department of Environmental and Occupational Health

Jorge D. Abad, Ph.D. Assitant Professor, Department of Civil and Environmental Engineering

Vikas Khanna, Ph.D. Assitant Professor, Department of Civil and Environmental Engineering

Dissertation Director: Xu Liang, Ph.D., Professor, Department of Civil and Environmental Engineer

Copyright © by Yi Xu

2013

INVESTIGATION OF ENVIRONMENTAL IMPACTS OF BENEFICIAL REUSE OF BAUXITE RESIDUE IN COAL-REFUSE AREA BASED ON A HYDRO-THERMAL-GEOCHEMICAL MODEL

Yi Xu, PhD

University of Pittsburgh, 2013

The waste of coal mining results in numerous piles, which produce acid mine drainage (AMD) and deteriorate water quality. Also ions from the refuse piles, including sulfate, ferric and ferrous iron are continuously leached from these coal-refuse piles. Bauxite residue, a byproduct from alumina refining process, has a relatively high pH. If bauxite residue is innovatively mixed with the coal refuse, the issues associated with these two wastes (e.g., high and low pH values) may be solved. Also, the concentrations of leached ions will be reduced significantly.

This study investigates the impacts of bauxite residue + coal refuse on the environment through a hydro-thermal-geochemical model (HTGCM) in combination with field measurements and laboratory analysis. This dynamic model accounts for the processes of water cycle, pyrite oxidation, oxygen diffusion, solute transport, thermal transport, pH calculation and other secondary reactions. The Distributed Hydrology Soil and Vegetation Model (DHSVM) is the basic framework based on which the HTGCM model is developed. The HTGCM model developments include three main stages: (1) improving the DHSVM hydrological model and coupling the algorithm of pyrite oxidation to DHSVM, (2) developing thermal transport and including the heat transport from the oxidation process, and (3) coupling a geochemical model and calculating more chemical reactions.

The modeling studies and the field observations lead to the following main findings: (1) the chemical concentrations in the amended zone are reduced while the pH value is ameliorated

to be less acidic; (2) the chemical concentrations in the non-amended zone also decrease but not as significantly as in the amended zone in the short-term period; (3) it appears that there may be a range of preferred depth for the amended zone to be more effective; (4) heat released from the pyrite oxidation increases the soil temperature; (5) the effect of plants on soil temperature is restricted to a vegetation-impact depth; and (6) impacts of the amended zone on the deep non-amended zone can be seen through a long-term simulation.

This work provides new insights into the remediation studies and may lead to a paradigm shift in the AMD treatment strategy in the future.

TABLE OF CONTENTS

LIST OF TABLES

LIST OF FIGURES

ACKNOWLEDGMENTS

Pursuing Ph.D. degree is a challenging, interesting, exciting and hardworking process, which has not only given me a great opportunity to explore science and technology, but has also taught me how to overcome difficulties in research and life.

For this important experience, I am deeply grateful to my advisor, Professor Xu Liang, who has spent so much effort on training me in the thorough knowledge and I also really appreciate and thank her for the long-term support for my Ph.D. study. Her high-level academic insights and professional dedication are so impressive to me and she is a great example for my future career.

I am also indebted to the members of my dissertation committees: Professor Jorge D. Abad, Professor James Peterson and Professor Vikas Khanna. Thanks for their time and great suggestions for my work. I appreciate very much their help.

I would like to thank our main collaborators and team members who I have worked with during our research project: Dr. Judodine Nichols, Dr. Tyler Davis, Dr. Jaw K. Fu, Dr. Jason Monnell, Peter Koranchie-Boah, Huiqi Deng and Yipei Wen.

Finally and importantly, I have to thank my parents for their spiritual encouragement in my study. Their infinite love always makes me go forward.

1.0 INTRODUCTION

1.1 BACKGROUND AND MOTIVATION

It is known that during the long-term development of the coal mining industry, coal waste was dumped from the target mineral. This waste has been accumulated into many hills that we call coal-refuse (CR) piles, which are continuously releasing metal ions and anions such as Fe^{2+}, Fe^{3+}, SO_4^{2-}, and H^+ into soil water because of the pyrite oxidation. This causes the acid mine drainage (AMD) in CR piles and decreases the pH value in soil water and stream flow. AMD has been an important issue for the mining regions in world since coal is still widely used as one of the significant sources of energy. A lot of environmental scientists and engineers have been exploring the different approaches of remediation to deal with the AMD issue in order to maintain a sustainable environment for our future generations. However, there still remain a few questions, such as what kind of remediation is good for a site and how to evaluate and predict the results of the remediation in future? In this research, the remediation is to use bauxite residue (BR) to neutralize the acidic water from CR. And this approach is investigated by a scientific model combined with field measurement and laboratory experiment. The modeling results will provide a few suggestions to guide the remediation on the right track.

Currently, there are quite a lot of remediation approaches and technologies for coal waste, but most of them are expensive due to the huge consumption of caustic chemicals or

inefficiency in the utilization of materials. The many types of technologies developed to date to treat AMD can be typically classified as either active or passive methods [*Johnson and Hallberg,* 2005]. The active type requires continuous addition of typically caustic material to neutralize pH and precipitate metals, while the passive type includes natural wetlands or constructed eco-systems and takes advantage of natural chemical and biological reactions to neutralize the AMD. Active treatment is effective but always expensive due to the materials and lots of labor. The passive-abiotic approach may be not as effective as the active treatment, but it is relatively less expensive to implement since it does not require as many materials and maintenances as the active systems do. Both of the two approaches may include abiotic and biological types. The abiotic type directly relies on alkalinity of materials to neutralize AMD while the biological method uses microorganisms to produce alkalinity. In summary, both of them have their own strengths and weaknesses.

In order to evaluate the current remediation method correctly, two critical parts have to be addressed in CR area: 1) hydro-thermal processes including evapotranspiration, infiltration, runoff generation, overland flow, stream flow, heat generation and energy transport 2) geochemical processes including pyrite oxidation, oxygen diffusion, other mineral reactions, precipitates of metals and anions, chemical advection and dispersion. To involve all the above processes together in one model, there are many problems that have to be addressed.

To date, hydro-thermal processes have been simulated by a few hydrological models and land surface models. Different models are designed with different features which depend on spatial scale, terrain characteristic, runoff mechanism and thermal transport etc. For example, the Variable Infiltration Capacity model [*Liang et al.,* 1994] has been widely applied from medium scale to macro scale to simulate hydrological processes and energy cycle. MIKE SHE model [*Xu*

et al., 2011], a commercial model, is usually used in small ~ medium scales catchments to calculate the surface water and groundwater, while the thermal module is not included. In terms of the terrain characteristics, some models are able to perform well in hilly regions. For instance, TOPMODEL [*Ziemkiewicz et al.*, 1997] introduced a topographic index to consider the impact of slope on the surface water movement and subsurface water movement. This concept has been used in the other hydrological models. Regarding the mechanism of runoff, two typical categories, namely saturated runoff and infiltration excess runoff, are widely discussed. The Xinanjiang model [*Zhao et al.*, 1980; *Zhao*, 1992; *Zhao et al.*, 1995] is one of the models that include both of these two mechanisms. However, it is not able to calculate the energy cycle and it is a lumped model which is limited to the simple characteristic of land surface. Therefore, a sophisticated hydro-thermal model needs to be created to address the issues of complex terrains, multiple runoff mechanisms, heat generation and fine resolution in CR area.

Geochemical processes represent another essential part during the evaluation of remediation. First, the model has to identify the dominating reaction such as pyrite oxidation in the chemical system. It also must figure out the other minerals and reactions along with the pyrite oxidation. The identification of minerals is based on the field data and the results of X-Ray Diffraction (XRD). The mineral reactions are obtained from the database of the existing geochemical models. Subsequently, all the main minerals and the reactions can be designed into the current model. The pH-redox-equilibrium-equations speciation model (PHREEQC) [*Parkhurst et al.*, 1980; *Parkhurst*, 1995; *Parkhurst and Appelo*, 1999], which includes the features of mineral reactions, solid dissolution, precipitation and ion-exchange etc., has been widely applied in the geochemical field. MINTEQ2 [*Jacques et al.*, 2008] is another model for geochemical modeling as it is able to calculate the equilibrium reaction in aqueous systems.

Although it has a large database of the equilibrium reactions, it is inadequate to satisfy the non-equilibrium reactions in natural system. Even though PHREEQC has a larger database that includes the equilibrium reactions and non-equilibrium reactions, the physical processes of mineral reactions have not been reflected in the model.

According to the above reviews, it is time to combine the hydro-thermal models and the geochemical models together to investigate the remediation approach in CR regions. It is also the main task in this research to build such a new hydro-thermal-geochemical model. Currently, the concept of the remediation is to mix bauxite residue, a byproduct of the alumina refining process which has a high residual pH, with CR that has low pH leachate. It has a vegetative tier on the top of remedial materials. Briefly, it is a reuse of two wastes with the addition of vegetation to achieve a treatment for AMD. As a result, the new hydro-thermal-geochemical model should be able to incorporate all the relevant features of the CR and the remediated areas. In this thesis, the model developments and the results are described in Chapters 2.0 3.0 and 4.0 . The final conclusions of the entire research are summarized in Chapter 5.0 . The model setup and output are discussed in APPENDIX A.

1.2 SCIENTIFIC QUESTIONS

In this research, the purpose of the modeling evaluation for the AMD treatment is to address the following scientific questions:

- What is an appropriate remedial depth for the protection of CR region in terms of the AMD issue in the study site?
- How much soil temperature is affected by the heat from pyrite oxidation?

- What role does the vegetation play for soil temperature in the remedial process?
- What are the long-term impacts of remediation in the site?

1.3 RESEARCH DESIGN

In order to solve the above questions, the developments of this new hydro-thermal-geochemical model were separated into three stages: 1) first stage, basic hydro-geochemical model (HGCM) [*Xu et al.*, 2013a]; 2) middle stage, hydro-thermal-geochemical development (HTGCM v1.0) [*Xu and Liang*, 2013]; 3) sophisticated stage, sophisticated hydro-thermal-geochemical development with PHREEQC (HTGCM v2.0) [*Xu et al.*, 2013b].

- Development of the HGCM model is to combine hydrological processes, pyrite oxidation process and chemical advection-dispersion process all together. This is a framework with a few assumptions. The hydrological processes are designed based on the Distributed Hydrology Soil and Vegetation Model [*Wigmosta et al.*, 1994] version 3.0 (i.e. DHSVM v3.0) which has a good process-driven representation of the vegetation, hydrological expression and their interactions through water and energy cycles. DHSVM v3.0 has been widely applied in many watersheds across the country [*Leung et al.*, 1995; *Waichler*, 2000; *Leung and Wigmosta*, 2007]. DHSVM v3.0 provides the conditions for the investigation at the watershed scale in future. Here DHSVM 3.0 is improved further to address the hydrological processes in the complicated region (It is described in Chapter 2.0).

  For the pyrite oxidation process, there are different kinds of model including empirical models and geochemical-based models (A few geochemical models are discussed in Chapter 2.0). PYROX [*Wunderly et al.*, 1996] is one of geochemical-based models that is widely

used for the simulation of pyrite oxidation in coal waste areas. However, it does not include some of the hydrological features e.g. vegetation and the interactions among vegetation, soil and the pyrite oxidation, two mechanisms of runoff and the slope-impact infiltration in hilly region, which are fundamentally important if one wants to adequately evaluate the effectiveness of the new remediation approach in CR piles. Therefore, the combination of DHSVM and PYROX is a very significant stage in this research. DHSVM is an open-source model while PYROX has been programmed in this research based on the work of *Wunderly et al.* [1996]. The interaction between these two models is realized by the advection and dispersion. The sequential coupling approach is applied in this research and usually the results of the sequential method are similar to the implicit coupling methods [*Walter et al.*, 1994]. In this first stage, the model can simulate the hydrological process and pyrite oxidation process including SO_4 (total sulfate in all SO_4^{2-} solutions) and total Fe i.e. (Fe(Π) + Fe(ΙΙΙ) solutions) generation under a few assumptions. The model setup is listed in APPENDIX A. The model development in this stage and the sensitive analysis of amended layer are discussed in Chapter 2.0 .

- Development of the HTGCM v1.0 is to develop a thermal module into the above basic hydro-geochemical framework then it becomes the hydro-thermal-geochemical model, although the geochemical process is not pH-dynamic (calculating pH at each time step is referred to as pH-dynamic in this thesis) due to the constant pH assumption. The thermal cycle not only relates to the water cycle but also it may affect the reactions in the geochemical process. For example, the heat released from pyrite oxidation may increase the soil temperature. The higher soil temperature may accelerate the rate of pyrite oxidation. It would be a negative effect if the pyrite oxidation continuously occurs. Therefore, the thermal

module considering the heat from both chemical oxidation and biological oxidation is added into the model so that the heat from different sources can be concerned and it helps to assess the soil temperature during the remediation in the coal-refuse region.

In Chapter 3.0 , the model incorporates the features of PYROX, DHSVM, thermal generation, thermal transport and chemical transport. The heat and the soil temperature are simulated within every soil layer. The field measurement is used to calibrate the simulated soil moisture and the soil temperature. The sensitivity analysis of heat parameters and the different sources of heat generation are discussed in this chapter as well. Furthermore, the impact of vegetation on the heat generation and soil temperature is discussed further. Until this stage, the model becomes dynamic for thermal transport with the influence of vegetation. The interaction among the hydrological processes, heat transport and the half-geochemical process is realized in this stage. The model setup is in APPENDIX A.

- Development of the HTGCM v2.0 is to develop a sophisticated hydro-thermal-geochemical model that couples the middle-level model with a professional geochemical model. That is to combine part of PYROX, DHSVM, thermal module and PHREEQC all together. A few previous assumptions are not necessarily included in this stage, which allows the model to get close to the natural situation. For example in the new version, the pH value will change with time and the model is dynamic with the chemical reactions and physical processes. A general comparison of the existing models developed by other scientists is discussed in Chapter 4.0 as well.

It is worth mentioning that some laboratory experiments have been conducted to detect the chemical elements and the solid compositions in coal waste and bauxite residue. In the new version of the model, hydrological processes, heat transport process, geochemical

chemical process including pyrite oxidation and the other relative reactions are all concerned in this stage. The model is able to mimic the complicated situation with more chemical elements and more minerals. The appropriate depth of amended layer is further discussed and the long-term impact of amended zone will be predicted in Chapter 4.0 . Some discussions about the solid precipitation are also shown in this chapter. The model setup is listed in APPENDIX A.

None of the above model development is separated from the calibration and validation with the field data. Four experimental plots including the background plot (as benchmark) and the other three amended plots where different types of remediated materials are applied to the amended zone within the top 61 cm (24 inches) in plot 2 and plot 4 and 91 cm (36 inches) in plot 3. Plot 1 merely has coal-refuse (CR) and it is used as a benchmark, plot 2 is 90% CR mixed with 10% BR in the amended zone, plot 3 is 85% CR mixed with 10% BR and 5% mushroom compost (C), plot 4 is 70% CR mixed with 30% limestone (LS). Meanwhile, plot 1 is not planted while all the other three plots are planted by the same types of vegetation including alfalfa, white clover, red clover and tall fescue. Figure 1.1a shows the CR pile in Mather, PA. There are four experimental plots locating at the north-facing slope of the CR pile. Figure 1.1b is the plots just reclaimed and Figure 1.1c shows the three months after the reclamation with BR. Firstly, the comparison of plots 1~4 are investigated in Chapter 2.0 . Then plot 1 and plot 2 are mainly discussed in Chapters 3.0 and 4.0 to analyze the heat transport in the remediated plot and show the impact of BR on the coal refuse respectively.

Additionally, a few laboratory tests were completed for the soil properties for example, soil porosity, soil bulk density and hydraulic conductivity, which are the basic variables in the model.

In summary, the whole work in this research includes the model development, calibration, validation, field sampling, laboratory experiments and tests to evaluate the remediation of CR region in the site.

(a) **(b)** **(c)**

Figure 1.1 Coal refuse pile in the Mather site: (a) original condition with barren lands, (b) with the top 61 cm surface pile just reclaimed, and (c) three months after the reclamation with BR. (These photographs were taken by Alcoa Inc.)

2.0 BASIC DEVELOPMENT AND APPLICATION OF A HYDRO-GEOCHEMICAL MODEL

2.1 INTRODUCTION

Small mountains of overburden and low-energy-value materials have been left behind from long-term industrial developments world-wide in what are commonly called coal refuse or "gob" piles. These deposits, which typically have a deep unsaturated soil layer, have a highly heterogeneous composition with the potential of releasing acidity, metals and other harmful elements into the environment. The most important of these are from the oxidation of sulfide minerals (e.g., pyrite) which results in acid mine drainage (AMD), a major environmental issue in natural waterways due to the considerable amount of coal-powered energy produced globally. Therefore, it is important to investigate an effective and economical approach to handle the issues presented by AMD through rigorous scientific modeling combined with field measurements in order to maintain a sustainable environment for future generations.

Treatments for AMD have been classified into two categories: active and passive methods [*Johnson and Hallberg*, 2005] as mentioned in Chapter 1.0 . Recently, a new approach aims at combining bauxite residue (BR), a byproduct of alumina refining process with a high residual pH, with coal refuse (CR) that has low pH leachates. The novelty of this approach (i.e., BR + CR) is the reuse of the two waste materials and the vegetation tier to achieve remediation

of the AMD issue. It has the characteristics of active approach. Moreover, it would be relatively cheaper as the remedial materials are residues. Meanwhile, the plant may play an important role in the remediation as the passive approach does. Therefore, this treatment includes the features of active and passive methods with the abiotic and biological processes.

Initial field experiments have shown encouraging testing results with this new remediation approach. To investigate and evaluate the effectiveness and efficiency of the environmental impacts of this new remediation approach over more conditions, we need to develop an appropriate numerical model. A new hydro-geochemical model is developed that considers the hydrological and pyrite oxidation processes and their interactions to assess the implications of this new remediation approach for CR.

Although there are existing numerical models that can represent the hydrological processes and the fate transport process, there is no model yet that has most of the important hydrological features in the hilly CR region with pyrite oxidation process represented together in a more physically-based manner. Some models represent the simplified characteristics of hydrology and fate and transport process, but they do not include a representation of the pyrite oxidation process in their models, and the vice versa. For example, the widely used Soil and Water Assessment Tool (SWAT) [*Neitsch et al.,* 2002] is a hydrologic model for predicting the movement of sediments, pesticides and/or nutrients within a watershed. Study regions of the SWAT model are divided into hydrologic response units over which the land and routing phases of the hydrologic cycle are simulated using water balance equations. However, it does not address the pyrite oxidation process. Even for models that represent the pyrite oxidation process, the process is mainly represented empirically.

The other widely used model is HYDRUS [*Šimůnek et al.*, 1998] which utilizes the advection-dispersion equation and incorporates a sequential first-order decay process to mimic the movement of the soluble chemicals in the soil water. HYDRUS is a multi-phase model that is usually applied to field scale (e.g., HYDRUS-2D [*Šimůnek et al.*, 1999]) or to a soil profile (e.g., HYDRUS-1D). Despite being able to simulate the transport of numerous chemicals, neither SWAT nor HYDRUS considers the process of pyrite oxidation which is a primary cause for the AMD problem. Also both of these models may not represent a good infiltration in the hilly region.

Models that describe the pyrite oxidation process are mainly empirical and/or based on experimental measurements made during the solute transport. For example, *Chen et al.* [1998] developed the Watershed Analysis Risk Management Framework (WARMF) to evaluate water quality at the watershed scale. *Herr et al.* [2003] later incorporated a first-order decay equation for kinetic pyrite oxidation into WARMF based on the experimental summary of the *Ohio State University Research Foundation* [1971]. This was applied to the Cheat River Watershed, located in the Ohio River Basin in the eastern United States, with a constant rate of pyrite oxidation in the presence of atmospheric oxygen. A second example is the pH-redox-equilibrium-equations speciation model (PHREEQC) [*Parkhurst et al.*, 1980; *Parkhurst*, 1995; *Parkhurst and Appelo*, 1999]. This one dimensional model, developed by U.S. Geological Survey personnel, has been widely used in the geochemical field. It has been designed with a graphical user interface [*Charlton et al.*, 1997]. The model calculates the rate of pyrite oxidation by utilizing a derived function based on measurements [*Williamson and Rimstidt*, 1994]. Even although, PHREEQC has been coupled with HYDRUS in the HP1 model [*Jacques et al.*, 2006; *Šimůnek et al.*, 2008], pyrite oxidation was not calculated in a physical manner. Another example is that *Xu et al.*

[2000] used the constant values to represent the rates of pyrite oxidation in saturated and unsaturated subsurface flow, which is a simplified approach for describing pyrite oxidation process.

Different from these experiment-based pyrite oxidation models, *Wunderly et al.* [1996] developed a more physically-based model called PYROX that simulates one-dimensional, kinetically controlled oxygen diffusion within the vadose zone of tailings impoundments. This model can simulate the geochemical and the physical processes of the pyrite oxidation based on the coupling of an oxygen diffusion module and a shrinking core module [*Davis and Ritchie*, 1986] linked together with a simple reactive transport model. *Gerke et al.* [1998] used a similar concept for simulating pyrite oxidation on overburden mine spoils. In this approach, the pyrite oxidation process is coupled with a two-dimensional advection-dispersion transport model on a 2D cross-sectional domain. The Richard's equation is applied to calculate the soil water movement. Although it has been coupled with HYDRUS-2D in unsaturated waste rock pile call POLYMIN, it was designed at field scale [*Molson et al.*, 2004].

As the above brief reviews, these existing models do not integrate all the significant processes of hydrology and pyrite oxidation with water, oxygen and H^+ in a physical manner for the investigation of remediation. However, development of such an integrated model is fundamentally important if one wants to adequately evaluate the environmental impacts of the new remediation approach (i.e., BR + CR) or other similar approaches at a spatial scale from a field to a larger area. This is because water, oxygen and an acidic environmental condition are all essential to pyrite oxidation process in the field or watershed. An effective remediation approach would be one that is able to significantly reduce or "block" these "supplies" for CR piles. In this

chapter, we present a new hydro-geochemical model to fill in the gap so that an adequate investigation of the new approach (i.e., BR + CR) on reducing AMD in CR piles can be carried.

This new model employs the partial of PYROX sub-model to represent the geochemically-based pyrite oxidation process and the Distributed Hydrology Soil Vegetation Model [*Wigmosta et al.*, 1994] version 3.0 (i.e., DHSVM v3.0) to represent the soil-water-vegetation processes and their interactions through water and energy cycles. The DHSVM v3.0 is selected due to its ability in evaluating scenarios requiring high spatial resolution in hilly terrain (e.g., small mountainous areas similar to CR piles). In addition, the DHSVM v3.0 includes some of the important soil-water-vegetation processes such as evapotranspiration, infiltration and saturation excess runoff, baseflow, overland flow, and river flow routing as well as impacts of topography on surface and subsurface flow. The new model is available for field scale and watershed scale. To date, the model is test within a field scale.

This chapter is organized as follows: the model development is presented in section 2.2. A brief description of the study site and the field data is provided in section 2.3. In section 2.4, the new model is tested using the data collected from four experimental field plots of a pilot study. Analysis of the impact of remediation in CR pile, impact factors on pyrite oxidation and the depth of the amended zone are discussed in section 2.5. Section 2.6 provides conclusions.

2.2 BASIC MODEL DEVELOPMENT

The new hydro-geochemical model HGCM [*Xu et al.*, 2013a] developed in this study is based on the DHSVM v3.0 [*Wigmosta et al.*, 1994] and a pyrite oxidation model (PYROX) [*Wunderly et al.*, 1996]. Four improvements were made to the DHSVM model which better suit the

application for CR pile studies. These improvements are outlined in section 2.2.1. Section 2.2.2 describes the governing equations of the advection-dispersion model and section 2.2.3 details the processes of the pyrite oxidation model (partial of PYROX). The coupling process is explained in section 2.2.4.

2.2.1 Improvements to DHSVM v3.0

The first modification made to the DHSVM v3.0 is the addition of two more soil layers within each soil column. In the default mode of model, there are only four soil layers considered. In the new model, two extra layers are added. One of them is the buffer layer i.e. Layer 2 in Figure 2.1, which includes half amended layer and half non-amended layer. Apparently, above this layer, there are amended zone while the layers below is non-amended zone. The other layer added is a thick bottom layer since the coal waste could reach more than 10 meters. The thicknesses for each layers are as follows: 0.2 m, 0.2 m, 0.42 m, 1.5 m, 4.0 m, and the thickness of the bottom layer varies from approximately 4.0 m to ~10.0 m. This allows the model to simulate amended and un-amended regions at the same time.

The incorporation of steep slope effects on the infiltration process is the second improvement to the DHSVM v3.0. CR piles are typically characterized as having steep slopes. Therefore it is important to consider impact of the slope on the infiltration process as mentioned by Philip [*Philip*, 1991] that the impact on infiltration along a slope is not significant when the slope is less than 30 °, but becomes significant when the slope is greater than 30 ° [*Chen and Young*, 2006]. This is because more water becomes surface runoff rather than being infiltrated into the soil under such a steep slope condition. Therefore, a simple expression, i.e., cosine of

slope angle timing with rainfall, has been incorporated to the DHSVM v3.0 to account for the perpendicular rainfall on the slope, which leads to a more accuracy infiltration on the slope.

The final improvement made to the DHSVM v3.0 relates to its lower boundary condition. In the original DHSVM v3.0, there is a zero boundary condition (i.e. flow rate is zero) at the bottom of the deepest layer. This allows water to accumulate from the bottom to the up quickly. In order to make a more accurate portrayal of the soil conditions in the deep unsaturated field, the lower boundary condition of the soil is changed to free drainage instead of the zero boundary condition.

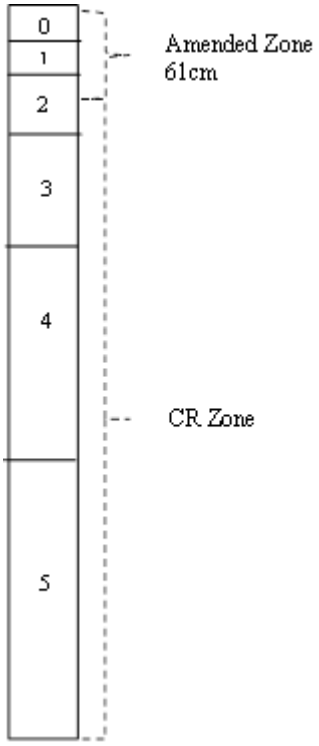

Figure 2.1 Soil profile in the coal-refuse region. The interface of 61 cm locates at the middle depth of Layer 2. Above 61 cm, it is the amended zone and below 61 cm it is coal refuse.

2.2.2 Advection-dispersion module

The advection-dispersion equation (ADE) is the key component in the model since it relates the pyrite oxidation process to hydrological processes. This equation is typically expressed as follows:

$$\frac{\partial \theta C}{\partial t} + \frac{\partial \rho s}{\partial t} = \frac{\partial}{\partial z}\left(\theta D^w \frac{\partial C}{\partial z}\right) - \frac{\partial qC}{\partial z} - S \tag{2-1}$$

where θ is the volumetric soil moisture content [$L^3 \cdot L^{-3}$], ρ is soil bulk density [$M \cdot L^{-3}$] , C and s are the chemical concentrations in liquid [$M \cdot L^{-3}$] and solid [$M \cdot M^{-1}$], respectively, q is water flow in soil [$L \cdot T^{-1}$], D^w is the dispersion coefficient in water [$L^2 \cdot T^{-1}$], and S is the source/sink term[$M \cdot T^{-1} \cdot L^{-3}$]. In this study, S represents total sulfur and total iron generated from the pyrite oxidation process. Note that Eq. (2-1) is only capable of reflecting the transport of sulfur and iron within the soil column, while impacts of other reactions are not considered in this chapter. Such a simplification is reasonable based on the premise that pyrite oxidation is a dominating process in the generation of AMD. In the model, Eq. (2-1) is solved by the finite difference method as Eq. (2-2) shows:

$$\begin{aligned} &\frac{(\theta C)_m^n - (\theta C)_m^{n-1}}{\Delta t} + \frac{(\rho s)_m^n - (\rho s)_m^{n-1}}{\Delta t} - \frac{(\theta D^w)_m^n - (\theta D^w)_{m-1}^n}{\Delta z} \cdot \frac{C_m^n - C_{m-1}^n}{\Delta z} - \\ &(\theta D^w)_m^n \frac{C_{m+1}^n - 2C_m^n + C_{m-1}^n}{\Delta z^2} + \frac{(qC)_m^n - (qC)_{m-1}^n}{\Delta z} + S = 0 \end{aligned} \tag{2-2}$$

where the superscript n denotes the time step and m is the number of the soil layer. The absorption and desorption are considered in the model with a coefficient k timing concentrations to replace s in Eq. (2-2) i.e. $k \times C$, while k can be negative or positive. Eq. (2-2) then becomes:

$$\frac{(\theta C)_m^n - (\theta C)_m^{n-1}}{\Delta t} + \frac{(\rho k C)_m^n - (\rho k C)_m^{n-1}}{\Delta t} - \frac{\left(\theta D^w\right)_m^n - \left(\theta D^w\right)_{m-1}^n}{\Delta z} \cdot \frac{C_m^n - C_{m-1}^n}{\Delta z} - \left(\theta D^w\right)_m^n \frac{C_{m+1}^n - 2C_m^n + C_{m-1}^n}{\Delta z^2} + \frac{(qC)_m^n - (qC)_{m-1}^n}{\Delta z} + S = 0 \quad (2\text{-}3)$$

2.2.3 Pyrite oxidation module

The pyrite oxidation process can be simplified into two reactions represented below by Eqs. (2-4) and (2-5) [*Wunderly et al.*, 1996]. These two reactions can also be combined into a single expression shown in Eq. (2-6).

$$FeS_2 + H_2O + 7/2O_2 \Rightarrow Fe^{2+} + 2SO_4^{2-} + 2H^+ \quad (2\text{-}4)$$

$$Fe^{2+} + 1/4O_2 + H^+ \Rightarrow Fe^{3+} + 1/2H_2O \quad (2\text{-}5)$$

$$FeS_2 + 1/2H_2O + 15/4O_2 \Rightarrow Fe^{3+} + 2SO_4^{2-} + H^+ \quad (2\text{-}6)$$

Applying the algorithm of PYROX developed by *Wunderly et al.* [1996], the pyrite oxidation process can be represented with two sub-modules: an oxygen diffusion sub-module and a shrinking-core sub-module [*Davis and Ritchie*, 1986]. Under saturated soil conditions, oxygen diffusion is considerably lower than that in the air, thus limiting the pyrite oxidation process [*Gerke et al.*, 1998]. In this model, pyrite oxidation is assumed to occur only within the unsaturated soil layers of CR pile.

In the oxygen diffusion sub-module, the advection-dispersion of oxygen in the pore space is described by Eq. (2-7):

$$\frac{\partial \theta_a(z) \cdot [O_2]_a}{\partial t} = \frac{\partial}{\partial z}\left(\theta_a \cdot D_a(z) \cdot \frac{\partial [O_2]_a}{\partial z}\right) - S_{O_2}(z,t) \quad (2\text{-}7)$$

where $\theta_a(z)$ is the air content [$L^3 \cdot L^{-3}$], $D_a(z)$ is the oxygen diffusion coefficient [$L^2 \cdot T^{-1}$] in the pore space, $[O_2]_a$ is the concentration of oxygen in the pore space [$M \cdot L^{-3}$], S_{O_2} is the oxygen consumption treated as a sink term [$M \cdot L^{-3} \cdot T^{-1}$], z is soil depth[L], and t is time [T]. $D_a(z)$ is calculated by the method of *Elberling et al.* [1993]:

$$D_a(z) = \alpha \cdot D_a^{O_2} \cdot (1-\phi)^{\beta} + \frac{\phi \cdot D_w^{O_2}}{H} \tag{2-8}$$

where α is equal to 0.273 and β is equal to 3.28, $D_a^{O_2}$ is the oxygen diffusion coefficient in air [$L^2 \cdot T^{-1}$], $D_w^{O_2}$ is the oxygen diffusion coefficient in water [$L^2 \cdot T^{-1}$], ϕ is the relative water saturation which is equal to $\theta \cdot (\theta_s - 0.01)^{-1}$ where θ_s is porosity [$L^3 \cdot L^{-3}$] and the residual water content is 0.01, H is equal to 2.63 (Henry's constant), $D_a^{O_2}$ and $D_w^{O_2}$ are equal to 1.8×10^{-5} m^2/s and 2.1×10^{-9} m^2/s, respectively, based on the data provided by *Gerke et al.* [1998].

In the shrinking-core model, it is assumed that the mineral particles are spherically shaped and homogeneously distributed throughout CR pile. The radius of average soil particles is represented as R and the radius of the unreacted mineral cores is r_c. For the purposes of this study, R is set 2.0 mm and the initial r_c for each layer is 1.95 mm. The speed of the pyrite oxidation process is estimated by the shrinking size of the unreacted particle radius represented by Eq. (2-9) [*Wunderly et al.*, 1996; *Gerke et al.*, 1998]:

$$\frac{dr_c}{dt} = -\frac{D_w(1-\theta_s)}{\varepsilon \rho_s} \frac{R}{r_c(R-r_c)} \frac{[O_2]_a}{H} \tag{2-9}$$

where D_w is the effective oxygen diffusion coefficient containing the diffusion properties of the water and the oxidized mineral particle [$L^2 \cdot T^{-1}$] and is equal to 3.2×10^{-11} m^2/s [*Gerke, Molson et al.* 1998], ρ_s is the sulfur bulk density [$M \cdot L^{-3}$] which is equal to $f \times \rho_b$ where ρ_b is soil bulk density [$M \cdot L^{-3}$] and f is the proportion of sulfur in the soil [$M \cdot M^{-1}$], ε is the mass ratio of the

consumption of oxygen to the consumption of sulfur based on the reaction stoichiometry and it is determined by Eq. (2-10) as follows,

$$\varepsilon = \frac{Mass\ of\ oxygen}{Mass\ of\ sulfur} = \frac{\frac{7}{2}\cdot W_{O_2}\cdot ratio + \frac{15}{4}\cdot W_{O_2}\cdot(1-ratio)}{2\cdot ratio\cdot W_s + (1-ratio)\cdot 2\cdot W_s} = \frac{\frac{15}{4}\cdot W_{O_2} - \frac{1}{4}\cdot W_{O_2}\cdot ratio}{2\cdot W_s} \quad (2\text{-}10)$$

where W_{O_2} and W_s are the molar mass for oxygen and sulfur respectively and *ratio* denotes the concentration of [Fe^{2+}] to total Fe:

$$ratio = \frac{[Fe^{2+}]}{[Fe(total)]} = \frac{1}{\left[K_{eq}\times(\frac{[O_2]_a}{H})^{0.25}\times 10^{-pH}+1\right]} \quad (2\text{-}11)$$

where $K_{eq} = 10^{7.7549}$ at 25 ℃ [*Wunderly et al.*, 1996].

Following the definitions of the shrinking-core module, the sink term, $S_{O_2}(z,t)$ in Eq. (2-7) can now be estimated using Eq. (2-12) derived by *Gerke et al.* [1998].

$$S_{O_2}(z,t) = D_w\frac{3(1-\theta_s)}{R^2}\left(\frac{r_c}{R-r_c}\right)\frac{[O_2]_a}{H} \quad (2\text{-}12)$$

After substitution, Eq. (2-7) now becomes:

$$\frac{\partial\theta_a\cdot[O_2]_a}{\partial t} = \frac{\partial}{\partial z}\left(\theta_a D_a\frac{\partial[O_2]_a}{\partial z}\right) - D_w\frac{3(1-\theta_s)}{R^2}\left(\frac{r_c}{R-r_c}\right)\frac{[O_2]_a}{H} \quad (2\text{-}13)$$

Based on Eq. (2-9) (i.e., the shrinking-core module) and Eq. (2-13) (i.e., the oxygen diffusion module), the unreacted particle radius (r_c.) and the oxygen concentration ($[O_2]_a$) for each soil layer can be solved. This allows for the estimation of SO_4 (total sulfate in all SO_4^{2-} solutions) and total Fe (i.e. Fe(П) plus Fe(Ш) in all Fe solutions) from the pyrite oxidation process. These

products are the estimates of the source term in Eq. (2-1). The formulas of the finite difference method used for solving Eq. (2-13) and Eq. (2-9) are shown as follows:

$$\frac{(\theta_a \cdot [\mathrm{O}_2]_a)|_m^n - (\theta_a \cdot [\mathrm{O}_2]_a)|_m^{n-1}}{\Delta t} = (\theta_a D_a)\Big|_m^n \left(\frac{[\mathrm{O}_2]_a|_{m+1}^n - 2[\mathrm{O}_2]_a|_m^n + [\mathrm{O}_2]_a|_{m-1}^n}{\Delta z^2} \right) +$$
$$\frac{(\theta_a \cdot D_a)|_m^n - (\theta_a \cdot D_a)|_{m-1}^n}{\Delta z} \cdot \frac{[\mathrm{O}_2]_a|_m^n - [\mathrm{O}_2]_a|_{m-1}^n}{\Delta z} - \left[D_w \frac{3(1-\theta_s)}{R^2} \left(\frac{r_c}{R - r_c} \right) \right]\Bigg|_m^n \frac{[\mathrm{O}_2]_a|_m^n}{H} \qquad (2\text{-}14)$$

$$r_c\big|_m^{n,j} = r_c\big|_m^{n,j-1} -$$
$$\frac{\left(r_c\big|_m^{n,j-1}\right)^2 \left(\frac{R\big|_m}{2} - \frac{r_c\big|_m^{n,j-1}}{3} \right) - \left(r_c\big|_m^{n-1}\right)^2 \left(\frac{R\big|_m}{2} - \frac{r_c\big|_m^{n-1}}{3} \right) + \frac{D_w \left(1 - \theta_s\big|_m\right) R\big|_m}{\varepsilon\big|_m^n \rho_s\big|_m H} \frac{[\mathrm{O}_2]_a|_m^{n-1} + [\mathrm{O}_2]_a|_m^{n,k}}{2} \Delta t}{r_c\big|_m^{n,j-1} \left(R\big|_m - r_c\big|_m^{n,j-1} \right)} \qquad (2\text{-}15)$$

where the superscripts *n* and *m* in Eq. (2-14) are the current time step and the number of the soil layer as in Eq. (2-2). In Eq. (2-15), *j* denotes the j^{th} iterative step of the shrinking-core equation and *k* denotes the iteration step of Eq. (2-14). Eq. (2-15) is obtained by applying the Newton–Raphson algorithm based on *Davis and Ritchie* [1986]**.** The derivation of Eq. (2-15) is quite similar to the formula given by *Gerke et al.* [1998].

In order to solve Eq. (2-14) by the finite difference method, the upper boundary of oxygen concentration in the air is set to be a constant with 0.31 kg/m^3 which is obtained based on a standard air condition. In the soil, an initial oxygen concentration profile, which decreases with depth, is assumed. The scheme to solve the above system of equations follows *Wunderly et al.* [1996], except that the finite difference method is applied in Eq.(2-14) instead of the finite element method and the pH value is assumed to be a constant over time in this study.

A brief iteration to solve $[O_2]_a$ and r_c is given here by using the mth layer at the nth time step as an example: 1) one begins with $r_c|_m^n = 2r_c|_m^{n-1} - r_c|_m^{n-2}$ and solves $[O_2]_a|_m^n$ in Eq.(2-14); 2) one calculates $r_c|_m^n$ in Eq.(2-15) with the solved $[O_2]_a|_m^n$ and the latest $\varepsilon|_m^n$; 3) one obtains the ratio of [Fe^{2+}] to Fe (total) using Eq.(2-11) with a constant pH and the solved $[O_2]_a|_m^n$, then updates $\varepsilon|_m^n$ by Eq.(2-10); 4) one uses the calculated $r_c|_m^n$ from step 2 to solve $[O_2]_a|_m^n$ in Eq.(2-14); 5) one repeats steps 2, 3 and 4 until $[O_2]_a|_m^n$ and $r_c|_m^n$ are converged. After these variables converge, the production of sulfur in the liquid is given by:

$$\Delta C_{S,liquid}^{oxid} = \frac{\rho_s|_m((r_c|_m^n)^3 - (r_c|_m^{n-1})^3)}{R|_m^3 \theta|_m} \tag{2-16}$$

where $\Delta C_{S,liquid}^{oxid}$ is the amount of sulfur produced by the pyrite oxidation from the solid phase into the liquid phase at one time step [M·L^{-3}], $\theta|_m$ is the soil moisture at the m^{th} layer [L·L^{-1}], $r_c|_m^n$ is the unreactive core at the n^{th} time step and $r_c|_m^{n-1}$ is the unreactive core at the $(n\text{-}1)^{th}$ time step. The concentrations of Fe (total) in the liquid can be derived by the following:

$$\Delta C_{Fe,liquid}^{oxid} = \frac{W_{Fe} \cdot \Delta C_{S,liquid}^{oxid}}{2.0 \times W_s} \tag{2-17}$$

where W_{Fe} is the molar mass for iron. Eq. (2-16) and Eq. (2-17) do not consider solid precipitates, however, the products from pyrite oxidation may precipitate. Currently, the model assumes the first-order decay processes for SO_4 and total iron to represent the precipitate reactions. As the result of that, Eq. (2-16) and Eq. (2-17) are rewritten as Eq. (2-18) and Eq. (2-19):

$$\Delta C_{S,liquid}^{oxid} = (1-(1-C_s)e^{-\lambda_S t})\frac{\rho_s\big|_m((r_c\big|_m^n)^3-(r_c\big|_m^{n-1})^3)}{R\big|_m{}^3\theta_w\big|_m} \tag{2-18}$$

$$\Delta C_{Fe,liquid}^{oxid} = (1-(1-C_{Fe})e^{-\lambda_{Fe} t})\frac{W_{Fe}\Delta C_{S,liquid}^{oxid}}{2.0\times W_s} \tag{2-19}$$

where (1-C_s) and (1-C_{Fe}) are the precipitating rates for SO_4 and total iron respectively, while λ_s and λ_{Fe} are the decay coefficients for SO_4 and total iron. All of them need to be calibrated based on the observed information.

2.2.4 Hydro-geochemical coupling

The next issue following the improvements to the DHSVM v3.0 and the creation of the ADE with pyrite oxidation modules is the coupling of these two parts. The specific procedures are: (1) applying the oxygen diffusion module and the shrinking-core module to calculate the production (i.e., SO_4 and total Fe) of pyrite oxidation, (2) using the results from (1) as the source for the ADE, (3) coupling the ADE with the improved DHSVM v3.0 and solve the ADE by the finite difference method, (4) calculating the mixing concentrations in the routing module including surface, subsurface and channel flow.

The key connections between the ADE and DHSVM v3.0 are soil moisture, θ, and water flow, q. These two variables respond to the forcing data and the hydrological processes and are updated at each time step. After the soil moisture is updated in each layer, these two variables are passed to the ADE. The ADE starts to run the solute transport process, which includes pyrite oxidation. However, not all the steps of pyrite oxidation occur in each soil layer and each grid

cell. The first step of the pyrite oxidation process, i.e. Eq. (2-4), happens whenever there is enough oxygen in the pore space and sufficient water in the soil, while the second step of pyrite oxidation process, i.e. Eq. (2-5), requires sufficient amounts of both oxygen and H^+.

The interaction of chemical concentrations between grids is realized by the surface and subsurface routing. Assuming the chemical concentrations are immediately mixed with input water, the concentration can be expressed by the mass balance:

$$C_{in,i,j}Q_{in,i,j} = \sum_{k=0}^{7} F_k C_{out,k} Q_{out,k} \tag{2-20}$$

where $C_{in,i,j}$ and $Q_{in,i,j}$ are the chemical concentration and inflow at the grid (i, j) respectively, F_k is the weight of the flow in each direction [*Wigmosta and Lettenmaier*, 1999], $C_{out,k}$ is the concentration in the k^{th} direction and $Q_{out,k}$ is the flow in the k^{th} direction.

2.3 STUDY SITE AND DATA

2.3.1 Study site

The study area is the Mather CR pile, remnants of the Pickand-Mather Collieries Mine which was in operation from 1918 to 1964. It is located along the south branch of Ten Mile Creek in Mather, Greene County, Pennsylvania. Previous reclamation work has reshaped a considerable portion of CR pile which now has a vegetated tier and large plateau as shown in Figure 1.1a. However, due to the acidity of the pile, much of the vegetated cover has died and is eroded away. Despite remediation attempts, CR pile still leaches AMD into the surrounding environment.

This study investigates the beneficial use of bauxite residue, a byproduct of the aluminum production process, in neutralizing the acid environment and enhancing the soil quality. In 2009, a two-acre region is prepared along the northern face of the Mather coal pile (Figure 1.1b and c). This region was divided into four plots (the area of each plot is 0.0024 km^2, 0.0021 km^2, 0.0010 km^2 and 0.0015 km^2 respectively), of which three were reclaimed according to the reclamation methods listed by the Pennsylvania Department of Environmental Protection (PADEP) and one left untouched (i.e., plot 1) as a control plot for comparison. The three remediated plots have been described in Chapter 1.0 .

2.3.2 Measurements and data

According to our laboratory measurements, the saturated hydraulic conductivity (Ks) of the CR is considerably larger than that of the surrounding soil. The large hydraulic conductivity and considerable depth of the CR (greater than 10 m) keep the pile in an unsaturated state. Table 2.1 illustrates the surface porosity and the ranges of hydraulic conductivity in the soil layers, which have been slightly calibrated based on measurements.

Table 2.1 Porosity and saturated hydraulic conductivity for each plot.

	Plot 1	Plot 2	Plot 3	Plot 4
Porosity	0.52	0.46	0.48	0.45
Ks ($m\ s^{-1}$)	$6\times10^{-5}\sim 8.5\times10^{-4}$	$6\times10^{-5}\sim 8.5\times10^{-4}$	$6\times10^{-5}\sim 8.5\times10^{-4}$	$6\times10^{-5}\sim 8.5\times10^{-4}$

Meteorological data required by the model (e.g., air temperature, wind speed, relative humidity and rainfall) were supplied by a local weather station (KPACLARK3) located within a two-mile radius of the study area. The weather station is a part of the Weather Underground PWS online network, which provides the forcing data from 6/1/2009 to 6/27/2010 (Figure 2.2). The short wave data was obtained from NOAA National Solar Radiation Data Base. After this time period, the chemical samples were very limited. High resolution, 3×3 meters, DEM (digital elevation model) data was downloaded from the US Geological Survey (USGS) website to characterize the complexity of the topography of CR pile.

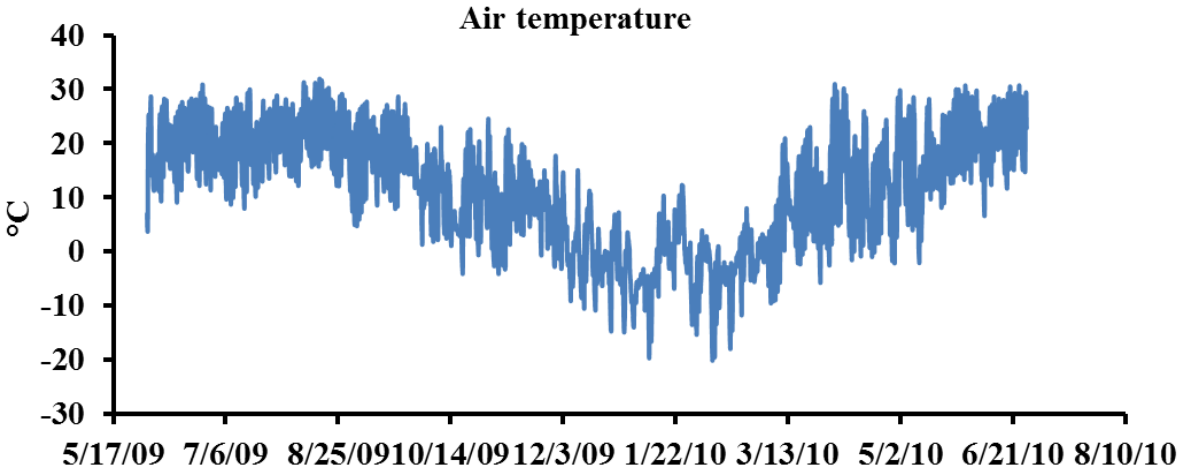

(a)

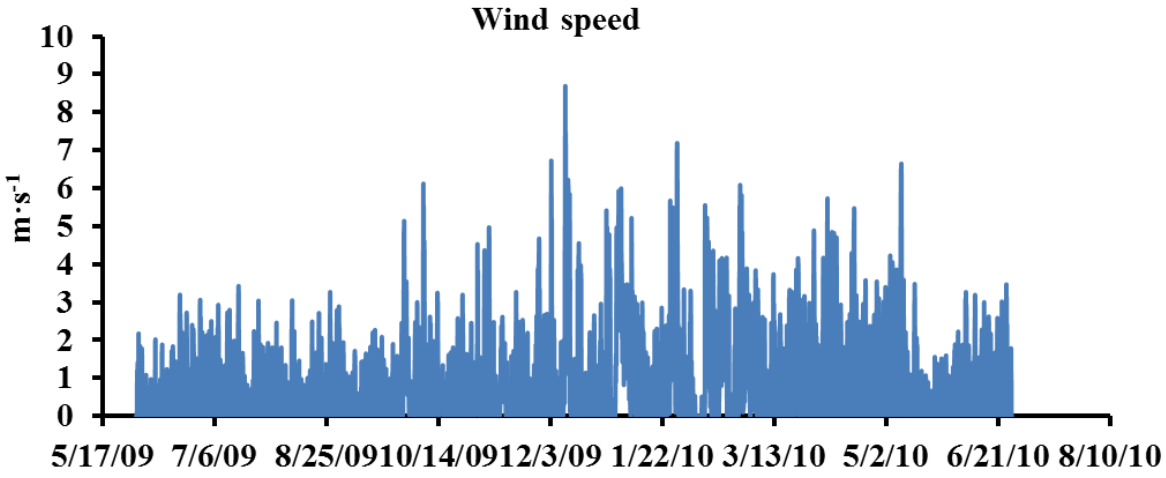
Wind speed
m·s-1
10
9
8
7
6
5
4
3
2
1
0
5/17/09
7/6/09
8/25/09
10/14/09
12/3/09
1/22/10
3/13/10
5/2/10
6/21/10
8/10/10

(b)

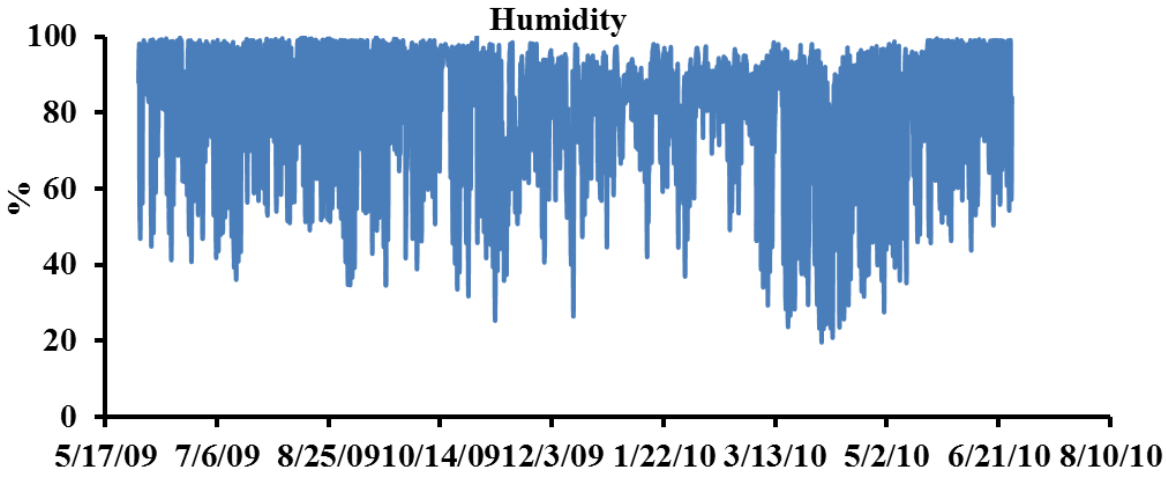
Humidity
%
100
80
60
40
20
0
5/17/09
7/6/09
8/25/09
10/14/09
12/3/09
1/22/10
3/13/10
5/2/10
6/21/10
8/10/10

(c)

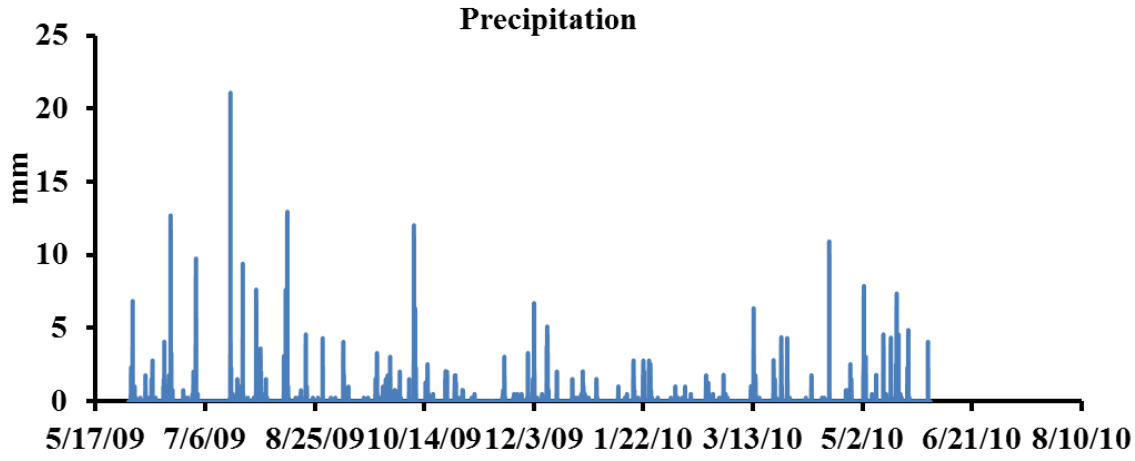

(d)

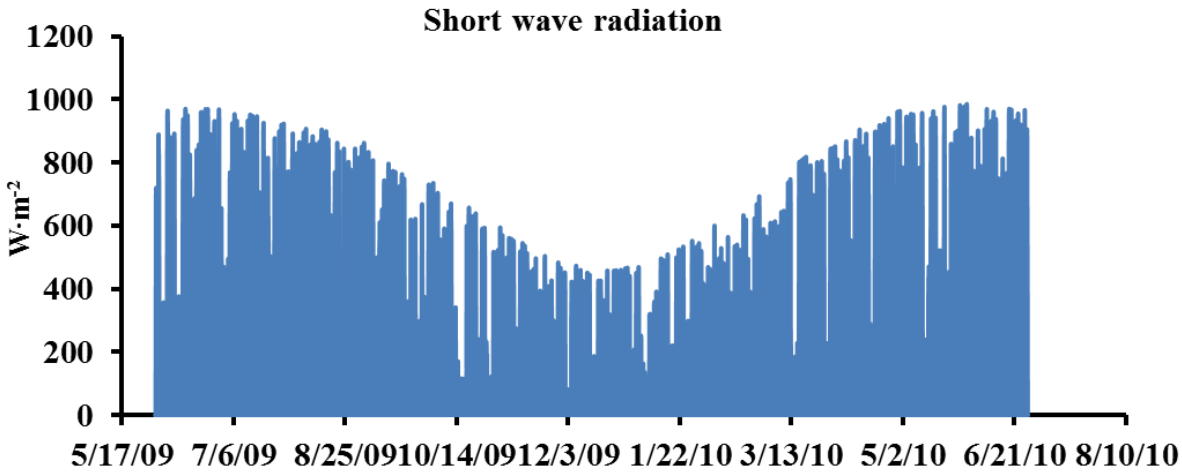

(e)

Figure 2.2 The weather information data in the calibration period from 6/1/2009 to 6/27/2010: (a) air temperature (b) wind speed (c) relative humidity (d) precipitation and (e) short wave radiation.

All the measurements were collected within a very small watershed ~0.06645 km^2 includes partial CR pile (pink area) and partial normal soil (grey region) in Figure 2.3a. Soil moisture sensors were installed at the middle location (green stars in Figure 2.3a) along the hill slope (Figure 2.3b) for each of the four plots. However, the sensors in plot 1 were damaged after installed a few months due to the acidic water. At each location, soil moisture was measured at the depth of 61 cm which is at the interface of the amended and non-amended zones except for plot 3 which has a deeper amended zone. The soil moisture data normally started from June 2010 and the hydraulic conductivities were slightly calibrated based on the range of Table 2.1 from June 2010 to February 2011.

To collect water samples in each plot, lysimeters were installed at middle location along the hillslope. At each location, water is collected at the depth of: 61 cm and 91 cm. The lysimeters located at the middle of the hillslope are close to the middle location where the soil moisture sensors are installed in each plot (Figure 2.3a). This chapter compares the model simulation with the field data at this location both for soil moisture and chemical concentrations.

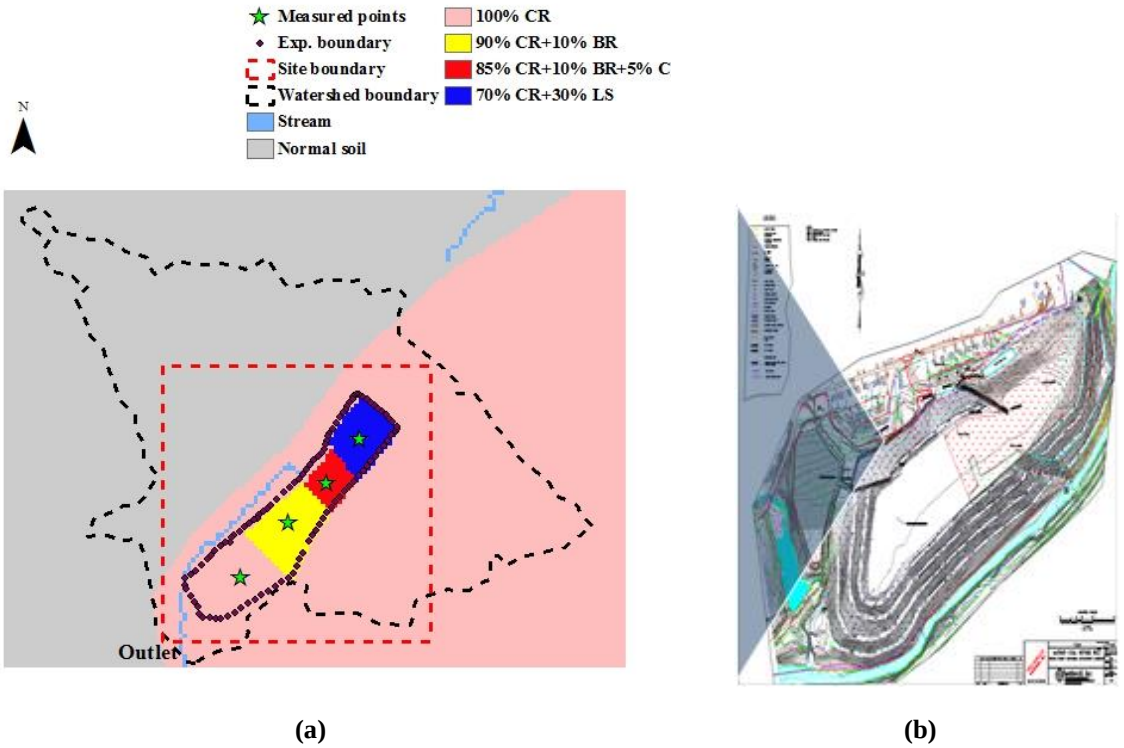

Figure 2.3 (a) Black dashed line is watershed boundary, red dashed line represents site boundary and purple dashed line denotes experimental boundary. Locations of measured points are shown in the four plots: the green stars are the middle locations along the hill slope where soil sensor and lysimeters are installed. Plot 1 merely has coal refuse without vegetation, plot 2 is 90% coal refuse mixing with 10% bauxite residue in the amended zone and vegetation on the top 61 cm, plot 3 is 85% coal refuse mixing with 10% coal refuse and 5% mushroom compost and vegetation on the top 91 cm, plot 4 is 70% coal refuse mixing with 30% limestone and vegetation on the top 61 cm. The coordinate of boundary for the four plots are given in APPENDIX B. (b) The hill slope of coal-refuse pile in Mather, PA (photo offered by Alcoa Inc.).

2.3.3 Statistical methods for data analysis

The modeling result is to minimize both of the errors of simulation and observation. The root mean square error (RMSE) Eq. (2-21), absolute error Eq. (2-22) and the absolute relative error Eq. (2-23) will be used in the entire thesis.

$$RMSE(X_{obs}, X_{cal}) = \sqrt{\frac{\sum_{i=1}^{n}\left(x_{obs}^{i} - x_{cal}^{i}\right)^{2}}{n}} \tag{2-21}$$

$$Abs.Error = \left|X_{obs} - X_{cal}\right| \tag{2-22}$$

$$Abs.\mathrm{Re}lativeError = \frac{\left|X_{obs} - X_{cal}\right|}{\left|X_{obs}\right|} \times 100\% \tag{2-23}$$

where X_{obs} and X_{cal} represent the series of observation and the series of simulation respectively, x_{obs}^{i} and x_{cal}^{i} are the observation and simulation at the i^{th} time step and n is the total time steps.

2.4 BASIC MODELING RESULTS

The model was running within the red dashed area 0.038018 ~ km^2 in Figure 2.3. Figure 2.4 shows the comparison between the simulation and the observation of the soil moisture at 61 cm in the amended plots (i.e., plots 2 through 4) for the period from 6/27/2010 to 2/13/2011. The observed soil moisture data were obtained by EC-5 soil moisture sensors (Decagon Devices, Inc.) and the accuracy is ±0.03 m^3/m^3. Plot 1 has no observed data for comparison due to the

strong acidity of the soil moisture which destroyed the moisture sensors. All of the plots demonstrated a higher soil moisture content in winter and lower soil moisture content in summer. There were a few spikes in the observed data in the amended plot which may be due to the result of the water pockets in the soil after the rain. Table 2.2 gives the comparison between the observations and model simulations for the soil moisture for the amended plots. The averages of the model simulated soil moisture are close to those of the observations. The relative errors between them are less than 5% and the root-mean-square errors (RMSE) are not greater than 0.05. These results suggest that the model performs well in simulating the soil moisture with the high resolution mesh.

Model simulation of the chemical concentrations is from 6/1/2009 to 6/27/2010. The oxidation time step is 2.5 days and the chemical transport time step is an hour. The initial concentrations of total sulfur (converted from sulfate) and total iron (Fe(Π) + Fe(ΙΙΙ)) in the model are listed in Table 2.3. The beginning oxygen concentration profile for the six soil layers, starting from the surface, is assumed as: 0.25 kg/m^3, 0.20 kg/m^3, 0.15 kg/m^3, 0.02 kg/m^3, 0.01 kg/m^3 and 0.01 kg/m^3. Impacts of these initial values disappear after an appropriate spin-up time following the model initialization.

Table 2.2 Simulation of soil moisture at 61 cm.

	Sim. Mean (VWC)	Obs. Mean (VWC)	Relative Error (%)	RMSE (VWC)
P2	0.19	0.20	5	0.05
P3	0.18	0.18	2	0.05
P4	0.14	0.15	5	0.05

Table 2.3 Model initial input: the concentrations of total sulfur (converted from sulfate) and Fe (total) in liquid for six layers in each plot. P1S, P2S, P3S and P4S represent total sulfur in plot 1, plot2, plot3 and plot4. P1Fe, P2Fe, P3Fe and P4Fe represent Fe (total) in plot 1, plot 2, plot 3 and plot 4.

	P1 S (kg/m^3)	P2 S (kg/m^3)	P3 S (kg/m^3)	P4 S (kg/m^3)	P1 Fe (kg/m^3)	P2 Fe (kg/m^3)	P3 Fe (kg/m^3)	P4 Fe (kg/m^3)
Layer 0	1.8	0.6	0.48	0.4	1.2	0.005	0.00012	0.0001
Layer 1	1.8	0.6	0.48	0.4	1.2	0.005	0.00012	0.0001
Layer 2	1.8	0.6	0.48	0.4	1.2	0.005	0.00012	0.0001
Layer 3	7.6	9.7	0.52	4.1	5.5	9.2	0.0002	2.6
Layer 4	7.6	9.7	0.52	4.1	5.5	9.2	0.0002	2.6
Layer 5	7.6	9.7	0.52	4.1	5.5	9.2	0.0002	2.6

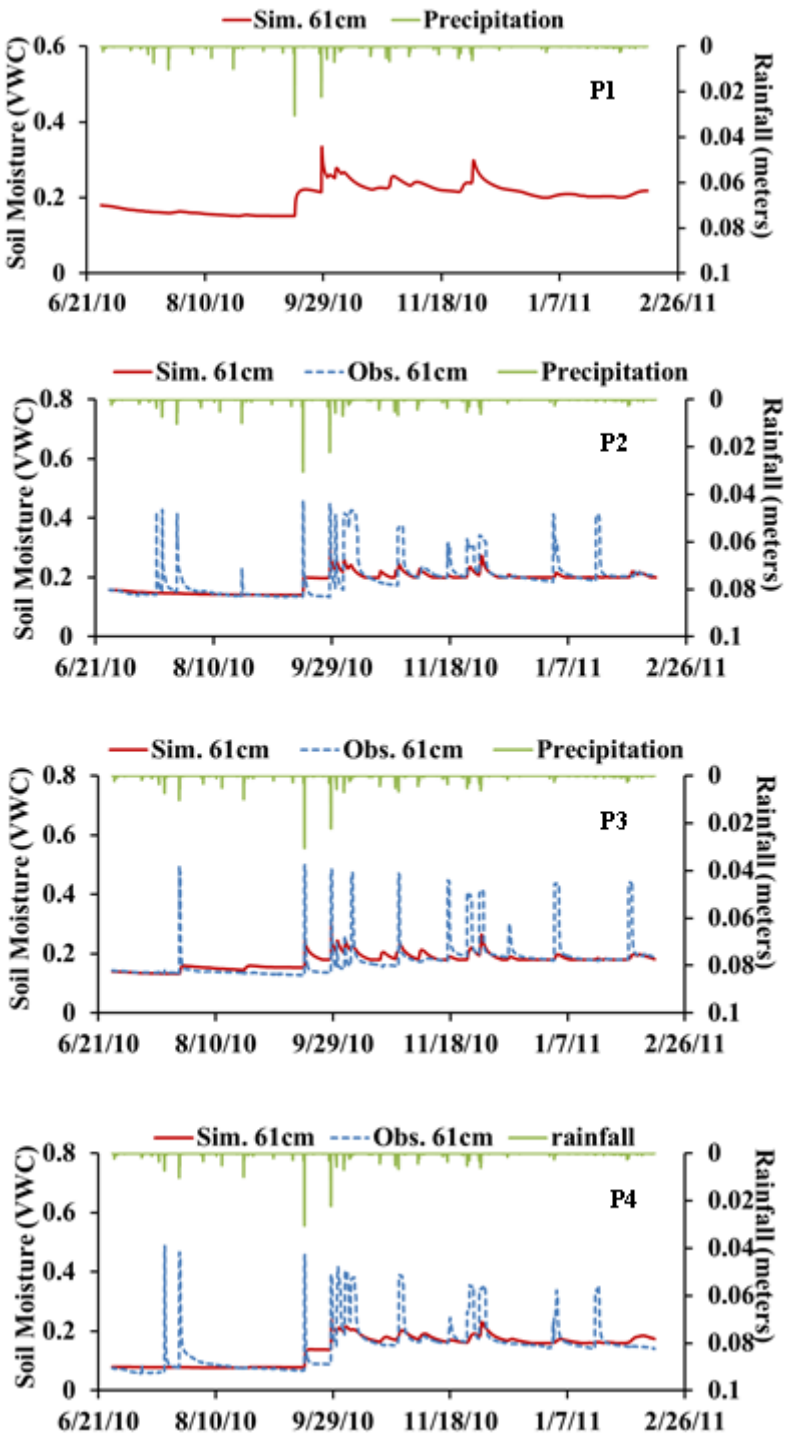

Figure 2.4 Comparison between simulated and observed soil moistures at the 61 cm depth of the middle location along the hillslope of each plot from 2010.6 to 2011.2, where P1, P2, P3 and P4 represent plot1 through plot4. The accuracy of observation is ±0.03 m^3/m^3.

There are three main assumptions made in this model. They include: (1) heat generated by the exothermic reactions such as pyrite oxidation is ignored. Such an assumption serves as a good 1st order of approximation. (2) Oxidation occurs in the unsaturated zone. The chemical transport is via the movement of water (including surface and subsurface flows). (3) The pH of the soil stays constant over time. The constant pH values given to each of the different zones (i.e., surface amended zone, layers 0 and 1; interface zone, layer 2; and non-amended zone, layers 3 through 5) are listed in Table 2.4. These pH values are one-year average values from the measurements. The pH measurements at 61 cm represent the interface zone, i.e. 40–82 cm, and the measurements at 91 cm denote the non-amended portion except for plot 3. In each remediated plot, the observed pH in the interface portion is higher than the non-amended zone. For the surface portion, i.e. 0–40 cm, the pH is assumed to be 7.0 in the amended plots, i.e. plots 2–4, while the surface portion in plot 1 is assumed to be same pH value as at the 61 cm. The amended zone for plot 3 is deeper than 91 cm and its pH values are listed in Table 2.4.

The simulations of SO_4 and Fe (total) in soil water at the middle of the hillslope for each plot are listed in Figure 2.5 and Figure 2.6 respectively. The simulation results capture the pattern of the observed data. In plot 1, both the observed data and the simulated data of SO_4 and Fe (total) show much higher than those in the other amended plots. This is because of the low pH in CR pile which may reduce the ability of precipitating SO_4 and Fe (total). The remediated plots, which have an amended top layer, were not as acidic as it was in plot 1 such that SO_4 and Fe (total) (especially Fe(III)) were more easily precipitated.

Table 2.5 lists the calibration result of precipitating rates and the decay coefficients for SO_4 and Fe (total): 1- C_S, 1- C_{Fe}, λ_s and λ_{Fe}. Plot 1, the un-amended plot, has the precipitating rate assumed to be zero in the model. For the other plots, precipitating rates of SO_4 are assumed lower than the rates of Fe (total), which lead to higher concentrations of SO_4 than Fe (total) in the amended plots. Moreover, Table 2.5 shows that the relative errors of SO_4 and Fe (total) in plot 1 are as low as 1.5%, which means that the model performs well in CR area. The relative errors in the remediated plots especially plot 4 are higher than plot 1. For example the relative error of Fe (total) in plot 4 is as high as 33.0%. However, the absolute error is as low as 0.00014 kg/m^3. It means that the model may not behave well in very low concentrations but the simulation still can capture the magnitude of the observation.

Table 2.4 The average pH values in the four plots. The second column is obtained by assumption. The third column and the last column are from the measurements at 61 cm and 91 cm. L3, L4 and L5 represent Layer 3, Layer 4 and Layer 5.

	pH (0~40cm) Layer 0,1	pH (40~82cm) Layer 2	pH (below 82cm) Layer 3, 4, 5
Plot1	2.2	2.2	2.4
Plot2	7.0	4.5	2.6
Plot3	7.0	6.9	L3:6.9; L4,5:2.9
Plot4	7.0	6.4	2.5

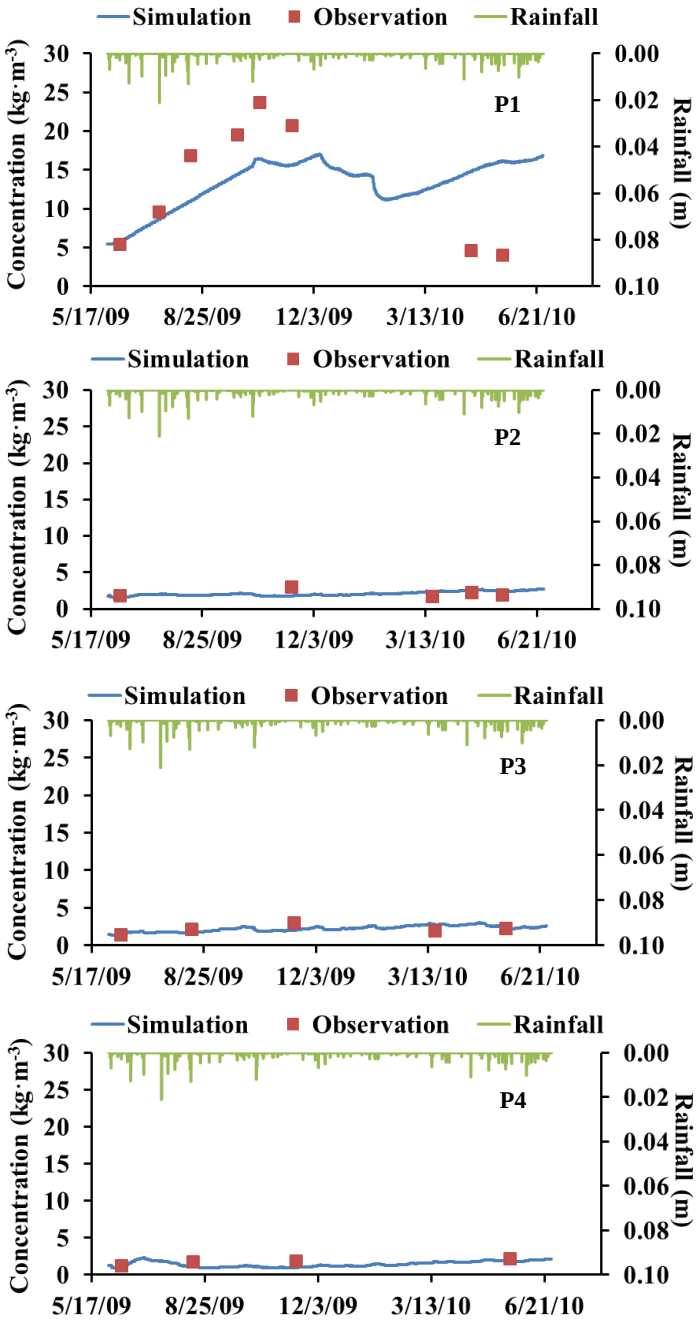

Figure 2.5 Comparison between simulated and observed concentrations of SO_4 at the 61 cm depth of the middle location along the hillslope of each plot from 2009.6 to 2010.6.

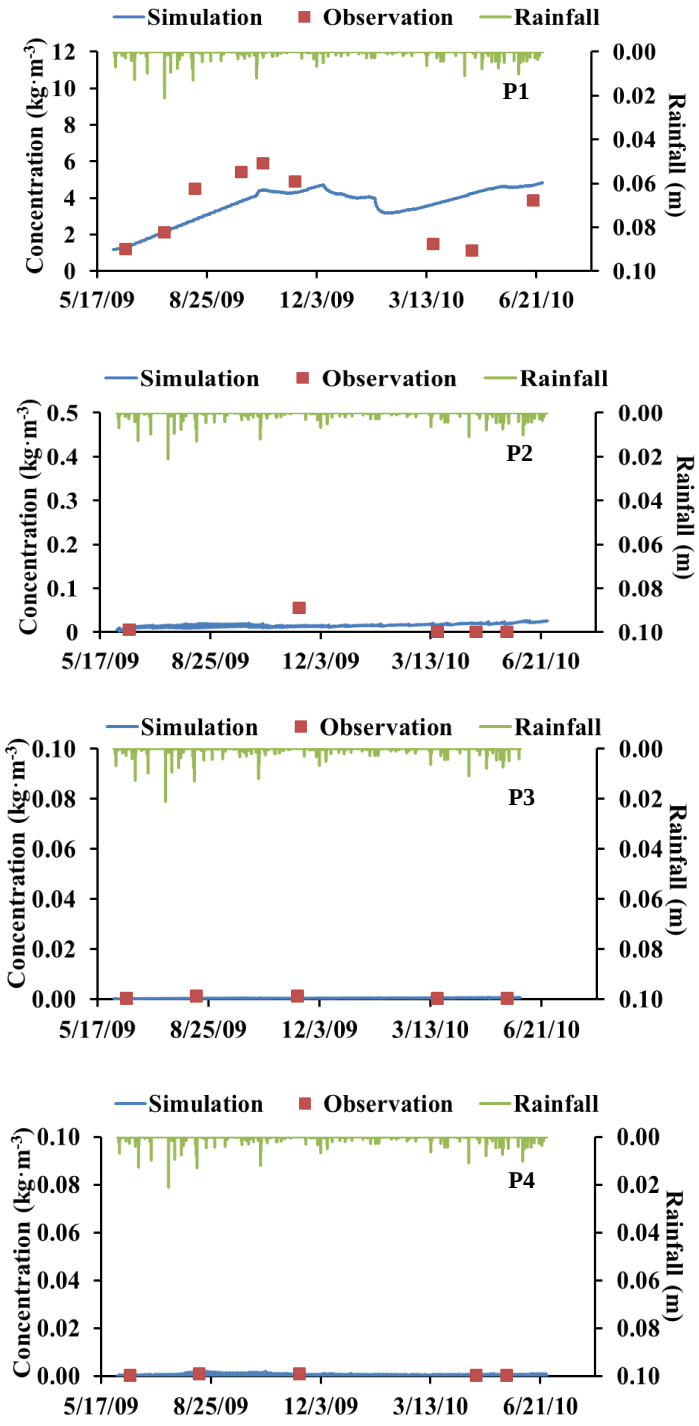

Figure 2.6 Comparison between simulated and observed concentrations of Fe (total) at the 61 cm depth of the middle location along the hillslope of each plot from 2009.6 to 2010.6.

Table 2.5 Precipitate rates and decay coefficients for SO_4 and Fe (total) at 61 cm in each plot and the simulation errors of SO_4 and Fe (total).

	$1-C_S$	λ_s	Abs. error ($kg\ m^{-3}$)	Relative error (%)	$1-C_{Fe}$	λ_{Fe}	Abs. error ($kg\ m^{-3}$)	Relative error (%)
P1	0		0.203	1.5	0		0.04903	1.5
P2	0.1	1.2×10^{-4}	1.2×10^{-4}	0.01	0.9	4×10^{-5}	0.00326	26.6
P3	0.08	1.0×10^{-4}	0.114	5.3	0.999	1×10^{-6}	0.00001	2.1
P4	0.25	1.5×10^{-4}	0.484	28.3	0.999	1×10^{-7}	0.00014	33.0

2.5 DISCUSSION

2.5.1 Factors affecting pyrite oxidation

The goal of remediation is not only to reduce the concentrations of SO_4 and Fe (total) in the amended zone, as indicated in Figure 2.5 and Figure 2.6, where the materials of CR and BR are mixed, but also to slow down the pyrite oxidation process in the non-amended zone. Figure 2.7 shows the measurements of the concentrations of SO_4 and Fe (total) in soil water at 91 cm at the middle location of the hill for each plot. It can be seen that the concentrations of SO_4 and Fe (total) are lower in the three remediated plots than the CR plot. Although the decreases are not as significant as they are in the amended zone, the Mann-Whitney U Test (It is a nonparametric test,

which does not require the samples to be normal distribution.) at the 95% confidence level shows that in the non-amended zone the difference between non-amended plot and amended plots indicated in Figure 2.7 are statistically significant. The significant decrease in the plot of 85% CR + 10% BR + 5% C (i.e., plot 3) is because this plot has its amended zone deeper than 91 cm. Reasons for the decreases of SO_4 and Fe (total) in the non-amended zone shown in Figure 2.7 are unclear yet in this chapter. The hypotheses are that (1) the amended zone facilitates the precipitates to form solids in the amended zone which then leads to limited SO_4 and Fe (total) in the liquid phase to be transported into the non-amended zone, and (2) "armor" (solid precipitates that attach to the surface of pyrite) is generated which prevents the oxygen and/or water going into the non-amended zone from the amended zone to react with the pyrite particles. Investigations into these hypotheses need more research in the future.

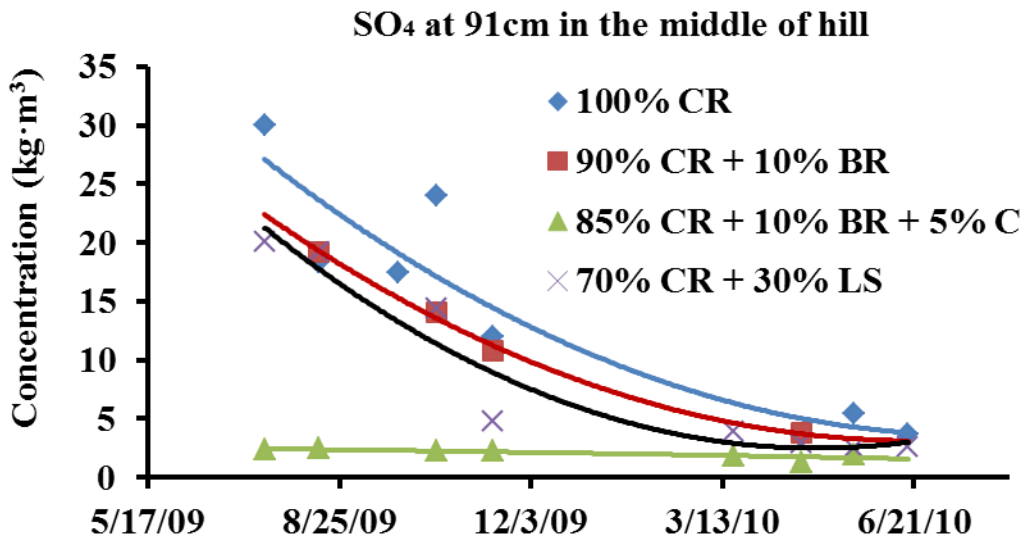

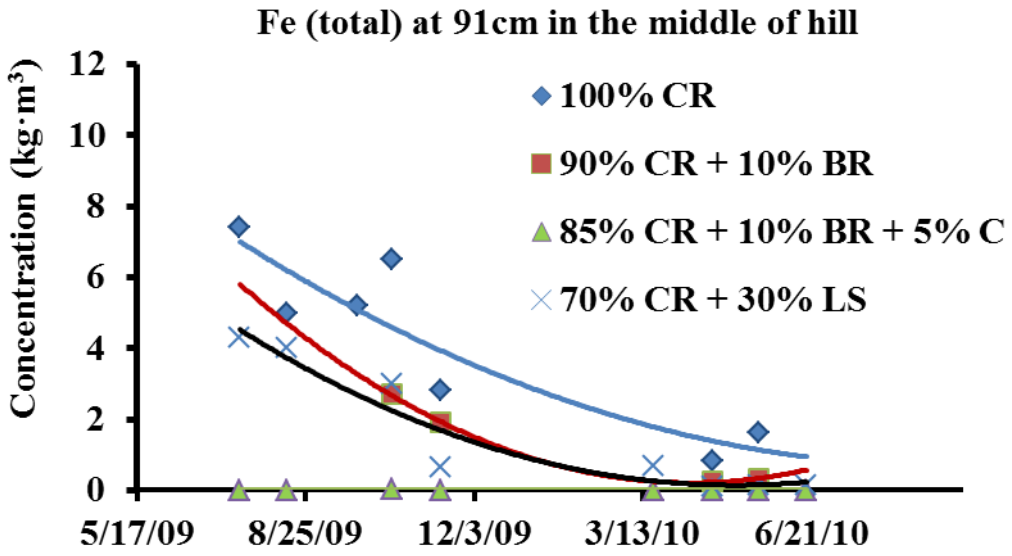

Figure 2.7 Measurements of the concentrations of SO_4 and Fe (total) at 91 cm at the middle of hill for each plot. C is mushroom compost and LS is limestone.

2.5.2 Sensitivity analysis of the thickness of amended zone

As we know, it is not feasible to mix the entire CR pile with bauxite residues to reduce the pyrite oxidation. Thus, we are interested in exploring impacts of the thickness of the amended zone on the pyrite oxidation process in the underlying non-amended zone. Five scenarios are designed with different amended zone thicknesses. They are: (1) 0 m, (2) 0.2 m, i.e. layer 0; (3) 0.4 m, i.e. layer 0 and layer 1; (4) 0.82 m, i.e. layer 0, layer 1 and layer 2; and (5) 2.32 m, i.e. layer 0, layer 1, layer 2 and layer 3. Layers 4 and 5 are always non-amended zone. The thickness of each layer is kept as the same as the values in the model calibration in section 2.4. The root depth is the depth of the amended thickness. Figure 2.8 shows the schematic of these five scenarios. The analysis of this design only focuses the remediation similar to plot 2, i.e. 10% BR + 90% CR. Most of the parameters are kept the same as the values in the model calibration. There is only a

slight change for pH values since there is no interface zone in this design. But the pH values in the amended zone and the non-amended zone are still defined the same values as the model calibration, which is 7.0 for the amended zone and 2.6 for the non-amended zone, respectively.

Figure 2.9 shows the concentrations of SO_4 and total Fe (i.e. Fe(II)+Fe(III)) within the six soil layers in plot 2 from 06/01/2009 to 06/27/2010. The left column of Figure shows the concentrations of SO_4 in each soil layer and the right column shows the concentrations of total Fe in each soil layer.

In layer 0, i.e. surface layer, it belongs to non-amended zone in Scenario 0 and pH is set to be 2.6, while the other four scenarios are designed to have BR mixed with CR and the values of pH are set to be 7.0 in the model. The concentrations of SO_4 and total Fe in Scenarios 1~4 are much lower than Scenario 0 as SO_4 and Fe(III) may precipitate into solid in the other scenarios. Also less concentration would be infiltrated into the deeper layer.

In layer 1, there is no remedial material in Scenarios 0 and 1, therefore, the simulation of SO_4 and total Fe in this layer are much higher than the other three scenarios. The concentration in Scenario 0 is higher than Scenario 1 since one-layer amended zone helps in reducing the concentrations in Scenario 1. The concentrations in Scenarios 2, 3 and 4 are close to each other.

However, the concentrations of SO_4 and total Fe in Scenario 2 are different from Scenario 1 in layer 2 although there is no remedial material in this layer for these two scenarios. The Mann-Whitney U-Test shows they are statistically different from each other and the RMSEs between Scenario 1 and Scenario 2 is 2.43 kg/m^3 for SO_4 and 0.82 kg/m^3 for total Fe. Such results suggest that the concentrations in the non-amended zone are relevant to the depths of the amended zone above it, even though the amended zone is as shallow as 40 cm. The concentrations in Scenario 3 and 4 are very low in layer 2 as they are within the amended zones.

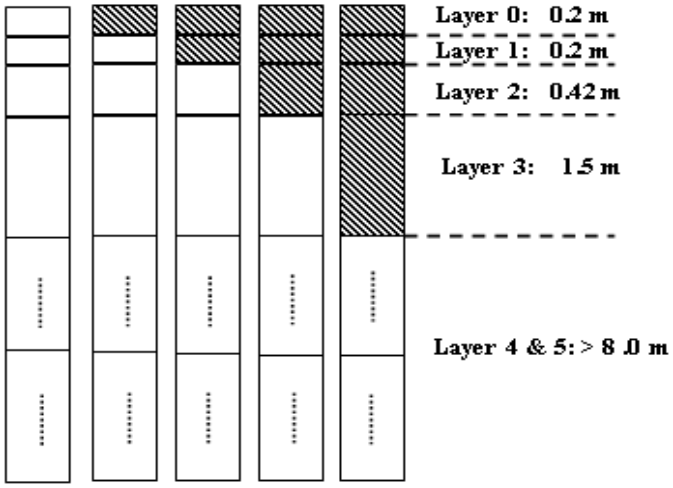

Figure 2.8 Design of five scenarios (from left to right) including no amended i.e. Scenario 0 and the other four of different amended scenarios; Scenario 1 amended zone: Layer 0 = 0.2 m; Scenario 2 amended zone: Layer 0 + Layer 1 = 0.4 m; Scenario 3 amended zone: Layer 0 + Layer 1 + Layer 2 = 0.82 m, Scenario 4 amended zone: Layer 0 + Layer 1 + Layer 2 + Layer 3 = 2.32 m. Notes: Layer 4 + Layer 5 > 8.0 m. The blank areas are coal refuse.

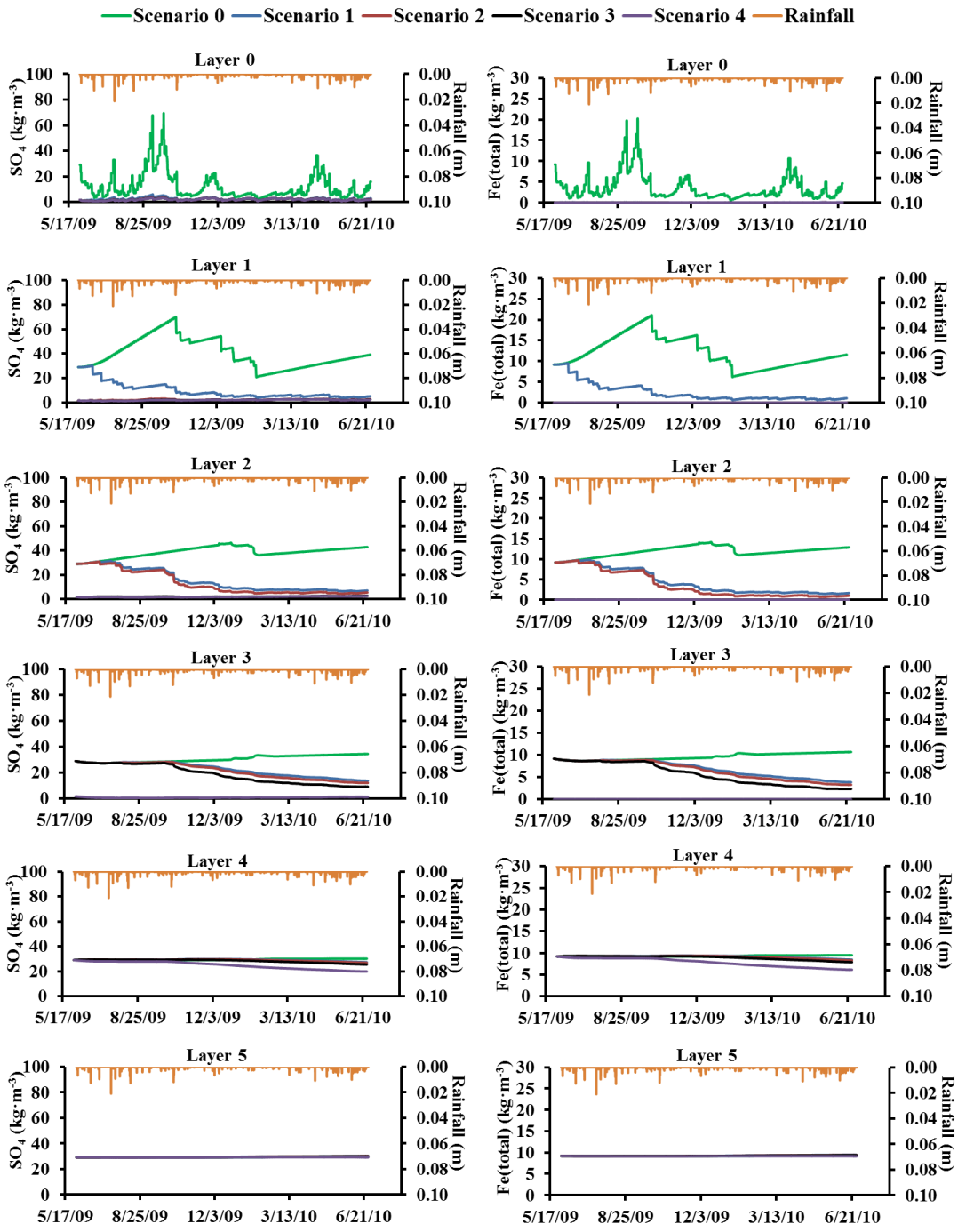

Figure 2.9 The simulation of the concentrations of SO_4 (left column) and total Fe (right column) for the four scenarios in the plot 2 i.e. 90% CR + 10% BR.

When the amended zone is 82 cm deep, there is a more significant decrease for the concentrations of $SO_4$and Fe (total) in the non-amended zone right beneath 82 cm than the shallow amended zone. That is not only because the Mann-Whitney U-Test indicates that the concentrations in Scenario 3 for layer 3 are statistically different from those for Scenarios 0, 1 and 2 in layer 3, but also the analysis of RMSEs among Scenarios 0~3 also proves that concentration in Scenarios 3 is more different from Scenarios 1 and 2 in layer 3. For example the concentrations of SO_4 in layer 3, the RMSE between Scenario 3 and Scenario 0 is 15.33 kg/m^3, the RMSE between Scenario 3 and Scenario 1 is 4.44 kg/m^3 and the RMSE between Scenario 3 and Scenario 2 is 3.15 kg/m^3; for the concentrations of Fe (total) in layer 3, the RMSE between Scenario 3 and Scenario 0 is 5.07 kg/m^3, the RMSE between Scenario 3 and Scenario 1 is 1.45 kg/m^3 and the RMSE between Scenario 3 and Scenario 2 is 1.01 kg/m^3. However, the concentrations of Scenario 1 and Scenario 2 are not much different since the RMSE between these two scenarios in layer 3 are 1.35 kg/m^3 and 0.46 kg/m^3 for SO_4 and Fe (total) respectively. Similar patterns are shown in Figure 2.9 for the concentrations in layer 4 among the four scenarios. That is, the concentrations in layer 4 for Scenario 4 are statistically lower than those for Scenarios 0, 1, 2, and 3. These model sensitivity results indicate that when the amended zone is thicker, the decrease of SO_4 and Fe (total) right below the amended zone is more significant than the effect of shallow amended zone. Such an initial sensitivity analysis provides a basis to further investigate the role of the amended depth and the reasons behind. It also provides a basis to seek for a potential appropriate amended depth.

The reason that the thicker amended zone leads SO_4 and Fe (total) decreased more in the non-amended zone is perhaps due to more SO_4, Fe (II) and Fe(III) being precipitated into solid in the thicker amended zone above so that the liquid transported to the deeper soil layer through

leach has a lower concentration level. Thus, Scenario 4 appears to be relatively more active in reducing the concentrations in the non-amended zone than Scenario 3 which is more effective than Scenarios 2 and 3. Regarding to the bottom layer i.e. layer 5, the concentrations of SO_4 and Fe (total) for the four scenarios are very close to each other in the short-term period e.g. one year. However, the effects of remediation on the deep layers may be shown in the long-term period, which is discussed in Chapter 4.0 .

Additionally, the variation of the amended zone thickness affects both the oxygen concentration and the soil moisture in the non-amended zone. Oxygen may be consumed more in the scenarios with thicker amended zones than the scenarios with thinner amended zones. Thus, less air oxygen may diffuse into the non-amended zone and the chance of pyrite oxidation would be reduced. Meanwhile, water has both positive and negative effects on the chemical fate and transport. On one hand, water is a basic condition for pyrite oxidation and it increases SO_4 and Fe (total) in the soil water (i.e., increasing chemical concentrations). On the other hand, water helps to dilute the concentrations of SO_4 and Fe (total) in the soil water. If "armor" is generated in the amended zone, limited oxygen and water would be allowed into the non-amended zone. However, the influence of "armor" is not included in this research yet.

2.6 CONCLUSIONS

A new hydro-geochemical model that incorporates the hydrologic processes and the kinetic process of pyrite oxidation is developed. This new model can be used to describe the behavior of the coal refuse in terms of its characteristics of soil moisture, SO_4 and Fe (total). The high-resolution model simulation, based on the framework of the DHSVM v3.0, makes it possible to

compare the observations of chemical concentration data and the soil moisture data with model simulated results at approximately the same locations in the piles. Due to field measurement restrictions, the model results can be compared at one representing point in each plot, although the model can simulate the entire four plots. Our model simulated results from all four plots show reasonably patterns for soil moisture and chemical concentrations and they compare well with the available observations. The new model is evaluated using field measurements.

The main findings of this study include: (1) comparing with plot 1, the combined mixtures in the remediated plots help to significantly reduce the concentrations of SO_4 and Fe (total) in the amended zone, especially for Fe (total); (2) the concentrations in the non-amended zone are relevant to the depths of the amended zone above it even though it is shallow (e.g., less than 40 cm); (3) the thicker amended zone decreases more concentrations of SO_4 and Fe (total) right below the depth of this amended zone than the impact of thinner amended zone at the same depth; and (4) the variation of the amended zone thickness affects both the oxygen concentration and the soil moisture in the non-amended zone. Oxygen may be consumed more by oxidation in the scenarios with thicker amended zones than the scenarios with thinner amended zones, which leads to less air oxygen being diffused into the non-amended zone and thus reduces the pyrite oxidation process. The advantages of the remediated plots prove to be beneficial when dealing with AMD issues in the coal-refuse region.

Overall, the beneficial use of two waste products presents a unique and effective approach for the remediation of the AMD legacy problem. Although the current state of the hydro-geochemical model has been successfully used to assess this remediation approach, it is not adequate to simulate all the situations to be encountered without the assumptions made in the chapter. Currently it paves the ways for developing a more sophisticated model. More

comprehensive modules are encouraged to be developed and integrated into this model. These more comprehensive modules should include the consideration of thermal transport and the calculation of a dynamic pH involving with more chemicals and reactions. With these additional recommended modules, future research can provide a more insightful view for the sustainable environment in regions with coal refuse.

3.0 DEVELOPMENT AND APPLICATION OF THERMAL TRANSPORT

3.1 INTRODUCTION

Oxidation of pyrite is widely recognized as one of the main causes for acid mine drainage in acidic coal-refuse piles as it is an exothermic reaction. The oxidation of pyrite's composition accelerates with increasing temperature [*Kawakami et al.,* 1988]. The laboratory experiment conducted by *Schoonon et al.* [2000] also showed that pyrite oxidation is highly temperature-dependent but it is difficult to describe this relation by a general equation. A lot of heat from pyrite oxidation in coal-refuse (CR) results in the rise of surrounding temperature and feeds back to increase the rate of oxidation by itself. So investigating soil temperature is a significant issue in CR areas. Coal oxidation also generates significant amount of heat that raises the temperature to over 40 ℃ [*Beamish et al.*, 2000], but it is not considered in this study.

If oxidation is suspended during the remediation of a CR region, then the heat and the soil temperature may be reduced. The extent of decrease is determined by the remediation approach. There are several factors that influence the soil temperature during the process of remediation especially the vegetative tier. This is due to vegetation being an insulator, preventing heating soil [*Coulson et al.*, 1993] and also reducing the loss of heat from soil in cold weather [*Zhang et al.,* 2002]. How much soil temperature is affected and what depth of soil layer is influenced by vegetation is not known. It is difficult to conduct these scenarios in the fields.

Therefore, computer simulation of heat generation is a practical solution to mimic or predict the results of different cases in the field. One of the most popular concepts of subsurface soil temperature modeling is using Fourier's Law and the energy conservation equation to solve the soil temperature for each layer. For example, *Cherkauer and Lettenmaier* [1999] applied this idea to investigate the frozen soil in a variable infiltration capacity model i.e. VIC model, which is a land surface hydrological model developed by *Liang et al.* [1994]. The concept was also used in HYDRUS [*Šimůnek et al.*, 1998] to simulate the heat transport in a one dimensional soil column. The similar application was extended to HYDRUS-2D and HYDRUS-3D [*Šimůnek et al.*, 1999]. It is almost the same in a geochemical model (i.e. PHREEQC) and heat transport was taken into account within each cell [*Parkhurst and Appelo*, 1999]. Most of the hydrological models or geochemical models emphasize heat transport under circumstances without the heat from chemical and biological processes, which should not be ignored in the coal mining region. This is because the soil temperature is not only influenced by the natural heat from solar radiation but also affected by chemical reactions and may be even more by biological processes [*Nicholson et al.*, 1988]. For instance, Acidothiobacillus ferrooxidans may enhance the rate of pyrite oxidation by five more orders of magnitude than the rate of abiotic oxidation [*Nordstrom*, 1982]. Currently, there are a limited number of models to describe all the sources of heat from natural radiation, chemical oxidation and biological process. *Jansson and Karlberg* [2004] developed a one dimensional model (i.e. Coupmodel) that incorporated heat and water transport in soil-vegetation system and *Hollesen et al.* [2011] improved the model by adding the temperature-dependent heat, which used two equations to represent the chemical and biological oxidations, respectively. They were successfully applied in Svalbard (78 ℃N). However, it is not adequate to consider the hydro-geochemical interaction between cells.

In order to address the above problems and include the characteristics of hydrology, chemistry and biology to simulate the soil temperature, this research couples the temperature-dependent heat module [*Hollesen et al.*, 2011] into HGCM model [*Xu et al.*, 2013a] and the model becomes a hydro-thermal-geochemical model (HTGCM v1.0) [*Xu and Liang*, 2013]. The new model reflects the heat sources of natural radiation, chemical process of pyrite oxidation and biological process of pyrite oxidation. The field measurement is combined with the simulation of soil temperature to calibrate and validate the model and the sensitivity analysis of parameters is discussed for the new model. The research is further extended to a more sophisticated model for the hydro-thermal-geochemical modeling involved with dynamic pH values in the next stage.

3.2 THERMAL TRANSPORT DEVELOPMENT

The model in this chapter is a hydro-thermal-geochemical model, which is developed from HGCM. HGCM is a model that solves the problems of runoff, evapotranspiration, surface flow, subsurface flow, flow routing and pyrite oxidation. Given that it has a basic heat module to calculate the surface temperature, the consideration of energy resources is limited to the natural radiation. An advanced module of thermal transport is added into HGCM connecting soil temperature with the temperature-dependent parameters.

Section 3.2.1 mainly describes the algorithm of heat module and section 3.2.2 shows the connection with the work in the last chapter. Additionally, in section 3.2.3, the statistical methods are mentioned for the calibration and the discussion of data analysis.

3.2.1 Algorithm of heat module

HTGCM v1.0 not only considers the impact of the natural heat flux on the soil temperature, but also, the heat from biological activity and chemical activity. This is accomplished by 1) using the concept of energy conservation to calculate the soil temperature following the approach of *Cherkauer and Lettenmaier* [1999], 2) coupling two existing equations to represent the heat from chemical& biological activities into the energy conservation equation. It may be a good approximation to reflect the heat generation in CR regions where solar radiation and pyrite oxidation are two of the main sources of heat generation.

Firstly, this heat module is based on the Fourier's Law Eq. (3-1) and energy conservation equation Eq. (3-2):

$$q_h = -k_h \frac{\partial T}{\partial z} \tag{3-1}$$

$$C_s \frac{\partial T}{\partial t} = \frac{\partial}{\partial z}\left(-q_h\right) + \rho_i L_f \left(\frac{\partial \theta_i}{\partial t}\right) \tag{3-2}$$

where q_h is the heat flux [MT^{-3}], k_h represents the soil thermal conductivity [$MLT^{-3}K^{-1}$], C_s represents the soil volumetric heat capacity [$ML^{-1}T^{-2}K^{-1}$], T denotes the soil temperature [K], z is the soil depth [L], ρ_i denotes the density of ice [ML^{-3}], L_f is the latent heat of fusion [L^2T^{-2}], θ_i represents the ice content in the soil layer [$L^3 L^{-3}$] , t denotes time [T]. It is similar with the formulas of *Cherkauer and Lettenmaier* [1999].

Inserting Eq. (3-1) into Eq. (3-2) and adding chemical heat $H_{chemical}$ [$ML^{-1}T^{-3}$] and biological heat $H_{biological}$ [$ML^{-1}T^{-3}$] as source terms, we obtain Eq. (3-3):

$$C_s \frac{\partial T}{\partial t} = \frac{\partial}{\partial z}\left(k_h \frac{\partial T}{\partial z}\right) + \rho_i L_f \left(\frac{\partial \theta_i}{\partial t}\right) + (H_{chemical} + H_{biological}) \tag{3-3}$$

Following the work of *Hollesen et al.* [2011], the heat from chemical process of pyrite oxidation can be expressed as Eq. (3-4)

$$H_{chemical} = heatpro\_A \times e^{(heatpro\_B \times T)} \tag{3-4}$$

where *heatpro_A* and *heatpro_B* are coefficients of heat from chemical oxidation. The O'Neill function [*Stange*, 2007] is used to calculate the heat from biological activity of pyrite oxidation.

$$H_{Biological} = heatpro\_A_2 \cdot \left(\left(\frac{T_{\max} - T}{T_{\max} - T_{opt}}\right)^n \times e^{n \times ((T - T_{opt})/(T_{\max} - T_{opt}))}\right) \tag{3-5}$$

where T_{opt} [K] is the optimum temperature when the rate of biological oxidation reaches its maximum value, T_{max} [K] is the maximum temperature when biological activity ceases, *heatpro_A*$_2$ is the rate of biological heat-production and *n* is the parameter of the O'Neill function; T_{opt} is 25.23 ℃ [*Stange*, 2007], T_{max} is assumed to be 55 ℃ and *n* is 10.73.

Due to the decay of pyrite oxidation [*Elberling et al.*, 1994], the heat decrease can be represented by an exponential function based on the work of *Hollesen et al.* [2011]:

$$H_{Chem\_or\_Bio} = H_{Chem\_or\_Bio} \cdot \exp(-decay\_chem\_or\_bio \times number\_of\_timesteps) \tag{3-6}$$

where *decay_chem_or_bio* is the half-life of chemical or biological activity, $H_{chem\_or\_bio}$ is the heat production at that time step.

3.2.2 Relation between soil temperature and reactive transport

The above heat module can update the soil temperature according to the amount of heat generated from natural radiation, chemical reactions and biological activity. At the same time, the rate of pyrite oxidation, other minerals reactive rates and diffusion coefficients are also dependent upon the changes in soil temperature. Increasing the soil temperature may cause a more acidic environment.

The Arrhenius equation [*Stumm and Morgan*, 1981] was introduced into HYDRUS to represent the effects of absolute temperature on transport coefficients. A more general version i.e. Eq. (3-7) was proposed by *Šimůnek and Suarez* [1993]. In this research, the other minerals reactions are not included, but the temperature dependence of the rate of pyrite oxidation and chemical diffusion are considered.

$$C_T = C_r \exp\left(\frac{E_a\left(T^A - T_r^A\right)}{R_u T^A T_r^A}\right) \tag{3-7}$$

Where C_T and C_r are the transport coefficients at an absolute temperature T^A and the reference temperature T_r^A, respectively; E_a [$ML^2T^{-2}M^{-1}$] is the activation energy of the particular reaction and R_u is the universal gas constant. In this research, the reference temperature is 25℃. The equation here is used for the diffusion coefficients of O_2, Fe(Ⅱ), Fe(Ⅲ) and SO_4 in liquid phase. Also the equilibrium constant of iron shown in Eq. (2-11) that is one of the factors influencing the pyrite oxidation is dependent on the temperature controlled by Eq. (3-7).

3.2.3 Statistical methods for data analysis

In this chapter, not only RMSE, absolute error and the absolute relative error will be discussed between the observation and simulation, but also the correlation coefficient will be shown between soil temperature and the weather information data. The equation is written as follows:

$$r_{xy} = \frac{\sum_{i=1}^{n}\left(x_i - \bar{x}\right)\left(y_i - \bar{y}\right)}{\sqrt{\sum_{i=1}^{n}\left(x_i - \bar{x}\right)^2 \sum_{i=1}^{n}\left(y_i - \bar{y}\right)^2}} \tag{3-8}$$

where x is soil temperature, $\bar{x}$ is the mean of soil temperature; y can be any other factors, $\bar{y}$ is the mean of y. r_{xy} is the correlation coefficient.

3.3 STUDY SITE AND FIELD DATA

3.3.1 Study site

The study site is one of the three remediated plots in Chapter 2.0 (there were four experimental plots including a non-remediated plot and three remediated plots in Figure 3.1a. The second plot (yellow) i.e. 90% CR + 10% bauxite residue (BR) within the top 61 cm is the plot discussed in this chapter since BR is the material we are interested in this research to treat CR. This second plot has vegetative tier on the surface as shown in Figure 3.1b. The 61 cm neutralized zone is given by Figure 3.1c and the roots of plants fill the entire amended zone. Below 61 cm depth, it is CR. The measured point is represented by the green star in Figure 3.1a. The observed soil temperature at the depth of 61 cm was taken by the temperature sensors at this point.

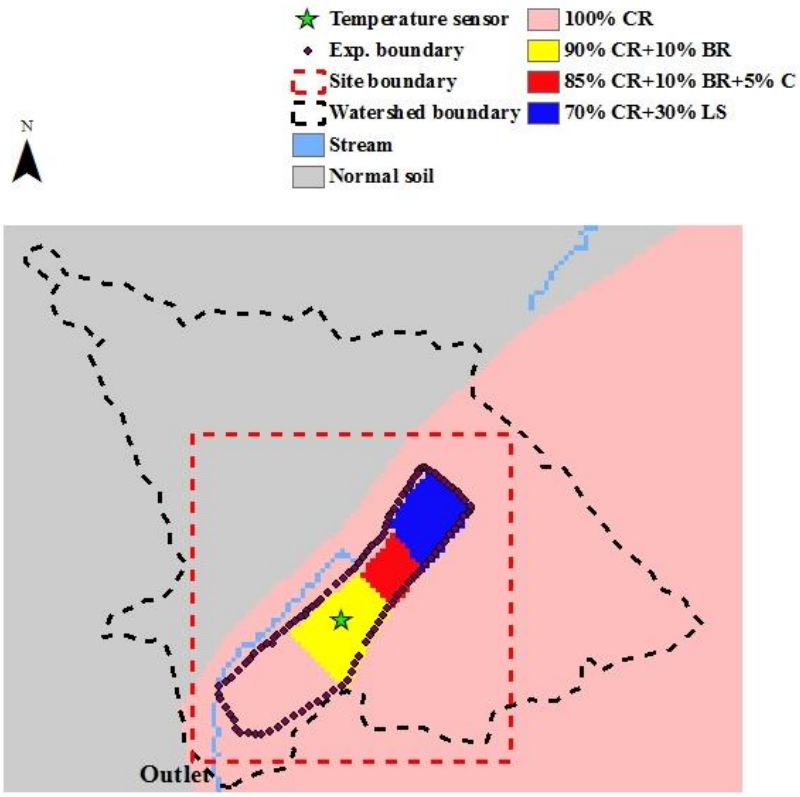

(a)

(b)

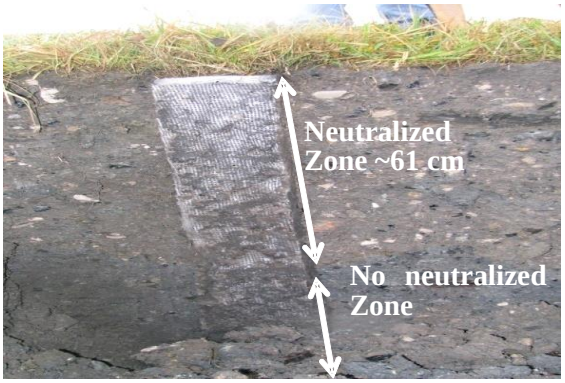

(c)

Figure 3.1 Studied plot at Mather, PA: (a) the boundary of study area and the measurement point for soil temperature, (b) the view of vegetation in plot 2, (c) the profile of neutralized zone (photo was provided by Alcoa) and none neutralized zone.

3.3.2 Field data analysis

This chapter uses the observed soil moisture and soil temperature to calibrate and validate the model in section 3.4. The weather information and the field data start from 5/4/2012 to 10/4/2012 that is from spring to autumn in this study area.

Figure 3.2 shows the weather information of air temperature, wind speed, humidity, rainfall, and solar radiation. Air temperature in Figure 3.2a increased from June and reached the highest point in July, then declined in fall. Wind speed was faster in fall except for a spike in June shown in Figure 3.2b. Figure 3.2d rainfall indicated significantly seasonal trends since June, July and August appeared wetter than May and October. The changes in humidity and short wave radiation are shown in Figure 3.2c and Figure 3.2e.

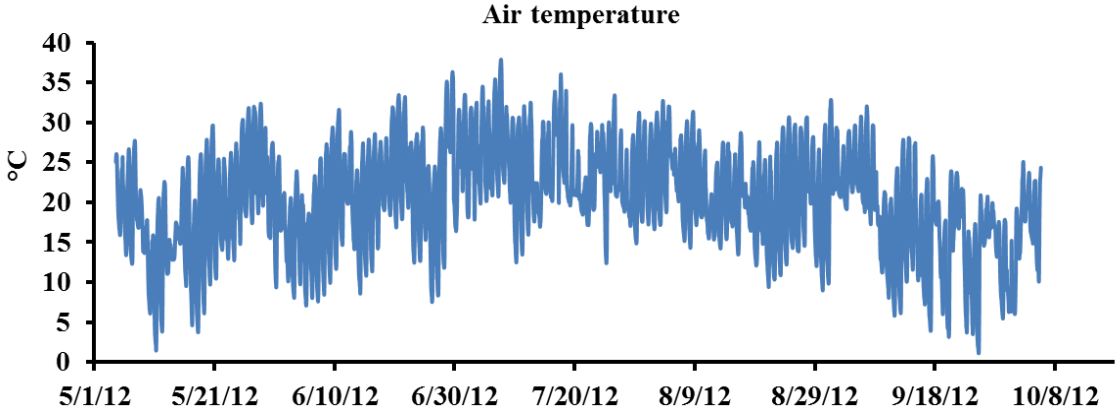

(a)

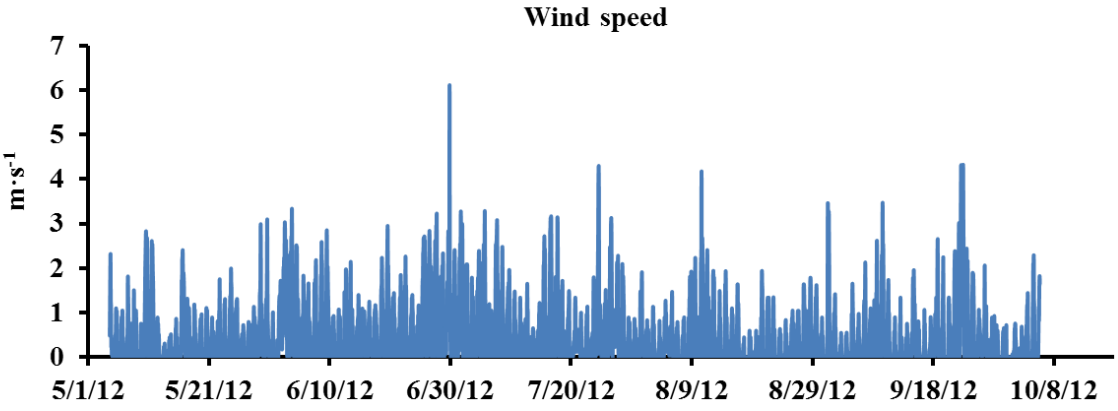
Wind speed
m·s-1
7
6
5
4
3
2
1
0
5/1/12
5/21/12
6/10/12
6/30/12
7/20/12
8/9/12
8/29/12
9/18/12
10/8/12

(b)

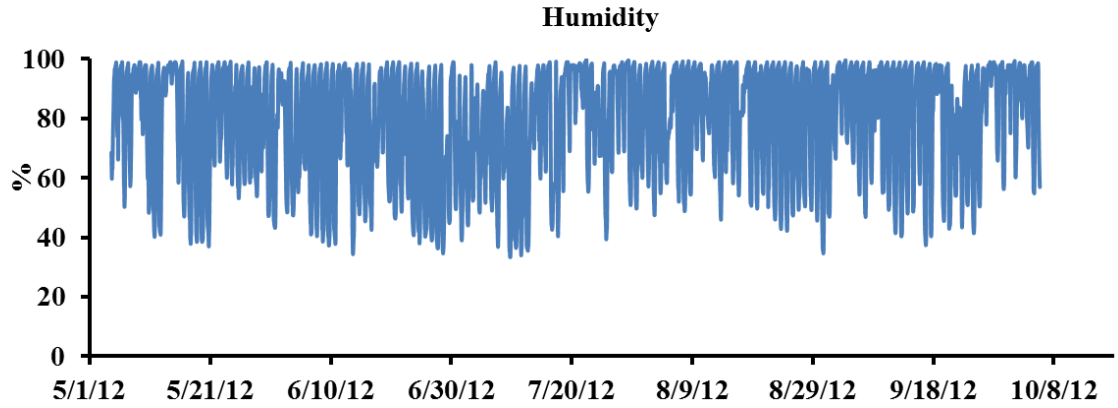
Humidity
%
100
80
60
40
20
0
5/1/12
5/21/12
6/10/12
6/30/12
7/20/12
8/9/12
8/29/12
9/18/12
10/8/12

(c)

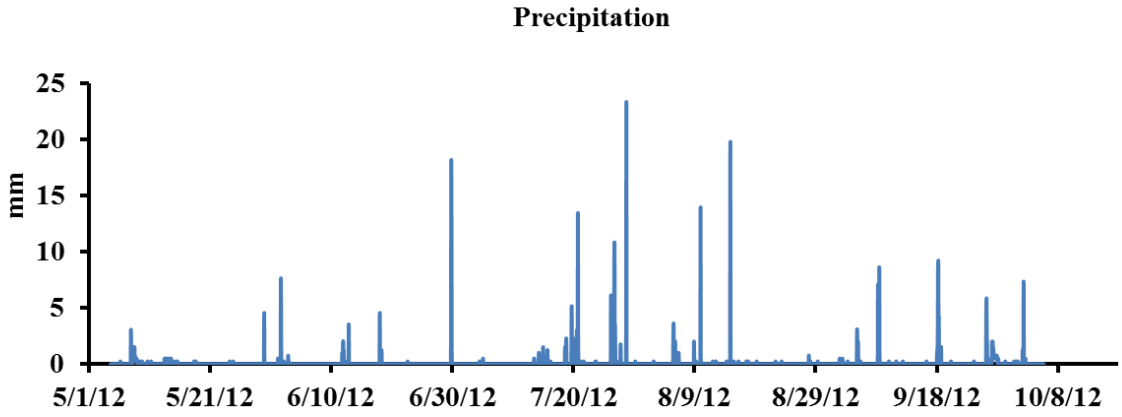
Precipitation
mm
25
20
15
10
5
0
5/1/12
5/21/12
6/10/12
6/30/12
7/20/12
8/9/12
8/29/12
9/18/12
10/8/12

(d)

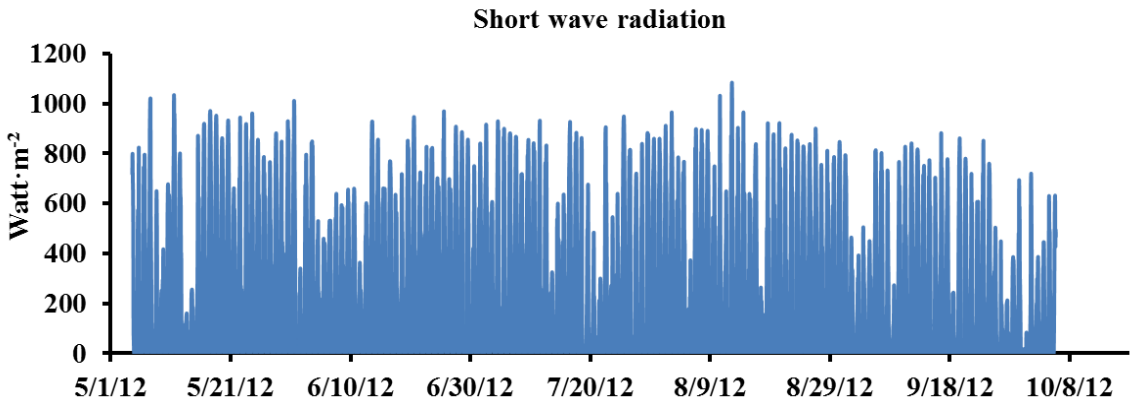

(e)

Figure 3.2 Weather information: (a) air temperature, (b) wind speed, (c) humidity, (d) precipitation, (e) short wave radiation.

Table 3.1 Correlation coefficients between the soil temperature and the other information including air temperature, wind speed, relative humidity, precipitation, shortwave radiation and soil moisture. Air T is air temperature; T61 is soil temperature at 61 cm.

	Air T	Wind speed	Humidity	Shortwave radiation	Precipitation	Moist
T61	0.329	0.034	-0.010	0.014	0.031	0.088

Here, the correlation coefficient is calculated to show the relationship between the field measurement of soil temperature and the other information in Table 3.1. The most related factor is air temperature followed by soil moisture, wind speed and rainfall, while humidity and shortwave radiation are less related. Among these impact factors, soil moisture is especially

important for soil temperature at the regional scale as air temperature is a climate factor at the large scale. Thus, the simulation of soil moisture is important for modeling soil temperature.

3.4 MODEL TEST

The model in this chapter has the features of hydrology, geochemistry and thermal transport. The final purpose of model calibration is to minimize the errors for soil temperature. But it is necessary to calibrate soil moisture before soil temperature as has been discussed in section 3.3.2. The cell size is 3×3 meters. And the 5TM sensor (moisture-temperature sensor, Decagon Devices, Inc.) was installed at the middle location of the slope shown in Figure 3.1a. The accuracy of observed soil moisture is ± 0.03 m^3/m^3 and the accuracy of observed soil temperature is ± 1 ℃.

The calibrated parameters are divided into: soil parameters, vegetation parameters and heat parameters. The specific parameters of each group are described subsequently. Then the calibration result was directly applied into the validation. As it mentioned in section 3.3 that the total length of time period was five months, the first three months (i.e. from 5/4/2012 to 8/8/2012) were used for the calibration and the other two months (i.e. from 8/8/2012 to 10/04/2012) for the validation. The model is running within the site boundary i.e. the red dashed line in Figure 3.1a and actually the results of Chapter 2.0 were also conducted in this area.

3.4.1 Model calibration

The soil parameters, vegetation parameters and heat parameters are discussed respectively in this section. These parameters are set according to the laboratory/field measurements, default database in DHSVM v3.0 and calibration results (the calibrated parameters are marked ** in Table 3.2, Table 3.3 and Table 3.4).

Table 3.2 Soil parameters in HTGCM v1.0.

Soil parameter	Value
Lateral conductivity (m s^{-1})	1.0e-6
Exponential decrease	2.0
Maximum infiltration (m s^{-1})	5.0e-4
Capillary drive	0.41
Surface albedo	0.2
Porosity	0.46
Pore size distribution	0.3
Bubbling pressure	0.14
Field capacity	0.2 **
Wilting point	0.16 **
Bulk density (kg m^{-3})	1360
Surface vertical conductivity (m s^{-1})	0.0003 **
Manning's coefficient	0.4 **

Table 3.3 Vegetation parameters in HTGCM v1.0.

Vegetation parameter	Value
Overstory present	FALSE
Understory present	TRUE
Maximum resistance (s m^{-1})	800
Minimum resistance (s m^{-1})	700 **
Moisture threshold	0.33 **
Vapor pressure deficit	4000
Fraction of shortwave radiation	10
Layer thickness (m)	0.2 0.2 0.42 1.5 4.0 **
Overstory root fraction	0.00 0.00 0.00 0.00 0.00
Understory root fraction	0.30 0.50 0.20 0.00 0.00
Overstory monthly LAI	1.0 1.0 1.0 2.0 3.0 3.0 3.0 3.0 1.0 1.0 1.0 1.0
Understory monthly LAI	1.0 1.0 1.0 2.0 5.0 5.0 5.0 5.0 1.0 1.0 1.0 1.0
Overstory monthly albedo	0.2 0.2 0.2 0.2 0.2 0.2 0.2 0.2 0.2 0.2 0.2 0.2
Understory monthly albedo	0.2 0.2 0.2 0.2 0.2 0.2 0.2 0.2 0.2 0.2 0.2 0.2

Table 3.4 Heat parameters in HTGCM v1.0.

Heat parameter	Value
Thermal conductivity (W m^{-1} K)	4.0 **
Thermal capacity (J m^{-3} K)	3.0e6 **
heatpro_A (J m^{-3} day^{-1})	24.0 **
heatpro_B	0.008 **
heatpro_A_2 (J m^{-3} day^{-1})	48.0 **
decay_chem	0.00006 0.00004 0.00001 0.000005 0.000001 0.000001 **
decay_bio	0.00006 0.00004 0.00001 0.000005 0.000001 0.000001 **
T_{opt} (℃)	25.23
T_{max} (℃)	55
n	1.1 **

First of all, the soil parameters are dependent on soil texture, including: lateral hydraulic conductivity, exponential decrease of lateral conductivity with soil depth, maximum infiltration, capillary drive, surface albedo, porosity, pore size distribution, bubbling pressure, field capacity, wilting point, bulk density, vertical hydraulic conductivity and Manning's coefficient (Table 3.2). Some of these parameters such as porosity, pore size distribution, bulk density, lateral hydraulic conductivity and vertical hydraulic conductivity were measured in the laboratory. However, the laboratory data may not be the same as the field value. So the slightly adjustment within a reasonable range is made for a few of them based on the experience and the multiple

measurements. For example, the vertical hydraulic conductivity on the ground surface is obtained based the magnitude in the laboratory. The calibration result of hydraulic conductivity is 0.0003 m/s and this value has been used for the entire thesis. The other calibrated parameters are field capacity, wilting point and Manning's coefficient. There are some other soil parameters are from the default database in DHSVM v3.0 for instance: exponential decrease, bubbling pressure, capillary drive and surface albedo.

The plants present in plot 2 are: alfalfa, white clover, red clover and tall fescue. The vegetation parameters representing the characteristics of these plants are listed in Table 3.3. These parameters include overstory present, understory present, maximum stomatal resistance, minimum stomatal resistance, moisture threshold, vapor pressure deficit, fraction of shortwave radiation, layer thickness, overstory root fraction, understory root fraction, overstory monthly LAI, understory monthly LAI, overstory monthly albedo and understory monthly albedo. Most of them are from the default database of DHSVM v3.0 except that minimum stomatal resistance, soil layer thickness and moisture threshold are slightly calibrated in Table 3.3.

As soil temperature is related to soil moisture, soil temperature is indirectly influenced by soil parameters and vegetation parameters. However, soil temperature may be dominated by the heat parameters more directly. These parameters are including: thermal conductivity, thermal capacity, *heatpro_A, heatpro_B, heatpro_A*$_2$*, decay_chem, decay_bio,* T_{opt}, T_{max} and n in Table 3.4. The first two parameters already exist in DHSVM v3.0 and the others are described in the algorithm of heat module (section 3.2.1). Thermal conductivity was calibrated within the range of 0.3 ~ 7.7 Wm^{-1} K [*Gier é and Stille,* 2004] and it was calibrated to be 4.0 W m^{-1} K. Thermal capacity 3.0e6 J m^{-3} K was calibrated within the range of 1.8 e6 ~ 4.18e6 J m^{-3} K [*Gier é and*

Stille, 2004]. The decaying parameters i.e. *decay_chem* and *decay_bio* were calibrated for 50 years. Regarding *heatpro_A*, *heatpro_B*, *heatpro_*A_2 and *n* were also obtained by the calibration.

According to the above classification of parameters, there are sixteen parameters needed to be calibrated. It is very tough to fulfill the task of the parallel calibrations for soil moisture and soil temperature at the same time. Some combination of parameters may not be reasonable for physical meanings although the observation and the simulation may match very well. In order to avoid this situation, the calibration process is divided into two steps: 1) moisture calibration and 2) soil temperature calibration. In the first step, keep the heat parameters to be constant and calibrate the soil and vegetation parameters in order to fit the simulated soil moisture to the observed soil moisture. The precondition is that the soil moisture is not sensitive to the heat parameters, which will be proved in section 3.5.1. In the second stage, keep the soil and vegetation parameters from the first step and adjust the heat parameters until the soil temperature is good enough with the observation.

Figure 3.3a and b give the calibration result at 61 cm for soil moisture and soil temperature respectively from 5/4/2012 to 8/8/2012. For the moisture simulation, Figure 3.3a shows that the simulated moisture captured the patterns of the observation and responded well to the rainfall which is indicated by the green line. However, the peak measurement of moisture may be overestimated by the sensor and the simulation could not reflect it correctly. The reason may be that the sensor was surrounded by some hard rocks, or precipitating chemicals, so that the water could not drain out as easily as in the normal soil. Table 3.5 shows that the RMSE of soil moisture between observation and simulation is 0.02 and the absolute error between the mean of simulation and the mean of observation is 0.01. The relative error of the two mean values is 5.00%. The RMSE of soil temperature is 1.51 ℃. The relative error of soil temperature

is 5.22% and the absolute value of the mean of simulation and the mean of observation is 1.02 ℃. Figure 3.3b shows that the observed air temperature (dense blue dashed line) vibrated stronger than the observed soil temperature at 61 cm (purple dashed line). The simulation and observation at 61 cm are plotted by the red solid line and the purple dashed line in Figure 3.3b. Both of them followed the pattern of air temperature but had milder vibration. They were gradually going up from May to August as well as the soil moisture since the season transits from spring to summer.

Table 3.5 Statistics analysis of calibration results.

	RMSE	Sim. mean	Obs. mean	Abs. error	Relative error
Soil moisture (VWC)	0.02	0.19	0.20	0.01	5.00%
Soil temperature (℃)	1.51	20.56	19.54	1.02	5.22%

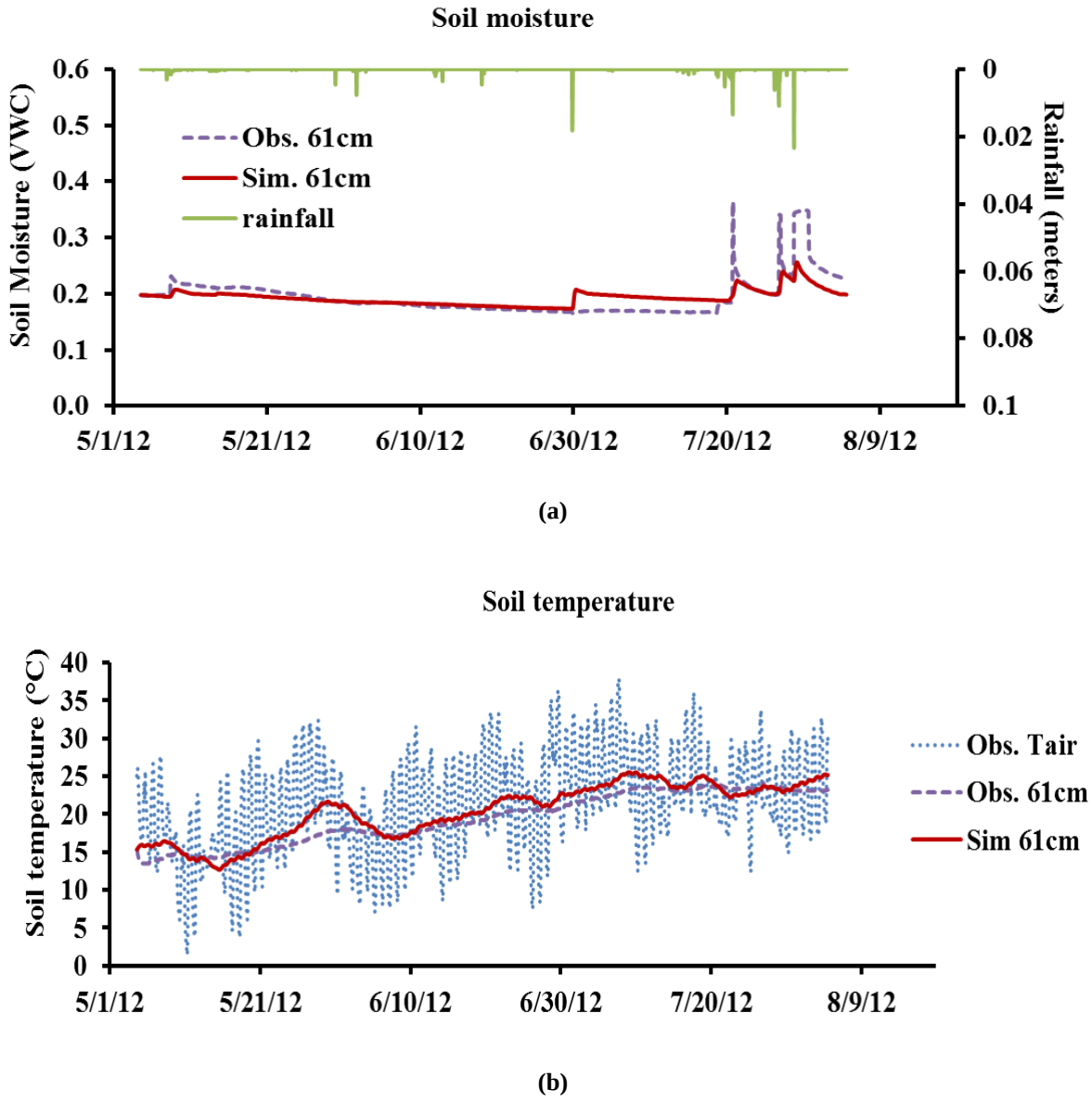

Figure 3.3 Calibration results of soil moisture and soil temperature at the time period of 05/04/2012 to 08/08/2012: (a) moisture comparison between observation and simulation at 61 cm, (b) soil temperature comparison between observation and simulation at 61 cm. The accuracy of observed soil moisture is ±0.03 m^3/m^3 and the accuracy of observed soil temperature is ±1 ℃.

3.4.2 Model validation

Figure 3.4a shows the results of soil moisture at 61 cm from 8/8/2012 to 10/04/2012. The validated moistures followed the same pattern as the observations and responded to the rainfall very well. The simulations still had the same issue that the peaks of moisture did not catch well with the observations due to the rock or chemical precipitates. In Table 3.6, the RMSE for the moisture simulation and the observation is 0.01. The absolute error between the simulated mean and the observed mean is 0.01 and the relative error is only 5.00%. Figure 3.4b shows that the observed air temperature changed more significantly than the soil temperature at 61 cm. The temperature trend was going down as the season was moving into fall. The comparison of soil temperature between simulation and observation at 61 cm is shown. All simulations captured the pattern of changing air temperature. The RMSE for the soil temperature in the validation period is 1.03℃, which is even lower than the calibration result. The absolute error between the simulated mean and the observed mean is 0.30℃ and the relative error is only 1.45%.

In general, the model performed very well in this area for modeling soil moisture and soil temperature. There is a supplementary in interpretation of the results. That is, all the simulations were calculated under a constant pH value, which may not be true in the field for a long time period. That is why it is necessary to incorporate a pH-dynamic environment module into the model as described in Chapter 4.0 .

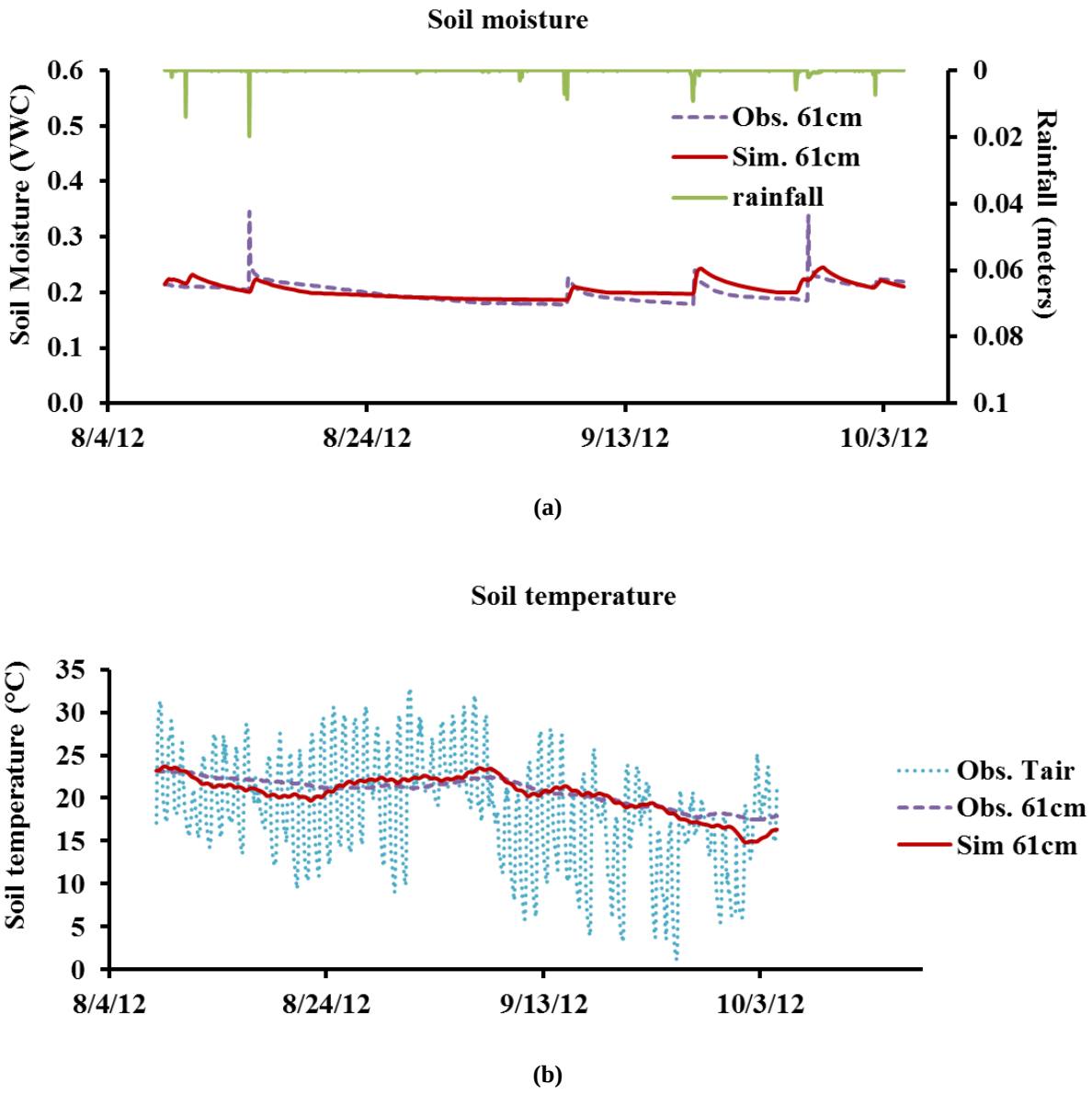

Figure 3.4 Validation results of soil moisture and soil temperature at the time period of 08/08/2012 to 10/04/2012, (a) moisture comparison between observation and simulation at 61 cm, (b) soil temperature comparison between observation and simulation at 61 cm.

Table 3.6 Statistics analysis of validation results.

	RMSE	Sim. mean	Obs. mean	Abs. error	Relative error
Soil moisture (VWC)	0.01	0.20	0.20	0.01	5.00%
Soil temperature (℃)	1.03	20.46	20.76	0.30	1.45%

3.5 DISCUSSION OF THERMAL TRANSPORT

Before further discussion about the model, it is necessary to prove the assumption in the first step of calibration that the soil moisture is not sensitive to the heat parameters so that soil and vegetation parameters obtained from this calibration approach are reliable. So firstly, the sensitivity analysis of heat parameters for soil moisture is shown. Then the sensitivity of heat parameters for soil temperature is also calculated. The soil parameters and the vegetation parameters are not described in this section as many documents about DHSVM have described about them. The comparison of the simulated soil temperature with and without modeling heat of the above two sources is discussed. Finally, results of the investigation of the impact of vegetation on soil temperature during the remediation are shown.

3.5.1 Sensitivity analysis of heat parameters

The impact of heat parameters for soil moisture and soil temperature is discussed in this section. The simulation time period is the same as model calibration in section 3.4.1. The sensitivity

analysis only aims at 61 cm within the third layer because the simulation results at this layer were calibrated by the field measurement. The changes of parameters are classified into five different ranges: -60%, -30%, 0%, 30% and 60%. For example, thermal conductivity is 4.0 W m^{-1} K in the calibration result, that is recognized as a benchmark for thermal conductivity i.e. 0% changes; -60% change denotes to subtract 60% values from the benchmark , that is 1.6 W m^{-1} K; 60% change means to plus 60% of benchmark value to itself, that will be 6.4 W m^{-1} K. The absolute value of relative error between the mean of observation and the mean of simulation is an important index in the sensitivity analysis for heat parameters. There are eight heat parameters calibrated in the model, therefore, the model has to run forty times with five different ranges of these heat parameters including the benchmark to obtain the sensitivity results.

Table 3.7 The absolute values of relative errors between the mean of observed soil moisture and the mean of simulated soil moisture.

Parameter/range	-60%	-30%	0%	30%	60%
Thermal conductivity	0.96%	0.96%	0.97%	0.97%	0.97%
Thermal capacity	0.97%	0.97%	0.97%	0.97%	0.97%
heatpro_A	0.96%	0.96%	0.97%	0.97%	0.97%
heatpro_B	0.96%	0.96%	0.97%	0.97%	0.97%
heatpro_A2	0.96%	0.96%	0.97%	0.97%	0.97%
decay_chem	0.96%	0.96%	0.97%	0.97%	0.97%
decay_bio	0.96%	0.96%	0.97%	0.97%	0.97%
n	0.97%	0.97%	0.97%	0.97%	0.97%

Table 3.7 is the sensitivity analysis of the eight heat parameters for the soil moisture. It shows that the absolute values of relative errors are 0.96% or 0.97%, which are close to the result using the benchmark parameters (benchmark error is 0.97%). It indicates that in the range of ±60% some heat parameters only leads to 0.01% change of soil moisture. For instance, reducing 60% of thermal conductivity, the absolute values of relative error of soil moisture merely deceased from 0.97% to 0.96%. Some heat parameters such as thermal capacity and n in the range of ±60% do not affect the absolute values of relative error of soil moisture. In terms of this, the soil moisture is not sensitive to the heat parameters at least within ±60%, which allows calibrating the soil moisture without changing the heat parameters.

However, compared to the soil moisture, the impact of heat parameters on the soil temperature shows much more significance in Table 3.8. The absolute values of relative errors obtained by the benchmark parameters are 5.23% (benchmark error). In the range of ±60% parameters, the biggest difference of the absolute value of relative error from the benchmark error is 1.35%. This means that *heatpro_A*$_2$ is the most sensitive heat parameter for the soil temperature among the eight parameters within the range of ±60% changes. The secondary sensitive parameter is thermal capacity and the difference of the absolute value of relative errors of the soil temperature from the benchmark error is 0.99% when subtracts 60% of thermal capacity. The sequence of the other parameters according to the sensitivity in Table 3.8 is: *heapro_A, n,* thermal conductivity, *heatpro_B, decay_bio* and *decay_chem*. Figure 3.5 improves further in the interpretation of Table 3.8 about the sensitivity of heat parameters for soil temperature by showing two characteristics:

Firstly, the absolute values of relative errors show three different trends for the eight parameters: downtrend, uptrend and almost constant trend (error vibration is within ±0.04%). For

the downtrend parameters, the absolute values of relative errors of soil temperature decrease with the increasing values of parameters such as thermal capacity, *n* and thermal conductivity, which are shown in the top three curves at the left hand side of Figure 3.5. For the uptrend parameters, the absolute values of relative errors of soil temperature raise with the increasing values of parameters for example *heatpro_A*$_2$, *heatpro_A* and *heatpro_B*, which are indicated in the top three curves at the right hand side of Figure 3.5. Regarding to the almost constant trend parameters, the absolute values of relative errors of soil temperature do not change much with the parameters such as *decay_bio* and *decay_chem*, which are shown at the bottom two curves in Figure 3.5. It means the soil temperature is not sensitive to the constant trend parameters.

Table 3.8 The absolute values of relative errors between the mean of observed soil temperature and the mean of simulated soil temperature.

Parameter/range	-60%	-30%	0%	30%	60%
Thermal conductivity	5.37%	5.32%	5.23%	5.13%	5.04%
Thermal capacity	6.22%	5.72%	5.23%	4.76%	4.30%
heatpro_A	4.40%	4.92%	5.23%	5.48%	5.68%
heatpro_B	5.06%	5.18%	5.23%	5.27%	5.31%
heatpro_A_2	3.88%	4.71%	5.23%	5.64%	5.97%
decay_chem	5.19%	5.23%	5.23%	5.23%	5.23%
decay_bio	5.19%	5.23%	5.23%	5.23%	5.22%
n	5.43%	5.33%	5.23%	5.14%	5.05%

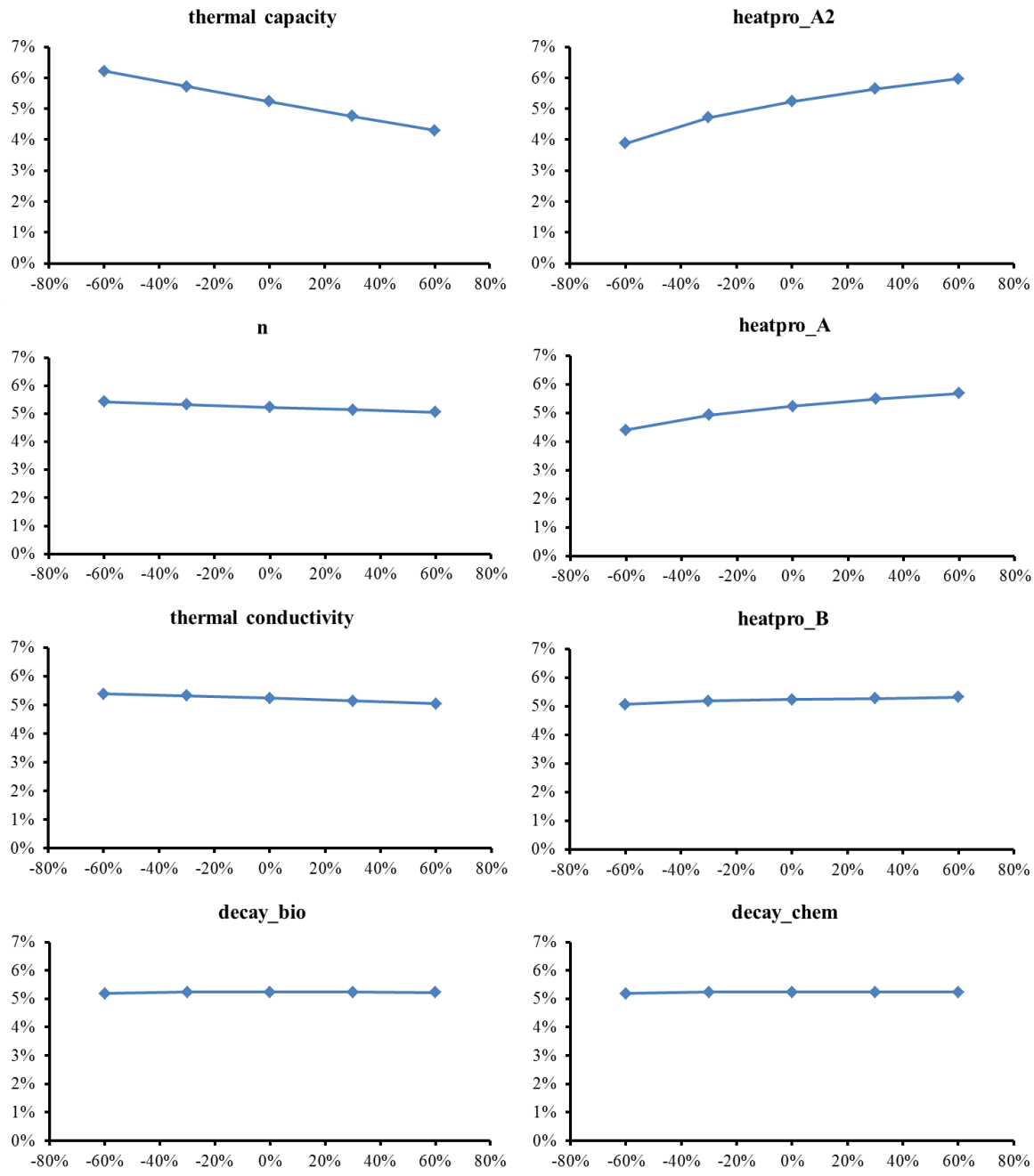

Figure 3.5 Sensitivity analysis of heat parameters for soil temperature. The vertical axis represents the change of soil temperature and the horizontal axis is the change of heat parameters.

The other characteristic is that the heat parameters of the biological activity are more sensitive for the soil temperature than the heat parameters of the chemical activity. For example, the rate of biological heat-product *heatpro_A*$_2$ is more sensitive than the rate of chemical heat-product *heatpro_A* and *heatpro_B* as the slope of *heatpro_A*$_2$ curve is steeper than the slope of the *heatpro_A* and *heatpro_B* curves in Figure 3.5. However, the sensitivity of the biological decay coefficient is close to the sensitivity of chemical decay coefficient.

In general, the above analysis shows the evidence that the soil temperature is much more sensitive than soil moisture to the heat parameters except the almost constant trend parameter. Since the soil temperature is influenced by the heat released from oxidation, it is necessary to figure out how much soil temperature is affected by the heat from total pyrite oxidations including biological and chemical oxidations.

3.5.2 The comparison of soil temperature with and without oxidation heat

The heats from biological and chemical oxidation of pyrite are the two important heat sources in the coal-refuse region. The total heat-production from oxidation in coal mining region is determined by many factors for example, the proportion of pyrite in soil, the bacteria for oxidation, the soil moisture and oxygen condition etc. In this study area coal refuse was mixed with bauxite residue so that the rate of pyrite oxidation may be inhibited during the remediation and the soil temperature may not show significant difference. Figure 3.6 gives the comparison of soil temperature simulation with and without the heat from biological activity and chemical activity (BC heat) during the calibration time period from 5/4/2012 to 8/8/2012 in the remediated plot. The simulation without BC heat is represented by the blue curve and the red curve denotes the simulation of soil temperature with BC heat. The figure shows that the patterns of two

scenarios are similar to each other and the maximum difference of soil temperature between two scenarios is around 3.5 ℃ in this remediated plot. However, the difference of soil temperature may be more significant in the CR plot.

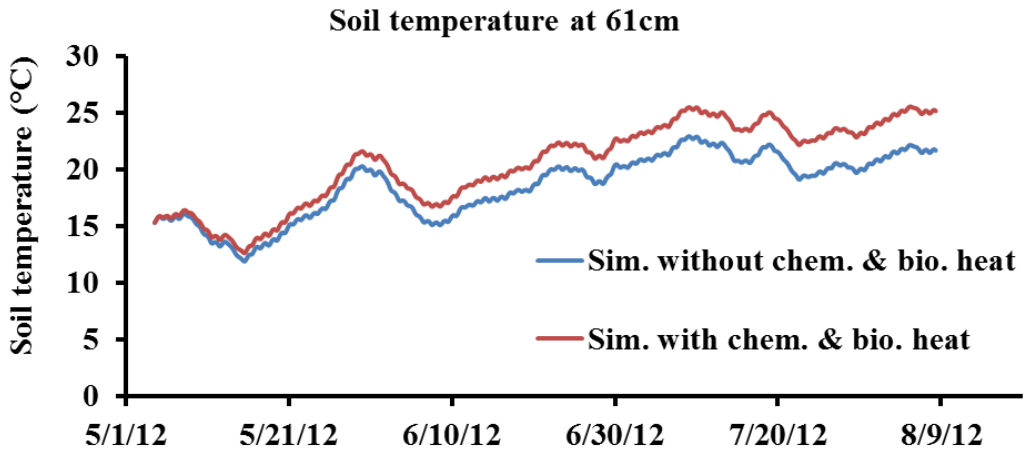

Figure 3.6 Comparison of the soil temperature with and without modeling heat from oxidation in remediated plot.

But the difference of soil temperature between the two scenarios may be more significant in pure coal refuse since pyrite oxidation is stronger in pure CR regions. To date, there was no soil temperature data obtained in the CR plot as the acidic water would damage the sensors in the coal refuse.

Moreover in the process of remediation, the soil temperature is not only influenced by the remedial materials but also by the vegetation. It is a combined effect on the heat from pyrite oxidation. It is necessary to investigate how vegetative tiers to influence the soil temperature in remediation.

3.5.3 The impact of vegetation on soil temperature in remediation

The impact of vegetation on soil temperature is to slow heat transport into soil, which was mentioned at the beginning of this chapter, but it may also block heat transport out. So it is difficult to say if the vegetation makes soil temperature decrease or increase. However, how much difference there is with and without vegetative tier and how deep is the influences on the soil can be investigated by modeling.

In order to solve the above questions, it is necessary to set a background scenario without a vegetative tier in the remediated plot so as to compare with the remediated plot with 0.82m root depth. Here RMSE is calculated between the soil temperature simulation without vegetative tier and the simulation with the vegetative tier in each soil layer. Figure 3.7 shows the results of RMSE versus soil depth in the remediated plot. This figure eventually answers the questions above. Firstly, RMSE is an index to show the difference of soil temperature between two scenarios. The value of RMSE in the surface layer is 4.0℃, which is significantly greater than the values of RMSE at the other depth. It means that the vegetative tier has the most important impact in the surface layer. Secondly, the values of RMSE decrease with the soil depth. The RMSE values are 1.6℃, 0.9℃, 0.3℃, 0.0℃ and 0.0℃ at the depths of 0.30m, 0.61m, 1.57m, 4.32m and 8.32m respectively. The data shows that the difference between the two scenarios is reduced in the deeper layer. RMSE value at the depth of 4.32m is getting to zero shown in Figure 3.7. Based on the simulation result, it suggests that the impact of vegetation on soil temperature could be almost ignored below 4.32m. This is called the vegetation-impact depth. However, this special depth would change if different vegetation was planted since the roots depth and the height of vegetation would be different.

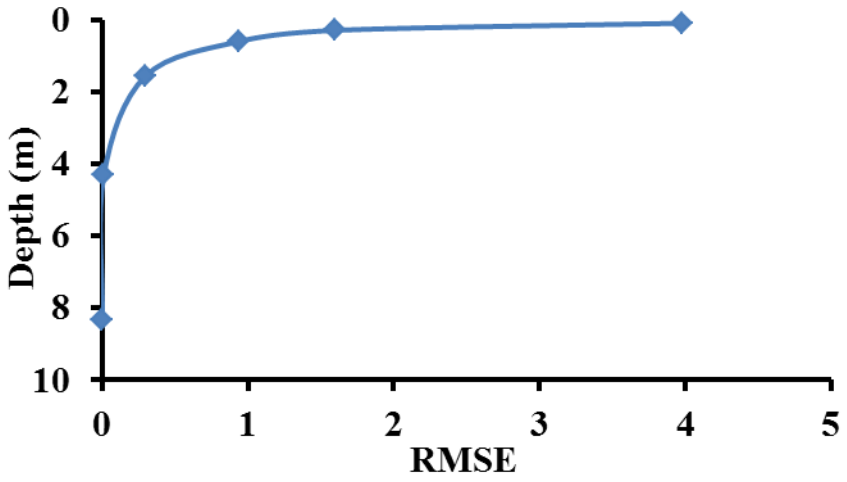

Figure 3.7 The root-mean-square errors of soil temperature between vegetation and non-vegetation.

Overall, the soil temperature influence by the vegetative tier is limited to some depth range. The impact is most significant on the surface and this impact may vanish below the vegetation-impact depth. Actually the impact of remediation on pyrite oxidation is also limited within a specific depth, which is dependent on the amount of remedial materials. However the vegetation–impact depth is not identical to the appropriate depth of remediation, although both of them may affect the soil temperature. Thus, a more sophisticated model is needed to evaluate such an appropriate depth for remediation.

3.6 CONCLUSIONS

The observations show that soil temperature is seasonal in the remediated region and it is lower than the coal-refuse region. In order to investigate the soil temperature in the remediation process, HTGCM v1.0 was improved to be able to simulate the soil temperature profile. The soil parameters, vegetation parameters were first calibrated by the observed soil moisture and then the heat parameters were calibrated through the observation of soil temperature. The results of calibration validation show that HTGCM v1.0 performs well in the study site due to the fact that the relative error for each simulation was small enough as well as the relative error of soil moisture.

The model sensitivity analysis of the parameters indicates that the rate of biological heat production i.e. *heatpro_A*$_2$ is the most sensitive for soil temperature. Based on the sequence of the other seven heat parameters, thermal capacity and the rate of chemical heat production *heatpro_A* are just following the rate of biological heat production. Moreover, as the rate of biological heat production is more sensitive than the rate of chemical heat production, more attentions should be paid to the heat from biological oxidation.

The heat from biological activity and chemical activity enhance the soil temperature in this remediated plot, i.e. plot 2, although pyrite oxidation is inhibited to a certain extent in this plot. The soil temperature in plot 1 (i.e. CR plot) is supposed to be higher than plot 2 because of the stronger pyrite oxidation. This model provides a useful tool for the investigation of the soil temperature in the remediated CR region.

The HTGCM v1.0 also shows that the difference in soil temperature between the non-vegetation scenario and the vegetation scenario is associated with the soil depth. The impact of

vegetation on the deep layer is not as significant as the surface layer. The different plants may have different vegetation-impact depth as it is dependent on the vegetation properties.

In sum, the soil temperature has been successfully investigated by the new model. HTGCM v1.0 has addressed the different scenarios to analyze the impact factors of soil temperature, which not only assesses the remediation impact for the soil temperature, but also will pave the way for improving the remediation approach in CR region with respect to heat pollutant. Despite consideration of natural heat, biological heat and chemical heat to calculate soil temperature, the heat generated from coal burning is not yet included in the model. It remains to be improved in the future research.

4.0 DEVELOPMENT OF A HYDRO-THERMAL-GEOCHEMICAL MODEL WITH PHREEQC

4.1 INTRODUCTION

Due to the complicated characteristics in a coal-refuse (CR) area and the different treatments in this area, the previous models in Chapters 2.0 and 3.0 may not be adequate to deal with the pH-dynamic situation. It is necessary to have a more sophisticated model to include the aspects of hydrology, heat transport and geochemical transport to investigate remediation in a CR region.

A few hydro-geochemical models with dynamic pH values have been present based on the framework of HYDRUS-1D/2D [*Šimůnek et al.*, 1998; *Šimůnek et al.*, 1999], which plays an important role simulating the hydrological processes and solute transport. Some different geochemical models with pyrite oxidation have been coupled into HYDRUS. For example, POLYMIN [*Molson et al.*, 2005] was developed based on HYDRUS-2D. It includes the features of the shrinking core model [*Davis and Ritchie*, 1986] and MINTEQA2 [*Allison et al.*, 1991] to be able to simulate the hydro-geochemical processes in the profile of a CR pile. Another model THERMOX [*Silva*, 2004] for modeling acid mine drainage (AMD) in waste rock combined HYDRUS-2D with the early version of PHREEQC [*Parkhurst et al.*, 1980]. In 2009, the speciation module in PHREEQC [*Parkhurst*, 1995] and shrinking core model were also coupled into THERMOX [*da Silva et al.*, 2009]. The other model HP1 [*Jacques et al.*, 2006; *Šimůnek et*

al., 2008] is a 1D hydro-geochemical model which was developed based on HYDRUS-1D and PHREEQC v2.0 [*Parkhurst and Appelo*, 1999]. The process of pyrite oxidation in this model is solved in the functions of PHREEQC.

Some other models do not use the framework of HYDRUS. For instance, TOUGH AMD [*Lefebvre*, 1994] was developed based on TOUGH2 [*Pruess*, 1991], which emphasized the flow movement in porous media. The idea of the shrinking core model was also applied into TOUGH AMD to mimic the process of pyrite oxidation. It is the same as MIN3P [*Mayer et al.*, 2002] which includes the shrinking core model and possesses its own hydrological processes.

Different from the above models, HTGCM v1.0 [*Xu and Liang*, 2013] in Chapter 3.0 is a hydro-thermal-geochemical model based on the framework of DHSVM [*Wigmosta et al.*, 1994] model. It is able to deal with the processes of hydrology, thermal transport and geochemical transport at field scale and watershed scale. The shrinking core model, the heat generation modules, the different runoff mechanisms e.g. saturated runoff and infiltration excess runoff in DHSVM and the infiltration in the hilly region are all included. However, the pH value is assumed to be constant in HTGCM v1.0. This assumption does not allow the model to be applied in the pH-dynamic environment, although the characteristic of pyrite oxidation is represented better than in the other pollutant transport models such as HSPF [*Bicknell et al.*, 2001] and SWAT [*Neitsch et al.*, 2002]. In order to enlarge the capability of the model, it is desirable to remove the restriction of constant pH. Moreover, more chemical elements should be considered and the model must not be limited to the simulation of SO_4 and Fe (total) (i.e. Fe (II) plus Fe(III) in all Fe solutions) . Accordingly, a hydro-geochemical model with dynamic pH values is discussed in this chapter i.e. HTGCM v2.0 [*Xu et al.*, 2013b].

In order to realize the above expectation in HTGCM v2.0, it is important to couple a well-developed model for pH calculation. WATEQ [*Truesdell and Jones*, 1973] is one of the models for pH calculation. However, it is limited to a small range of ionic strength e.g. lower than the ionic strength of seawater ~0.72. The range of ionic strength in other models e.g. MINTEQA2 is even smaller, which is around 0~0.5 [*Deutsch*, 1997]. Although they may be temporarily available for acid mine drainage, as the ionic strength of AMD in the field is lower than 0.5, they may not be able to work for sites with high ionic strength.

PHREEQC has been widely used in the aqueous geochemical field. It has all the features of MINITEQA2 and WATEQ, but moreover, it includes a large dataset base for a number of reactions. Meanwhile, the range of ionic strength in PHREEQC has been enlarged to be wider in the latest version [*Parkhurst and Appelo*, 2013] than WATEQ and MINTEQA2 due to the Pitzer aqueous model in PHREEQC. Because of these advantages, PHREEQC is a good option to be coupled into HTGCM v1.0. On the one hand, PHREEQC compensates the weakness of pH calculation in the model and allows HTGCM v2.0 to be used in a pH-dynamic environment. On the other hand, pyrite oxidation is controlled by the shrinking core module and oxygen diffusion module instead of the function in PHREEQC in order to maintain the pyrite oxidation in a physical manner. Thus, HTGCM v2.0 should adopt the advantages from both of HTGCM v1.0 and PHREEQC.

The objective of this research is to develop such a sophisticated model i.e. HTGCM v2.0. The short-term simulations are conducted to compare with the previous results and investigate further how much depth of the amended zone is appropriate in plot 2 i.e. 90% CR mixed with 10% bauxite residue (BR) with the vegetative tie within the top 61 cm. Some questions remaining from the previous chapters are discussed further in this chapter. The impact of remediation in the deeper non-amended zone is seen through a long-term simulation.

4.2 MODEL DEVELOPMENT

4.2.1 Model description

Due to the limitation of constant pH in HGCM and HTGCM v1.0, combining PHREEQC is a milestone for HTGCM v2.0 since PHREEQC is able to calculate the chemical process based on stoichiometry. The latest version PHREEQC v3.0.6-7757 has many capabilities for example: (1) calculations of equilibrium reactions and a few kinetic mineral reactions; (2) simulation for one-dimensional transport including solid precipitation; (3) enlarging the range of ionic strength [*Parkhurst and Appelo*, 2013] and (4) inverse modeling to account for variation in composition. In order to be coupled easily to the other transport models, IPhreeqc [*Charlton and Parkhurst*, 2011] gave a flexible way for users to call the modules in PHREEQC, that is to link the static library with the models that we need to couple to, instead of coupling all the codes of PHREEQC into the models. This approach saves much time to write the codes and reduces the chance of error to occur. To date, IPhreeqc v3.0.6-7757 includes all the modules in PHREEQC v3.0.6-7757. The library of IPhreeqc is compatible with C, C++, FORTRAN, Python, Visual Basic and MATLAB. The HTGCM v2.0 is written in the same language as the original version of HTGCM v1.0 the C programming language.

4.2.2 Coupling strategy between HTGCM and PHREEQC

Firstly, this section lists the general coupling procedures and the details of the computer technology are described in APPENDIX A:

- Compile and generate the static library of IPhreeqc v3.0.6-7757.

- Include the path of library into HTGCM v2.0 that is to link the library of IPhreeqc with the new model. Also include the path of database of PHREEQC and the path of head files of PHREEQC into the "makefile" of HTGCM v2.0.
- The parameters communicated between HTGCM v2.0 and PHREEQC are mainly: soil moisture, water flow, pH, soil temperature, oxygen, cation and anion. They interact across different modules in the model. The modules and the main parameters are:

  Pyrite Oxidation module: SO_4 and Fe (total), oxygen concentration, pH and soil temperature (This module calculates pyrite oxidation and updates the production of SO_4, Fe (total) and hydrogen ions in solution);

  PHREEQC module: pH, soil temperature, oxygen concentrations, cations and anions in solution and minerals in solid (This module updates all the concentration increments of SO_4, Fe (total) and hydrogen ions from pyrite oxidation.);

  Advection-Dispersion module: the soil moisture, water flow, metal cation and anion solutions (This module connects the water cycle with the chemical transport.);

  Thermal Transport module: soil temperature (This module is able to calculate the soil temperature profile influenced by solar radiation and heat generation from pyrite oxidation. All the rates of reactions in the database are associated with soil temperature in PHREEQC, which are based on Van't Hoff's law. Also the transport coefficients are also temperature-dependent based on the Arrhenius equation [*Stumm and Morgan*, 1981] in the model.).
- Compile all the codes and run the executable file.

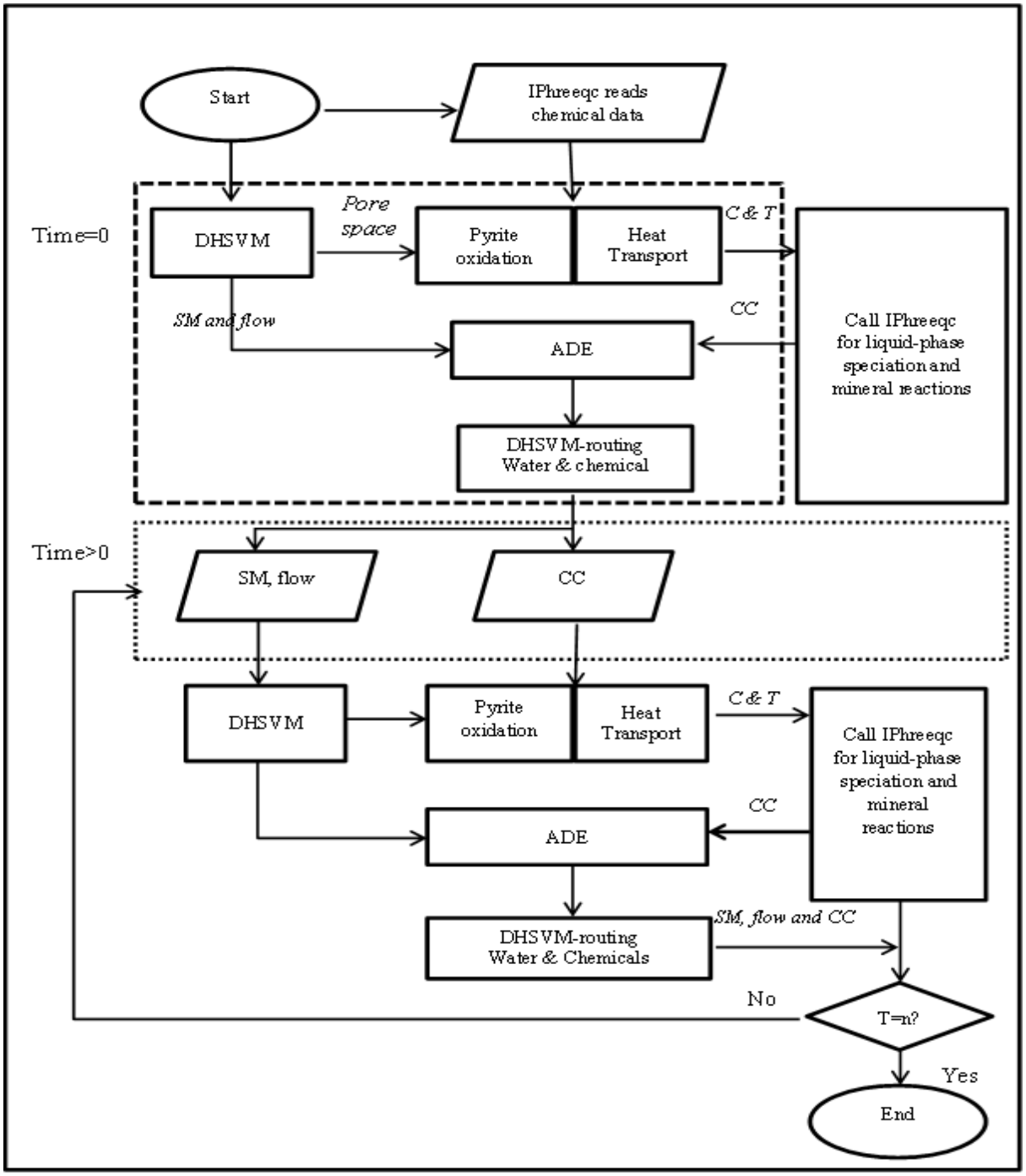

Figure 4.1 Flowchart of coupling HTGCM with PHREEQC. CC represent the concentrations of Fe (total), S (total), O (total), H (total), Al (total), Ca (total), Na (total), Mg (total), K (total), Si (total), P (total), Cl (total) and Mn (total) in solutions; C indicates the concentrations of Fe (total), S (total), O (total) and H (total) in solutions; SM is soil moisture, T is temperature, n is the ending time step and ADE is advection-dispersion equation.

The Figure 4.1 shows the coupling flowchart and the relationship between the new parameters and new modules in the model. The significant improvement in the new version is that not only the main elements i.e. Fe, S and O are concerned but also more chemical elements such as H, Al, Ca, Na, Mg, K, Si, P, Cl and Mn are included in the SOLUTION data block of PHREEQC. The new model allows more solid-liquid reactions controlled by the data blocks of EQUILIBRIUM_PHASE AND REACTION in PHREEQC. Also, all the elements are permitted to transport in the model and they are updated by SOLUTION_MODIFY for each time step.

4.3 STUDY SITE, DATA MEASUREMENT AND INITIALZATION

4.3.1 Study site and field measurement

Figure 4.2a indicates the compared points in plot 1 and plot 2 for this chapter, which are represented by the two green stars. Figure 4.2b gives the distribution of vegetation from 2009 to 2011. It has been mentioned that plot 1 was replaced by the materials of plot 2 in spring of 2011. However, we make the same assumption for plot 1 to be 100% CR as the benchmark all the time even after 2011, which is the same as in Chapter 3.0 in order to compare the benchmark with the remediation in plot 2. The parameters of soil property, vegetation property and thermal transport process are set based on Chapters 2.0 and 3.0 . Plot 3 and plot 4 are not discussed here since these two plots required the other remediated materials instead of BR.

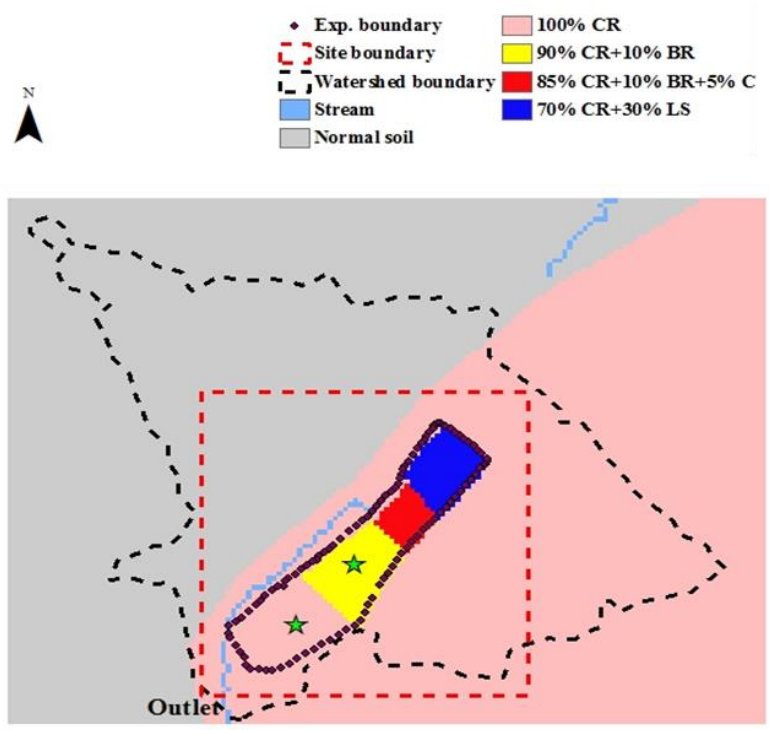

(a)

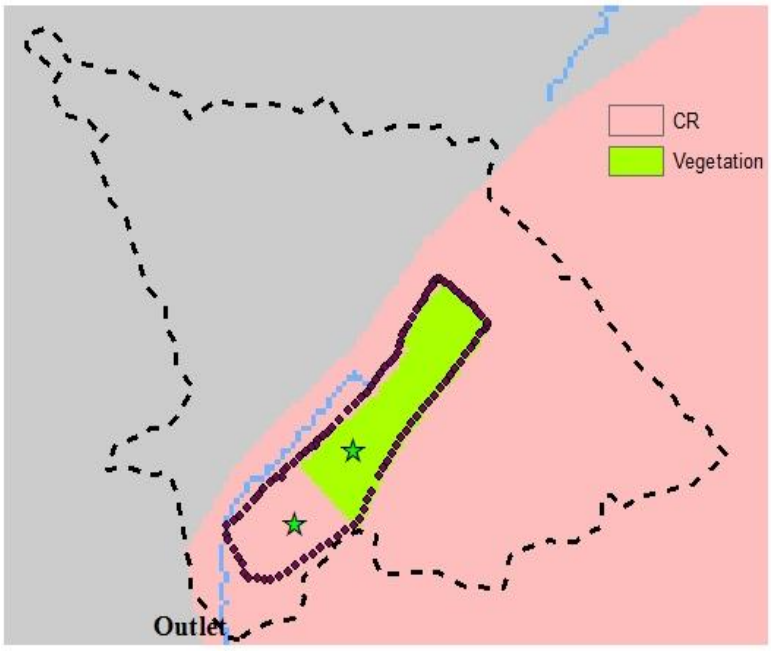

(b)

Figure 4.2 (a) Two compared points are shown in plot 1 and plot 2 indicated by the green stars, (b) green color represents planted area.

The short-term meteorological data (e.g., rainfall, air temperature, relative humidity, solar radiation and wind speed) are the same as provided in Chapter 2.0 , which is from 6/1/2009 to 6/27/2010. After that, another two years data have been collected to 06/01/2012. However, the forcing data (e.g. rainfall, wind speed, humidity, solar radiation etc.) during 2011 were lost from March 2011 to May 2011 due to that it was the time for the weather station maintenance. We simply compensated for these missing data by inserting the data from March 2012 to May 2012.

Despite most of the parameters and the driving data being identical to the previous version of the model, the input data in the new version require much more information such as more chemical information in the solution and the solid components that will be discussed in the following section in order to mimic the environment of the mining area.

4.3.2 Initial solution and solid composition

The representative solutions based on the observation were used to initialize the chemical concentrations and pH value in the liquid within 0~61 cm and below 61 cm respectively. Both plots i.e. 100% CR and 90% CR + 10% BR were given the different initial solutions for chemical elements in their total concentrations shown in Table 4.1 according to the measurement in June 2009 (this is the format of input data in PHREEQC). These input data contain the metals and nonmetals in the leachate.

These chemical elements in AMD would have different impacts on the environment. For instance, ferric ion as the product of pyrite oxidation could facilitate dissolving other heavy metal minerals. It is also suggested that precipitates such as ferric iron hydroxides could obstruct biological activities through burial of substrata, clogging of gill surfaces and reductions in light availability [*DeNicola and Stapleton*, 2002]. Also the high levels of sulfate released into the

AMD could result in sulfide toxicity and damage the roots of aquatic plants [*Lamers et al.*, 1998]. Meanwhile, some aluminum compounds are toxic such as Al_2O_3. Calcium dissolution could result in high values of hardness of water and potentially increase the cost of water treatment. Moreover, the concentrations of total Fe, total S, total Al and total Ca in the AMD are relatively higher the other elements. Thus, Fe, S, Al and Ca are the main elements to be discussed in this chapter. The compounds of these elements are the key solid components. For example, Pyrite (FeS_2), K-mica $KAl_2(AlSi_3O_{10}(OH)_2)$, Jarosite-K $KFe_3(OH)_6(SO_4)_2$, Kaolinite $Al_2Si_2O_5(OH)_4$, Calcite $CaCO_3$ and Gypsum $CaSO_4 \cdot 2H_2O$ which were all detected by X-Ray Diffraction (XRD) in CR. They are at equilibrium with the solution that is dominated by pyrite oxidation.

However, it is inadequate to detect the four elements to solve the proportions of the above six solid components in CR. In order to address this issue, we reduced the number of the unknown solid components and also measured one more element. Firstly pyrite which dominates the AMD system, was documented to be around 0.3% of the total mass of coal refuse in Mather site according to the measurement of coal refuse piles in Mather [*Neufeld*, 1990]. Meanwhile, we detected the proportion of one more element in 1kg CR. The solid sample was totally dissolved in the strongly acidic water and the chemical elements were detected by the atomic absorption spectrometer (AAS) and the ion chromatography (IC) shown in Table 4.2.

.

Table 4.1 Initial solutions of chemical elements in total concentrations for 100% CR and 90% CR + 10% BR. Concentration units: ppm.

Materials	100% CR		90% CR + 10% BR	
Depth	0~61cm	below 61cm	0~61cm	below 61cm
pH	2.2	2.4	4.5	2.6
S as SO_4	5880	22800	1818	29394
Fe	1200	5500	5	9200
Ca	430	460	570	520
Na	200	365	280	1570
Mg	65	65	12	500
K	7.6	4.8	7.2	0.5
Si as SiO_2	177.9	186.4	60	212.7
P	15	52	0.5	190
Al	280	2000	1.6	1300
Cl	100	100	155	155
Mn	8.9	39	0.7	48

Thus, we have five elements to solve five compounds i.e. K-mica, Jarosite-K, Kaolinite, Calcite and Gypsum in Table 4.3. The proportion of Quartz is the rest of the five components. Regarding the case of 90% CR + 10% BR, the proportion of each composition in 100% BR have been measured so 10% of it was plus with 90% compounds of CR. Table 4.4 lists the solid composition proportion for the amended zone in plot 2.

Table 4.2 Detection of chemical elements in 1kg 100% CR.

Elements	Mass (g/1kg mine rock)	Moles (mol/kg mine rock)
Fe	34.60	0.62
Al	66.15	2.45
K	31.22	0.80
Ca	6.15	0.15
S	14.36	0.45

Table 4.3 Solid compositions in 100% CR.

Composition	Percentage (%)
Quartz: SiO_2	55.62
K-mica: $KAl_2(AlSi_3O_{10}(OH)_2)$	24
Jarosite-K: $KFe_3(OH)_6(SO_4)_2$	9.9
Kaolinite: $Al_2O_32SiO_22H_2O$	8.26
Calcite: $CaCO_3$	1
Gypsum: $CaSO_4 \cdot 2H_2O$	0.92
Pyrite: FeS_2	0.3

Table 4.4 Solid compositions in 90% CR + 10% BR.

Composition	Percentage (%)
Quartz: SiO_2	50.358
K-mica: $KAl_2(AlSi_3O_{10}(OH)_2$	21.6
Jarosite-K: $KFe_3(OH)_6(SO_4)_2$	8.91
Kaolinite: $Al_2O_32SiO_22H_2O$	7.434
Dicalcium silicate: Ca_2SiO_4	5.7
Sodalite: $Na_8(Al_6Si_6O_{24})Cl_{l2}$	1.2
Calcite: $CaCO_3$	1.2
Gehlenite: $Ca_2Al(AlSiO_7)$	1
Gypsum: $CaSO_4 \cdot 2H_2O$	0.828
Hematite: Fe_2O_3	0.8
Pyrite: FeS_2	0.27
Calcium aluminum sulfate: $Ca_6Al_2(SO_4)_3(OH)_{12}$	0.2
Calcium titanium oxide: $CaTiO_3$	0.2
Titanium dioxide: TiO_2	0.2
Gibbsite: Al(OH)3	0.1

In order to simplify the model to be well controlled, Jarosite-K is excluded which was also not included in previous research [*Gerke et al.*, 1998] but it may need to be concerned in the future. So currently the possible chemical reactions are listed from Eqs. (4-1) ~ (4-8) in plot 1. Eqs. (4-1), (4-2) and (4-3) have already been included in the pyrite oxidation module and Eqs. (4-4) ~ (4-8) are included in the database of PHREEQC.

$$FeS_2 + H_2O + 7/2O_2 \Rightarrow Fe^{2+} + 2SO_4^{2-} + 2H^+ \quad (4\text{-}1)$$

$$Fe^{2+} + 1/4O_2 + H^+ \Rightarrow Fe^{3+} + 1/2H_2O \quad (4\text{-}2)$$

$$FeS_2 + 1/2H_2O + 15/4O_2 \Rightarrow Fe^{3+} + 2SO_4^{2-} + H^+ \quad (4\text{-}3)$$

$$CaCO_3 + 2\,H^+ \Leftrightarrow CO_2 + Ca^{2+} + H_2O \quad (4\text{-}4)$$

$$CaSO_4 \cdot 2H_2O \Leftrightarrow Ca^{2+} + SO_4^{2-} + 2\,H_2O \quad (4\text{-}5)$$

$$KAl_3Si_3O_{10}(OH)_2 + 10\,H^+ \Leftrightarrow K^+ + 3\,Al^{3+} + 3\,H_4SiO_4 \quad (4\text{-}6)$$

$$Al_2Si_2O_5(OH)_4 + 6\,H^+ \Leftrightarrow H_2O + 2\,H_4SiO_4 + 2\,Al^{3+} \quad (4\text{-}7)$$

$$SiO_2 + 2H_2O \Leftrightarrow H_4SiO_4 \quad (4\text{-}8)$$

For the simplification in plot 2, another three components i.e. Hematite (Fe_2O_3), Dicalcium silicate (Ca_2SiO_4) and Gehlenite ($Ca_2Al_2SiO_7$) were added into the reaction system represented by Eqs. (4-9) ~ (4-11), which have been included in PHREEQC.

$$Fe_2O_3 + 6H^+ \Leftrightarrow 2Fe^{3+} + 3H_2O \quad (4\text{-}9)$$

$$Ca_2SiO_4 + 4H^+ \Leftrightarrow 2Ca^{2+} + H_4SiO_4 \quad (4\text{-}10)$$

$$Ca_2Al_2SiO_7 + 10H^+ \Leftrightarrow H_4SiO_4 + 2Al^{3+} + 2Ca^{2+} + 3H_2O \quad (4\text{-}11)$$

HTGCM v2.0 is a pH-dynamic model with the main reaction i.e. pyrite oxidation and the other secondary mineral reactions. The products from the kinetic process of pyrite oxidation are assumed to react with the other minerals and achieve equilibrium at the each time step by using the function of EQUILIBRIUM_PHASE in PHREEQC. Moreover, the function of REACTION in PHREEQC allows the model to calculate the other kinetic source such as aluminum in CR and BR.

4.4 MODELING RESULTS

The model has been tested in different time series in Mather, PA. The first time series is identical to the period i.e. 06/01/2009-06/27/2009 in Chapter 2.0 to compare the results between the two chapters. Then the modeling period is extended to 06/01/2012 to verify a three-year result. This section discusses the two periods separately. A long-term simulation is presented in section 4.5.

4.4.1 One-year simulation

The model was tested within the field (red dashed line) in Figure 4.2a. The soil moisture and soil temperature will be presented in the three-year simulation. This section mainly focuses on the one-year result of chemical concentrations. All the initial moistures and chemical concentrations are the same as the previous settings including the oxygen concentration in pore space. Only one of the three assumptions in section 2.4 remains that oxidation occurs in the unsaturated zone, while the heat from oxidation has been concerned and pH value can change with time.

The simulations of SO_4, total Fe, total Ca (Ca^{2+} in all Ca solutions), total Al (Al^{3+} in all Al solutions) and pH in soil water at the middle of the hillslope at 61 cm in plot 1 and plot 2 are shown in Figure 4.3 and Figure 4.4 respectively. The simulations capture the pattern of all the observations. In Figure 4.3 i.e. plot 1, the simulations of SO_4 and Fe (total) do not change much with the results of the basic model in Chapter 2.0 . In the new version, the relative error between the observed SO_4 and simulation is 2% and the relative error for Fe (total) is 0.13% at 61 cm, while the relative errors in Chapter 2.0 for these two elements are also within 2%. The concentrations of total calcium and total aluminum were relatively low in plot 1 since the compounds of them were not the main reactants as pyrite in the AMD system. The minimum pH value in plot 1 is lower than 2 both in the measurements and the modeling results, which may not occur in the reality if SO_4^{2-} is equilibrium with HSO_4^-. It needs to pay more attentions to investigate the reason of such a low pH value in this CR area in the future. In plot 2, the results of SO_4 and Fe (total) from HTGCM v2.0 still behaved well to capture the patterns of observation in Figure 4.4 and it uses PHREEQC to calculate the solid precipitation instead of assuming first-order decay to represent the precipitate rates. The situation in plot 2 was different from plot 1 as

most of the chemicals were lower than plot 1 except total calcium. The reason is that the pH in plot 2 was higher and alkaline chemicals were added in the mixtures, which may allow SO_4^{2-}, Fe^{3+} and Al^{3+} to precipitate into the solid. Total calcium concentrations were low in both of plots. The reason may be due to that the extra calcium ions in plot 2 precipitated with sulfate. Then less amount of calcium ions were dissolved in the water. The calcium ions in plot 1 may be similar to this. However, ferric iron may easily precipitate because of the alkaline materials. It has been proved by laboratory experiment that yellow ferric compounds precipitate at the surface of the remediated zone i.e. 90% CR + 10% BR (Figure 4.5a) and also they were distributed in the amended zone unevenly (Figure 4.5b). In 100% CR, there was not such yellow solid shown in Figure 4.5c. This experiment was conducted in two 29-inch glass columns: one was full of 100% CR and the other was 12-inch 90% CR + 10% BR on the top of 17-inch 100% CR.

Comparing Figure 4.3 and Figure 4.4, pH at 61 cm in plot 2 was higher than plot 1. The pH at 61 cm in these two plots were stable for one-year simulation after coupling PHREEQC into the model, which is consistent with the real pH values in the field. It proves that the constant pH in Chapter 2.0 is a reasonable assumption for the short-term simulation. That is why the one-year simulations of SO_4 and Fe (total) in Chapter 2.0 are very similar to the results of this section for plot 1. And it also reflects that PYROX plays the main role in HGCM and HTGCM to catch the mechanism of pyrite oxidation. However, such an assumption of constant pH may not be good enough in the long-term scenario since pyrite may disappear after a long time period in plot 1 and pH value will change. Also the remedial plot may decrease the capability of neutralization for AMD after the alkaline substances in BR are consumed and pH value will not be stable as well.

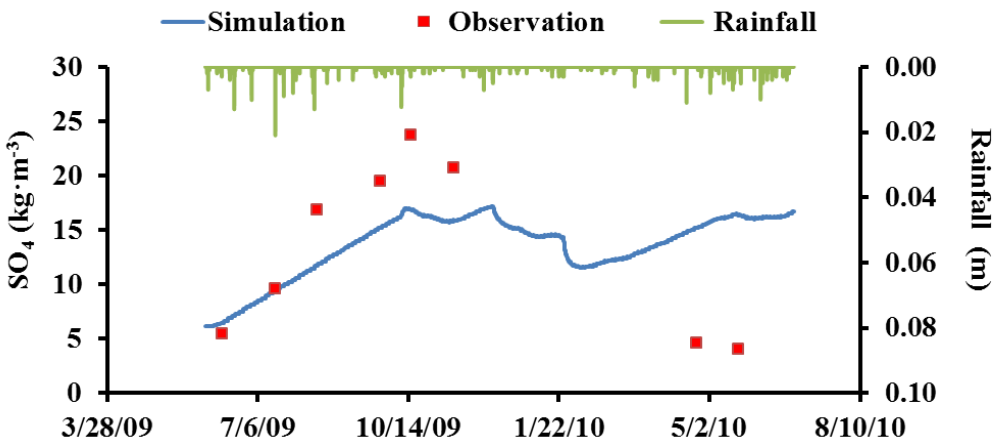
Simulation
Observation
Rainfall
30
25
20
15
10
5
0
SO4 (kg·m-3)
0.00
0.02
0.04
0.06
0.08
0.10
Rainfall (m)
3/28/09
7/6/09
10/14/09
1/22/10
5/2/10
8/10/10

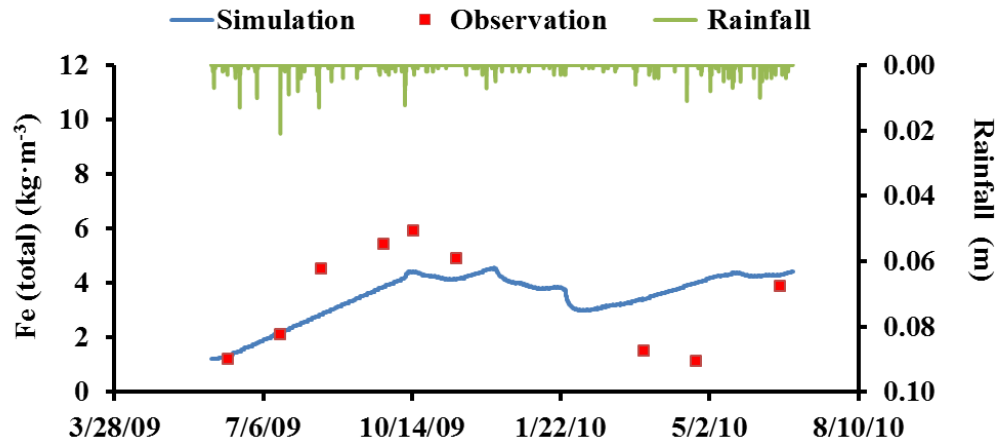
Simulation
Observation
Rainfall
12
10
8
6
4
2
0
Fe (total) (kg·m-3)
0.00
0.02
0.04
0.06
0.08
0.10
Rainfall (m)
3/28/09
7/6/09
10/14/09
1/22/10
5/2/10
8/10/10

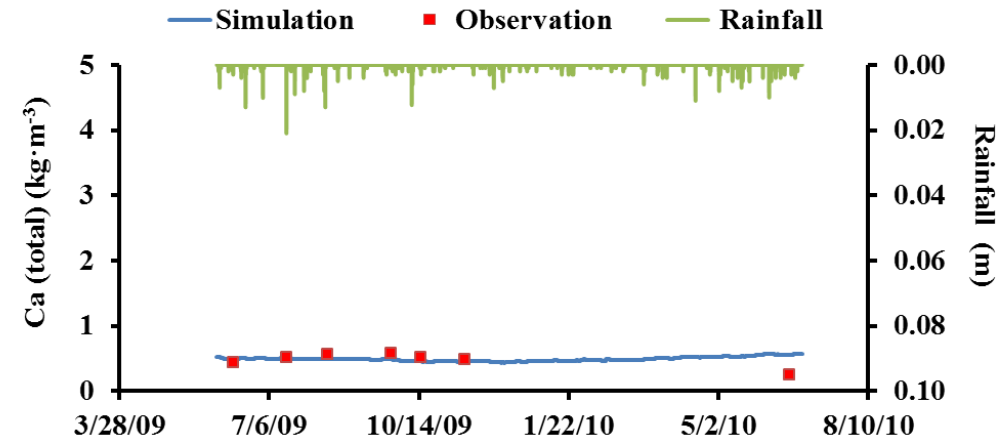
Simulation
Observation
Rainfall
5
4
3
2
1
0
Ca (total) (kg·m-3)
0.00
0.02
0.04
0.06
0.08
0.10
Rainfall (m)
3/28/09
7/6/09
10/14/09
1/22/10
5/2/10
8/10/10

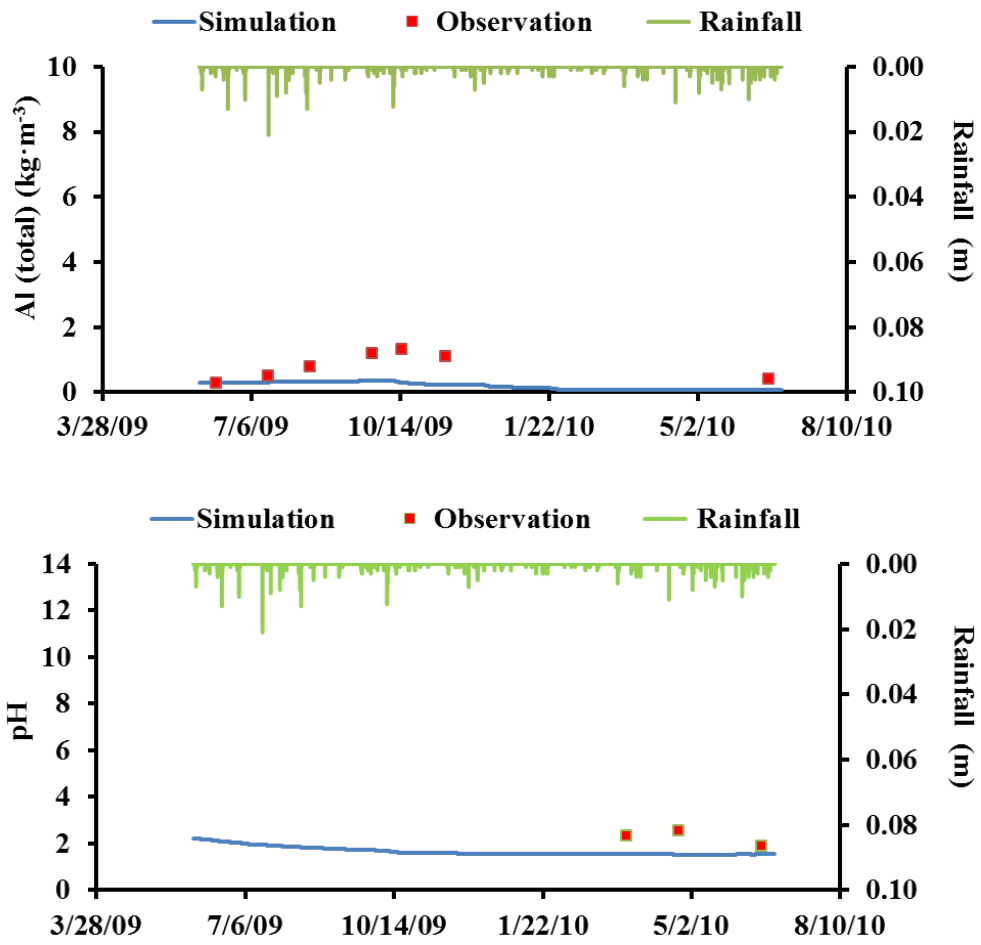

Figure 4.3 The simulations of SO_4, Fe (total), Ca (total), Al (total) and pH at the depth of 61 cm from 06/2009-06/2010 in plot 1.

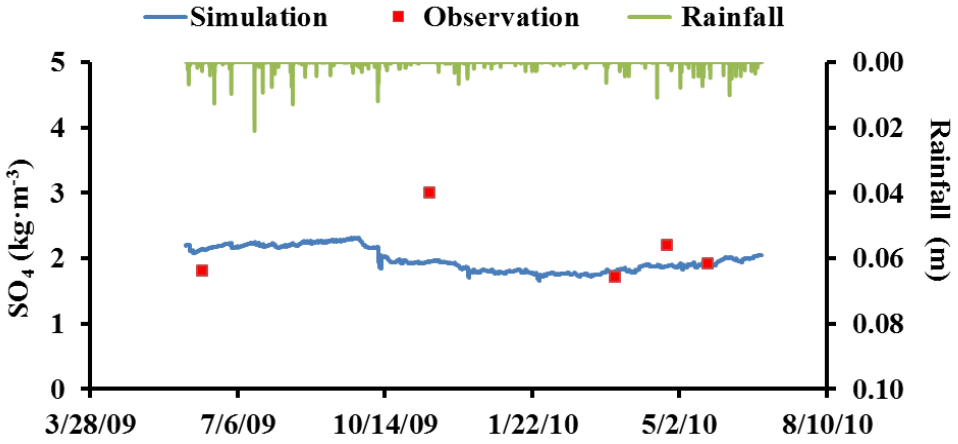

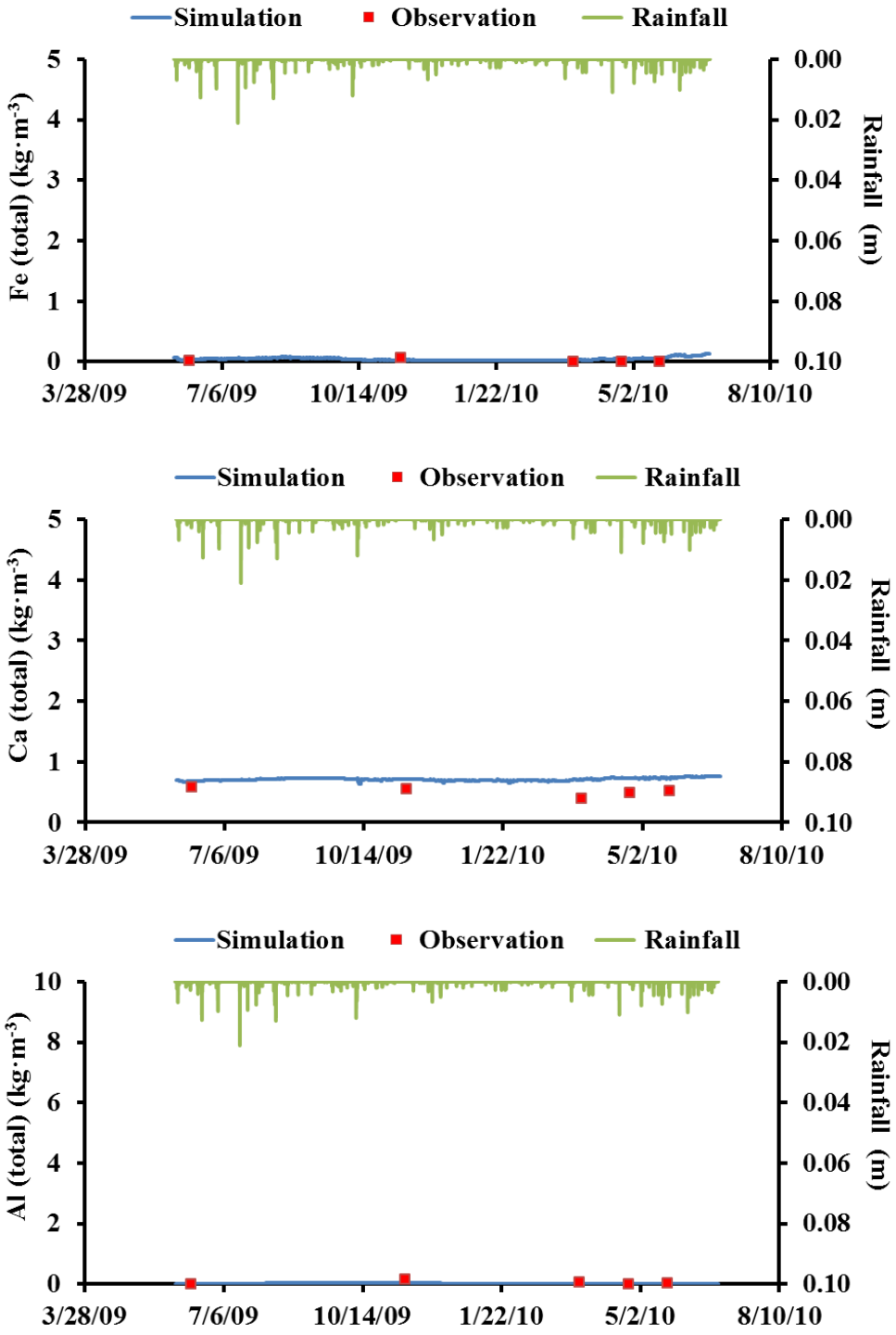
Simulation
Observation
Rainfall
Fe (total) (kg·m-3)
Rainfall (m)
0
1
2
3
4
5
0.00
0.02
0.04
0.06
0.08
0.10
3/28/09
7/6/09
10/14/09
1/22/10
5/2/10
8/10/10
Simulation
Observation
Rainfall
Ca (total) (kg·m-3)
Rainfall (m)
0
1
2
3
4
5
0.00
0.02
0.04
0.06
0.08
0.10
3/28/09
7/6/09
10/14/09
1/22/10
5/2/10
8/10/10
Simulation
Observation
Rainfall
Al (total) (kg·m-3)
Rainfall (m)
0
2
4
6
8
10
0.00
0.02
0.04
0.06
0.08
0.10
3/28/09
7/6/09
10/14/09
1/22/10
5/2/10
8/10/10

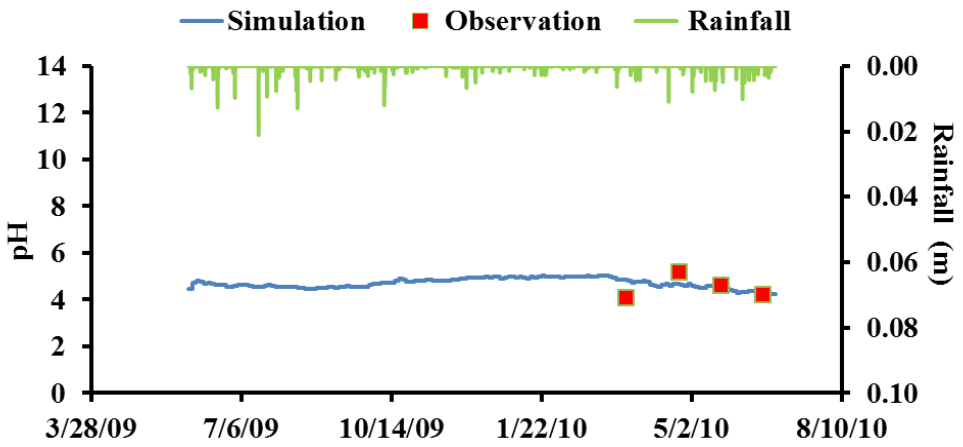

Figure 4.4 The simulations of SO_4, Fe (total), Ca (total), Al (total) and pH at the depth of 61 cm from 06/2009-06/2010 in plot 2.

(a)

(b)

(c)

Figure 4.5 (a) Ferric compounds at the surface of mixing zone in 90% CR + 10% BR, (b) ferric compounds precipitated within the mixing zone 90% CR + 10% BR, (c) 100% CR.

4.4.2 Three-year simulation

The three-year simulation is from 06/01/2009 to 06/01/2012. All the initial moistures and chemical concentrations are the same as the one-year simulation. The simulations of soil moisture in plot 1 and plot 2 at 61 cm are shown in Figure 4.6. The soil moistures responded to the rainfall. In Figure 4.7, the soil temperature performed seasonally and the soil temperature in plot 1 was higher than plot 2 due to that the heat from pyrite oxidation in plot 1 was more than plot 2.

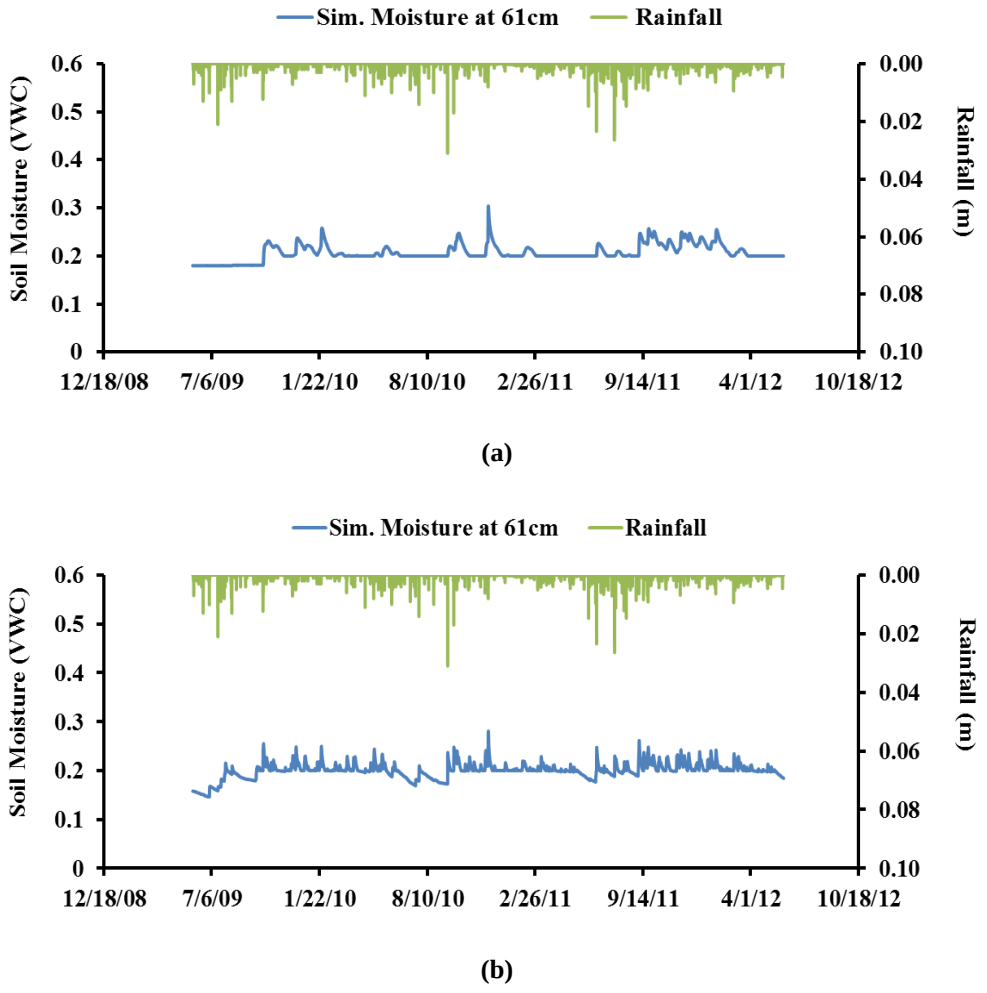

Figure 4.6 Soil moisture simulations in (a) plot 1 and (b) plot 2.

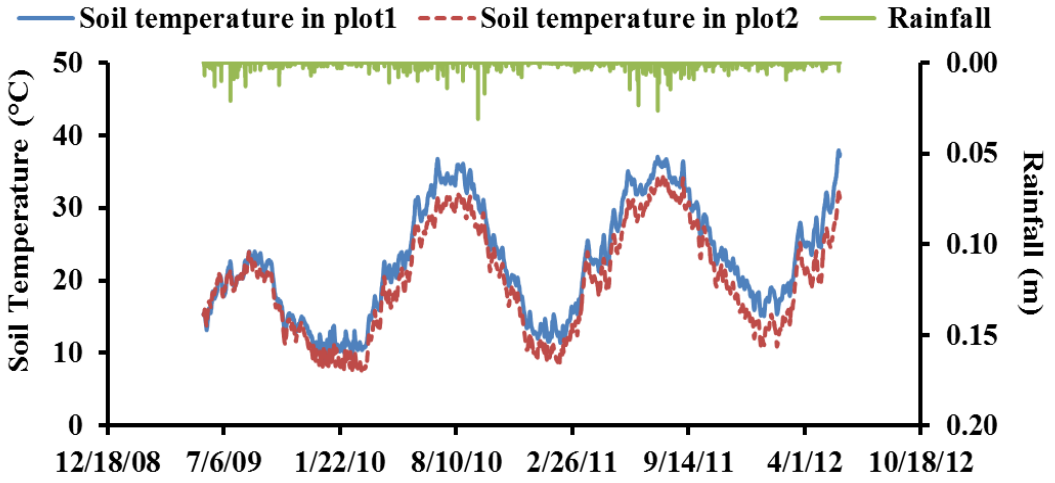

Figure 4.7 Soil temperature simulations from 06/2009-06/2012 in plot 1 and plot 2 at 61 cm.

Figure 4.8 and Figure 4.9 give the simulations of SO_4, Fe (total), Ca (total), Al (total) and pH in soil water at the middle of the hillslope in plot 1 and plot 2 respectively. The simulations in the two plots match the observation well even after 2010. The concentrations of SO_4 and total Fe were shown more seasonal in plot 1 as the concentrations of SO_4 and total Fe in plot 1 were higher than plot 2. The concentrations of total aluminum in plot 2 were also reduced compared to plot 1. But the concentrations of total calcium in the two plots are not much different as the one-year result. The pH value in plot 2 was higher than plot 1.

In sum, no matter if one-year results or three-year results are considered, HTGCM v2.0 has been able to reflect the hydro-thermal-geochemical processes for plot 1 100% CR and plot 2 90% CR + 10% BR correctly. The modeling results are consistent with the observation and plot 2 has shown the capability to neutralize acid water and decrease SO_4, total Fe and total Al. Although we have attempted to do the sensitivity analysis for the depth of amended layer in

Chapter 2.0 , the appropriate depth of amended zone still needs to be discussed further with the pH-dynamic model in this chapter. Also the long-term impact of amended zone will be presented.

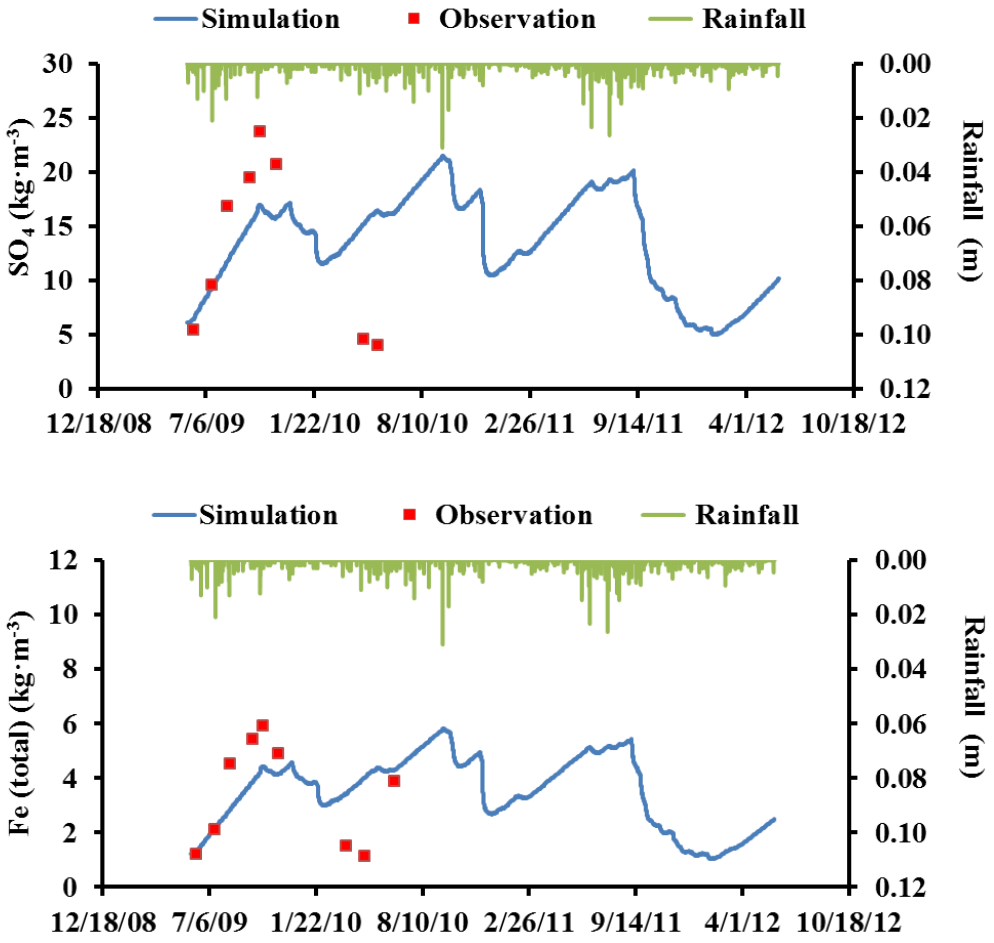

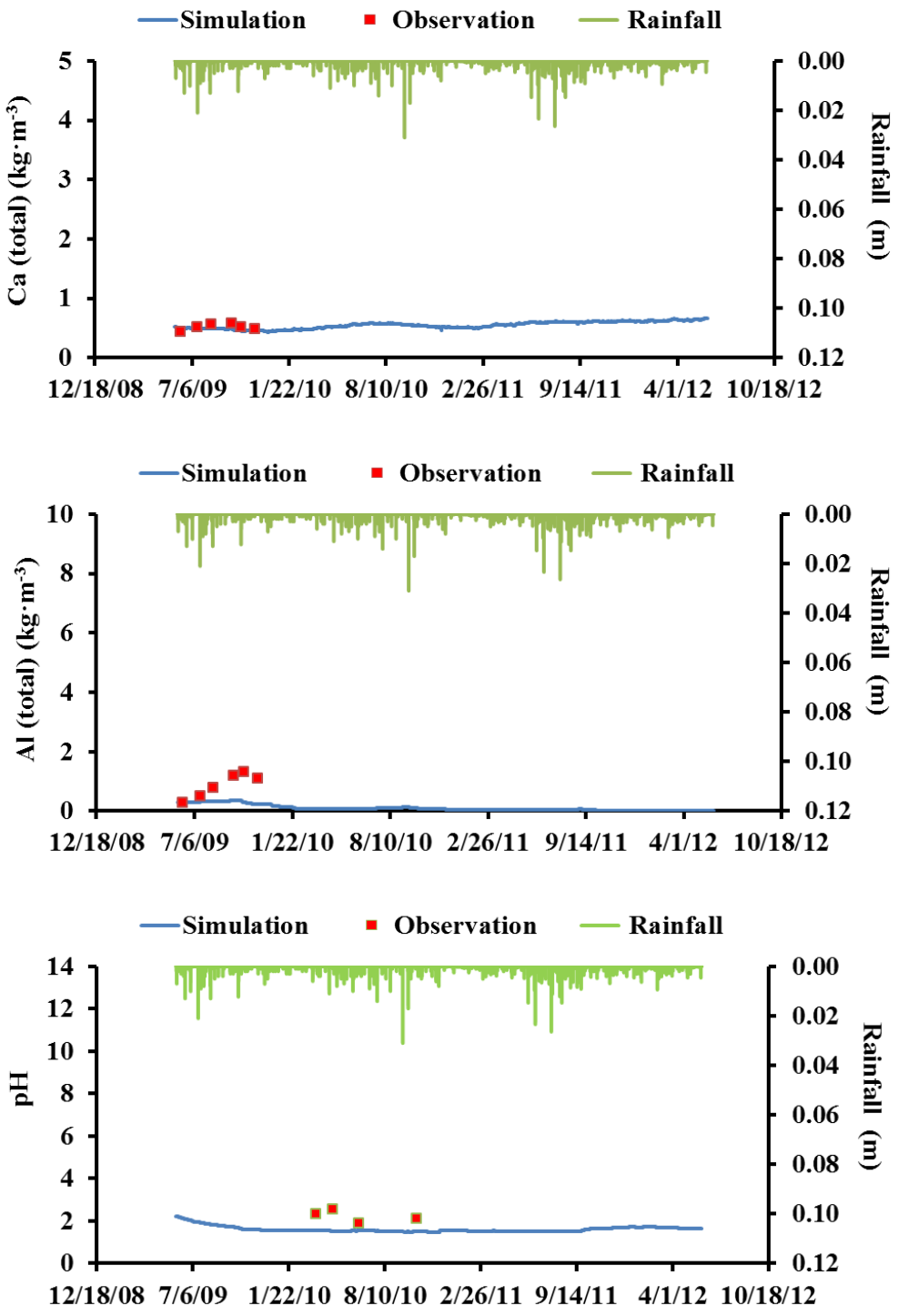

Figure 4.8 The simulations of SO_4, Fe (total), Ca (total), Al (total) and pH at the depth of 61 cm from 06/2009-06/2012 in plot 1.

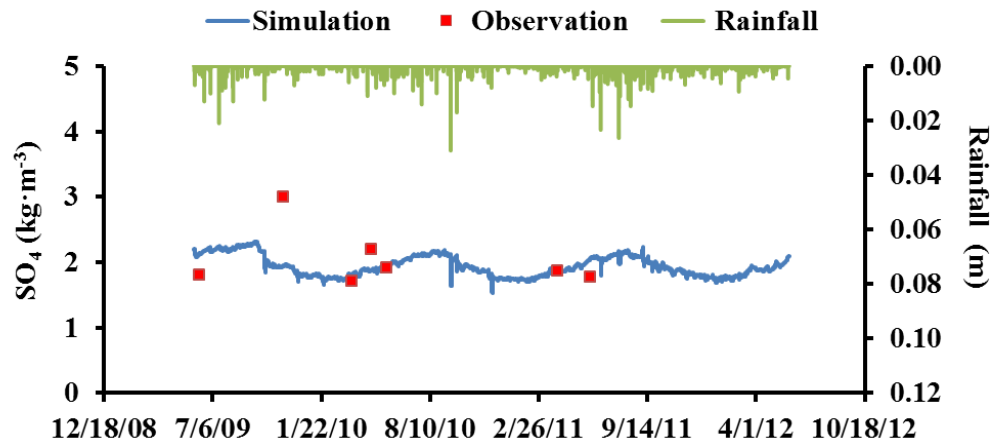
Simulation
Observation
Rainfall
SO4 (kg·m-3)
Rainfall (m)
0
1
2
3
4
5
0.00
0.02
0.04
0.06
0.08
0.10
0.12
12/18/08
7/6/09
1/22/10
8/10/10
2/26/11
9/14/11
4/1/12
10/18/12

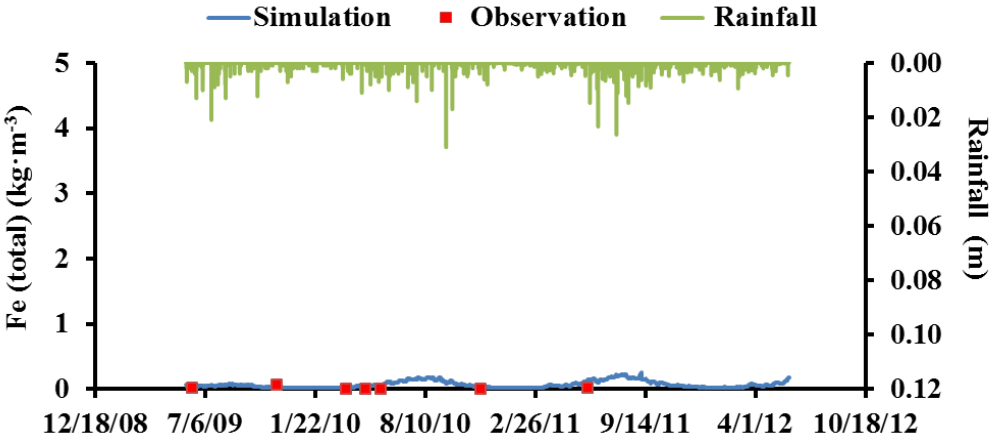
Simulation
Observation
Rainfall
Fe (total) (kg·m-3)
Rainfall (m)
0
1
2
3
4
5
0.00
0.02
0.04
0.06
0.08
0.10
0.12
12/18/08
7/6/09
1/22/10
8/10/10
2/26/11
9/14/11
4/1/12
10/18/12

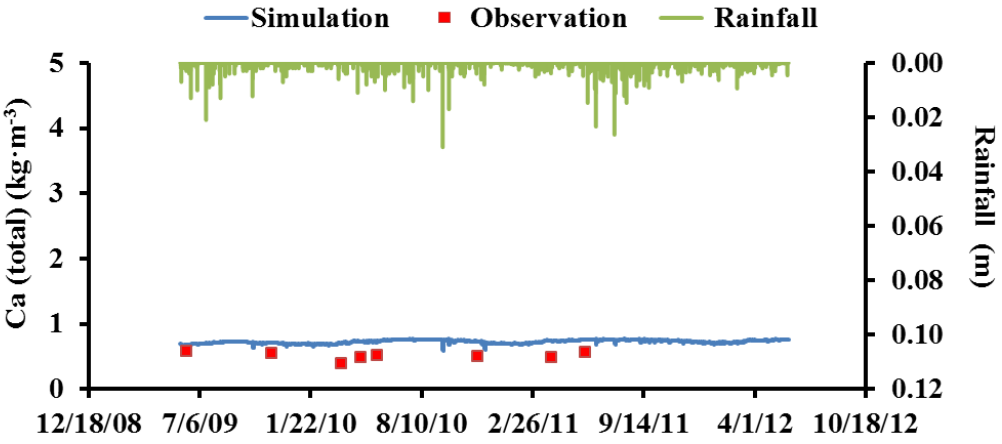
Simulation
Observation
Rainfall
Ca (total) (kg·m-3)
Rainfall (m)
0
1
2
3
4
5
0.00
0.02
0.04
0.06
0.08
0.10
0.12
12/18/08
7/6/09
1/22/10
8/10/10
2/26/11
9/14/11
4/1/12
10/18/12

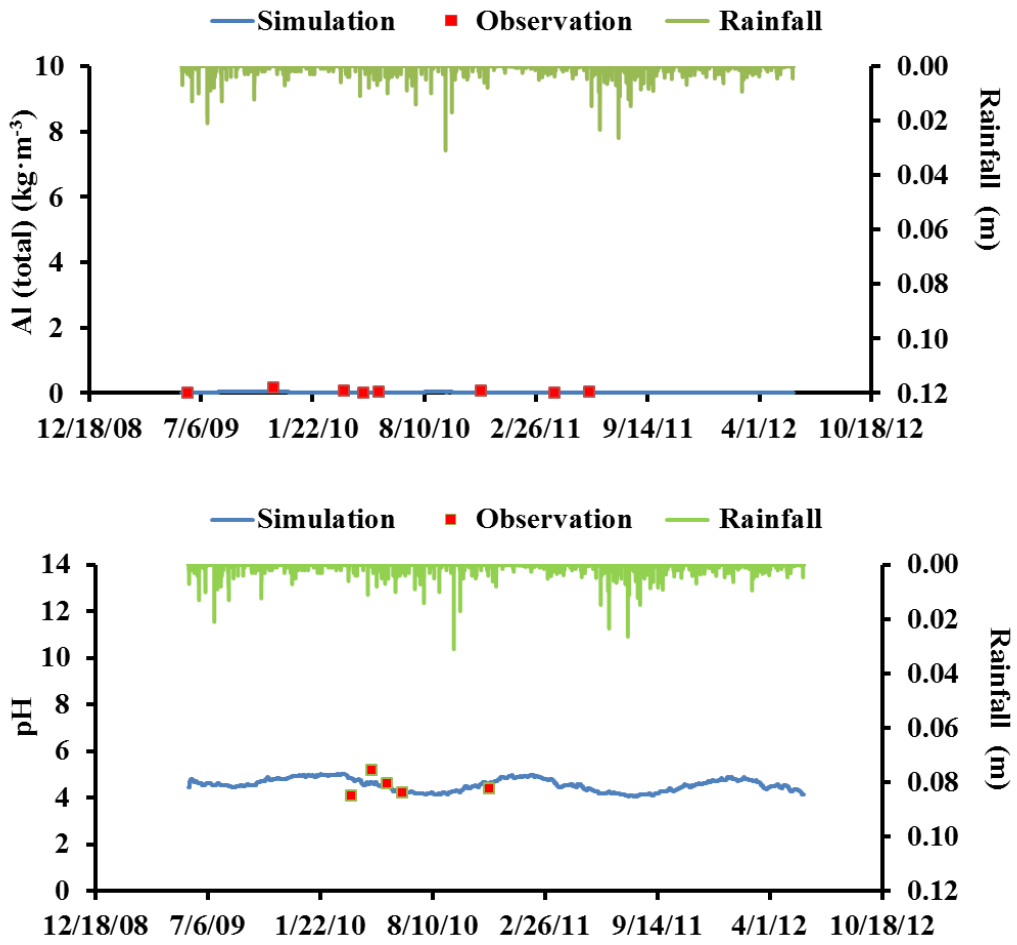

Figure 4.9 The simulations of SO_4, Fe (total), Ca (total), Al (total) and pH at the depth of 61 cm from 06/2009-06/2012 in plot 2.

4.5 DISCUSSION

4.5.1 The depth of appropriate amended layer

In Chapter 2.0 , it was mentioned that the thick amended zone results in more decrease in SO_4 and total Fe right below the amended zone than the effect of a thin amended zone at the same

depth. However, this conclusion was made under the ideal assumption that plot 2 i.e. 90% CR + 10% BR must be able to improve pH to 7.0 forever in the amended zone. Here, we investigate plot 2 again to see if this conclusion is still correct in a pH-dynamic environment and how much depth will be appropriate for the amended zone.

Similar to the sensitivity analysis in section 2.5.2, the same five scenarios are designed with different amended zone thicknesses in Figure 2.8 including one benchmark and four scenarios with different depths of amended zone. They are: (1) 0 m, (2) 0.2 m, i.e. layer 0; (3) 0.4 m, i.e. layer 0 and layer 1; (4) 0.82 m, i.e. layer 0, layer 1 and layer 2; and (5) 2.32 m, i.e. layer 0, layer 1, layer 2 and layer 3. Layers 4 and 5 are always non-amended zone. The root depth is the depth of amended thickness. Different from Chapter 2.0 , pH value is not constant any more. The initial pH in in the amended zone is defined to be 4.5 and the initial pH in the non-amended zone is still 2.6. All the initial chemical concentrations in the amended zone of the four remediated scenarios are given the same values as the value within 0~61 cm of plot 2 in Table 4.1. And the initial concentrations in the non-amended zone are the same as the values below 61 cm of plot 2 in Table 4.1. This design is much closer to the reality than the assumption in section 2.5.2.

The sensitivity simulations have been conducted in the same time period as section 2.5.2, that is from 06/01/2009 to 06/27/2010. Figure 4.10 shows the concentrations of SO_4 and total Fe within the six soil layers for plot 2. The left column is the concentrations of SO_4 in each soil layer and the right column are the concentrations of Fe (total). This figure is very similar to Figure 2.9 and it confirms that the conclusion made based on Figure 2.9 is also available in the pH-dynamic environment which has been mentioned at the beginning of this section. However, the sensitivity analysis of pH for each scenario in Figure 4.11 indicates that although pH value can be improved to around 5 in the amended zone, pH may not change much at a certain depth of

non-amended zone with the different depths of amended layers above it. For example in layer 2 i.e. 0.4~0.82 m, RMSE of pH between Scenario 1 and Scenario 2 is only 0.19. Also in layer 3 i.e. 0.82~2.32 m, pH is not improved much with the different depths of amended layers (i.e. Scenarios 1, 2 and 3) above it, even though the concentrations of SO_4 and total Fe in this layer are relevant to the thickness of above amended zone. RMSE of pH between Scenario 3 and Scenario 1 is 0.23, RMSE of pH between Scenario 3 and Scenario 2 is 0.14 and RMSE between Scenario 1 and Scenario 2 is 0.1. Thus, the thicker amended zone e.g. Scenario 3 does not improve pH dramatically.

In other words, it may not be necessary to design an amended zone as deep as 0.82 m as Scenario 3 (Layer 0 + Layer 1 + Layer 2) to neutralize the pH value at the depth of 0.82~2.32 m if this range of depth is non-amended. But it cannot be too shallow as the Mann-Whitney U-Test indicates that the pH value in layer 3 has no significantly difference only between Scenario 0 and Scenario 1 (0.2 m amended zone). So 0.4 m amended zone in Scenario 2 could be an appropriate choice if we want to neutralize the non-amended zone within 0.82~2.32 m. But this amended zone may not be adequate for the roots of plants. In future, a biological module may need to be considered in HTGCM to investigate the depth of amended zone dependent on both geochemistry and biology.

In the bottom layer 5, i.e. below 6.32 m, although the pH value is almost irrelevant to the depth of amended zone and the trends of pH seem very close to the scenario 0 in the short term e.g. one year, it is still hard to make a conclusion that the pH value in layer 5 will not be improved by the above remedial materials in future. The results of SO_4 and total Fe in such a deep layer are also not obvious in the short term. Thus the long-term simulation has to be conducted in the next section.

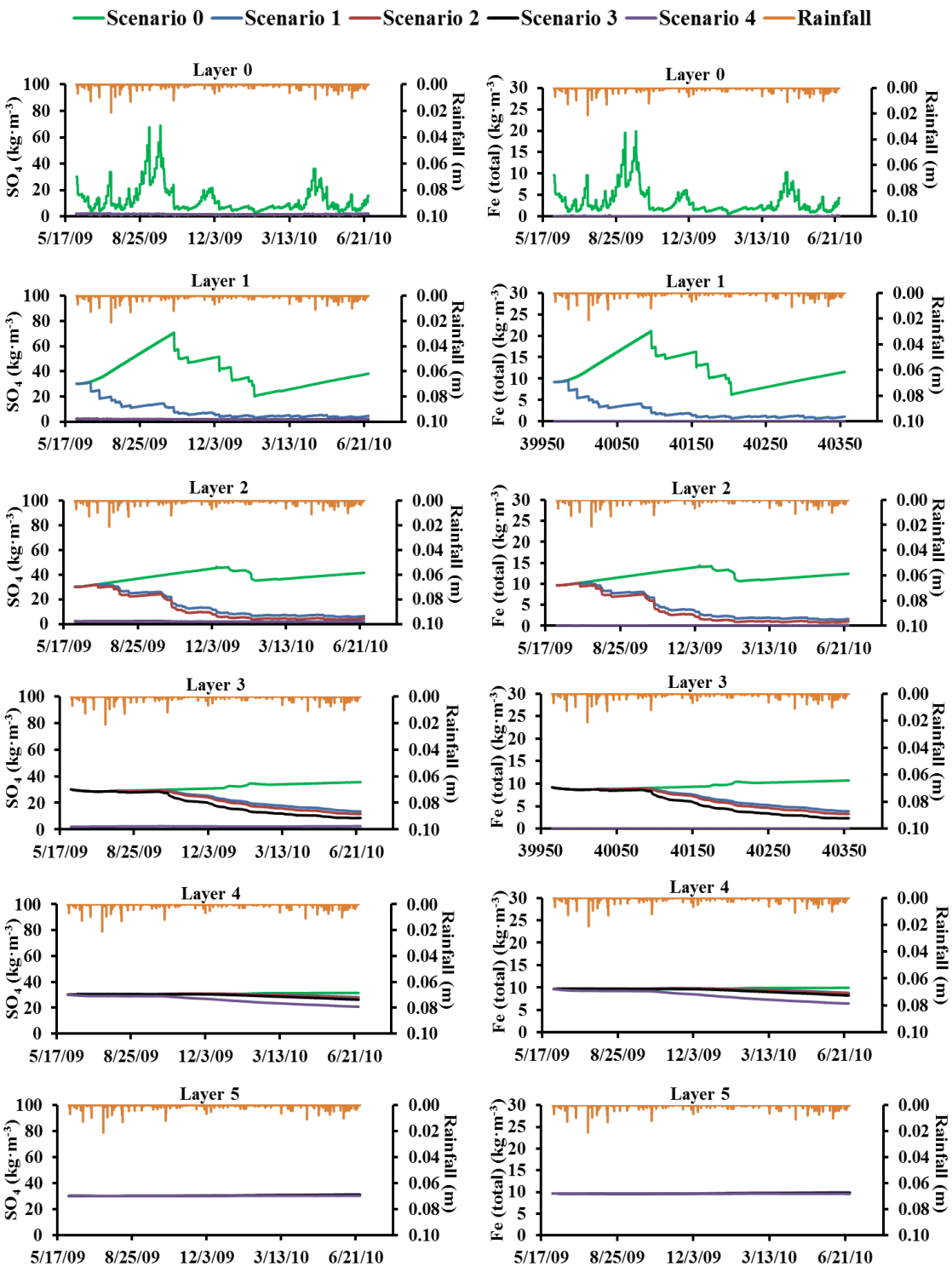

Figure 4.10 The simulations of the concentrations of SO_4 (left column) and total Fe (right column) for the four scenarios in the plot of 90% CR + 10% BR.

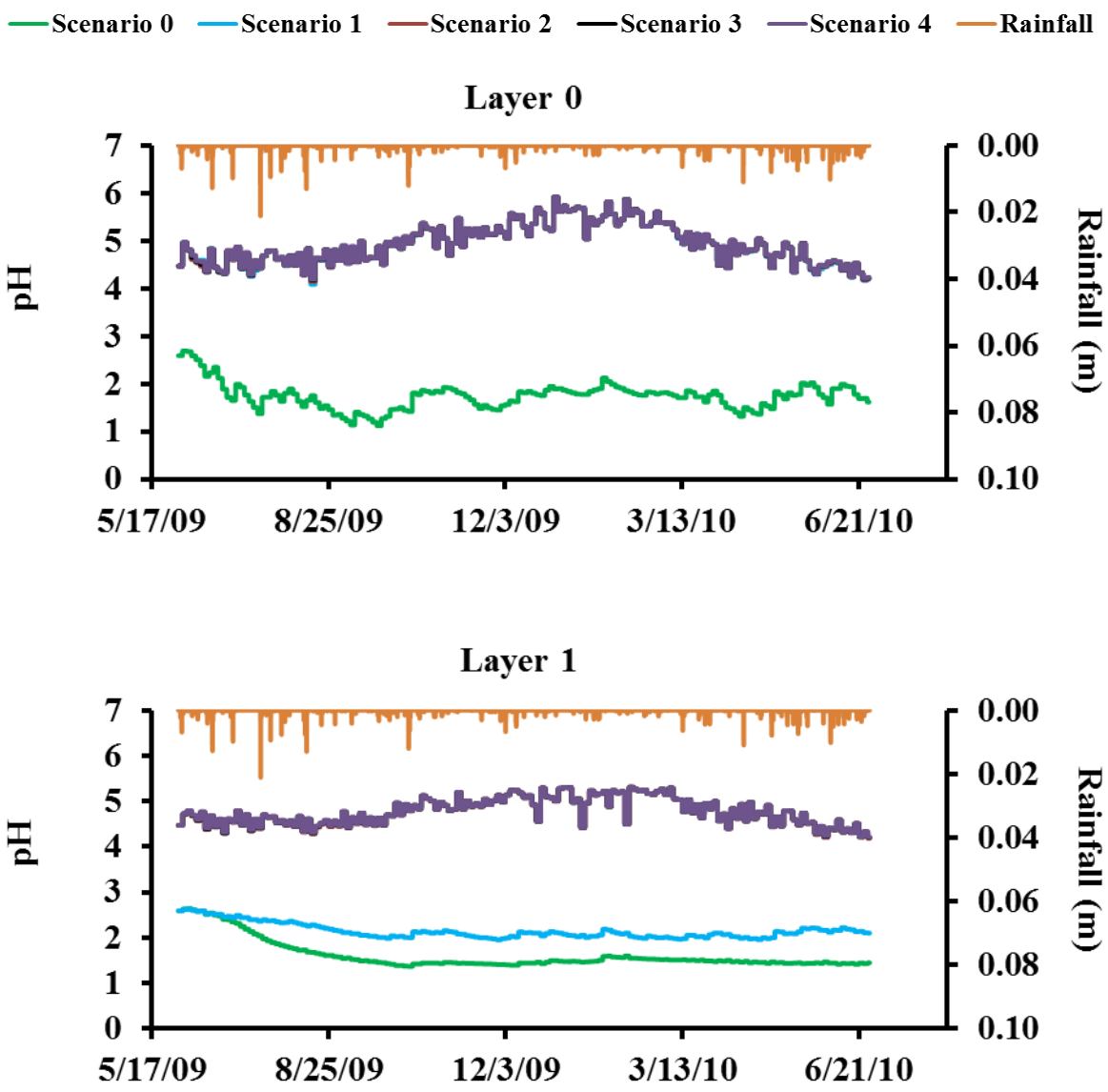
Scenario 0
Scenario 1
Scenario 2
Scenario 3
Scenario 4
Rainfall
Layer 0
pH
Rainfall (m)
7
6
5
4
3
2
1
0
0.00
0.02
0.04
0.06
0.08
0.10
5/17/09
8/25/09
12/3/09
3/13/10
6/21/10
Layer 1
pH
Rainfall (m)
5/17/09
8/25/09
12/3/09
3/13/10
6/21/10

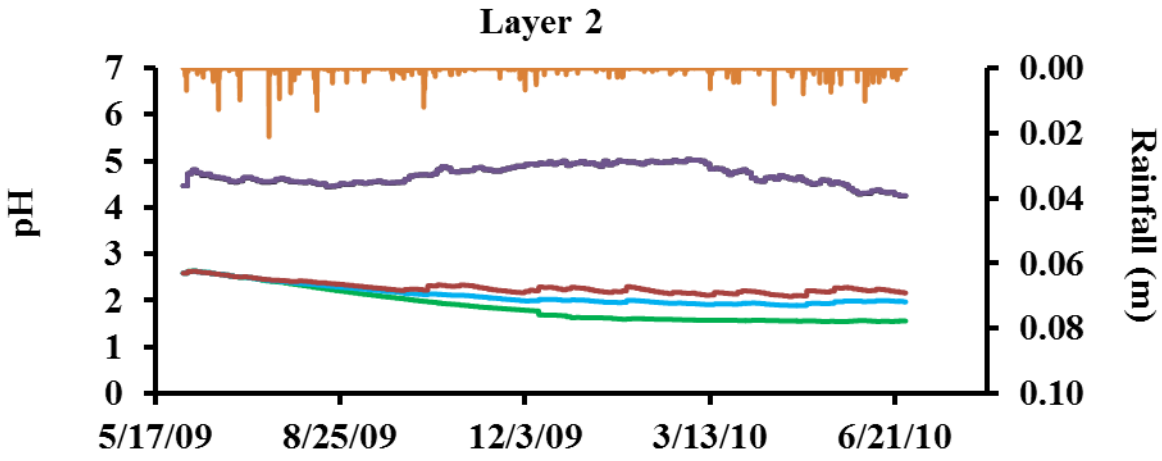
Layer 2
pH
Rainfall (m)
7
6
5
4
3
2
1
0
0.00
0.02
0.04
0.06
0.08
0.10
5/17/09
8/25/09
12/3/09
3/13/10
6/21/10

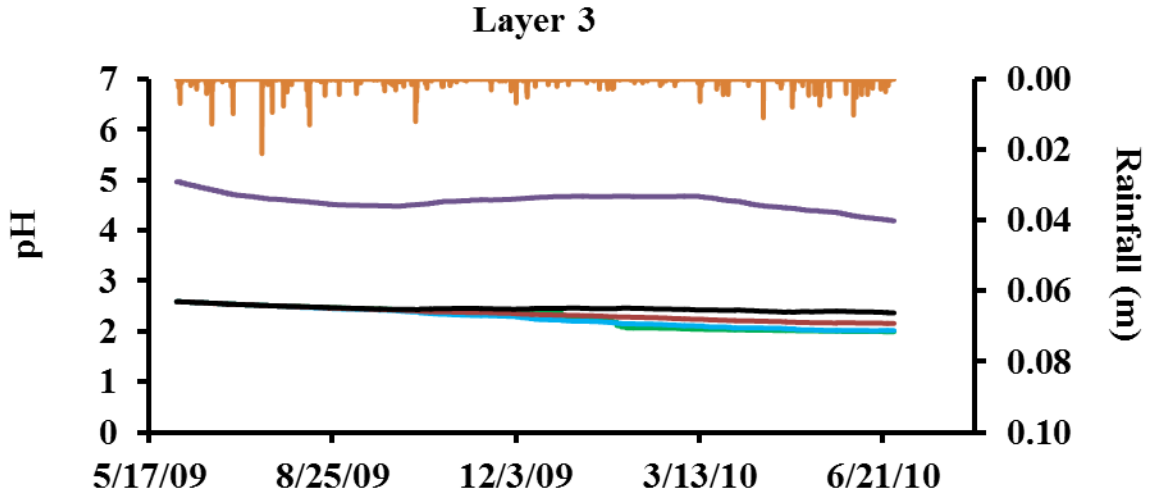
Layer 3
pH
Rainfall (m)
7
6
5
4
3
2
1
0
0.00
0.02
0.04
0.06
0.08
0.10
5/17/09
8/25/09
12/3/09
3/13/10
6/21/10

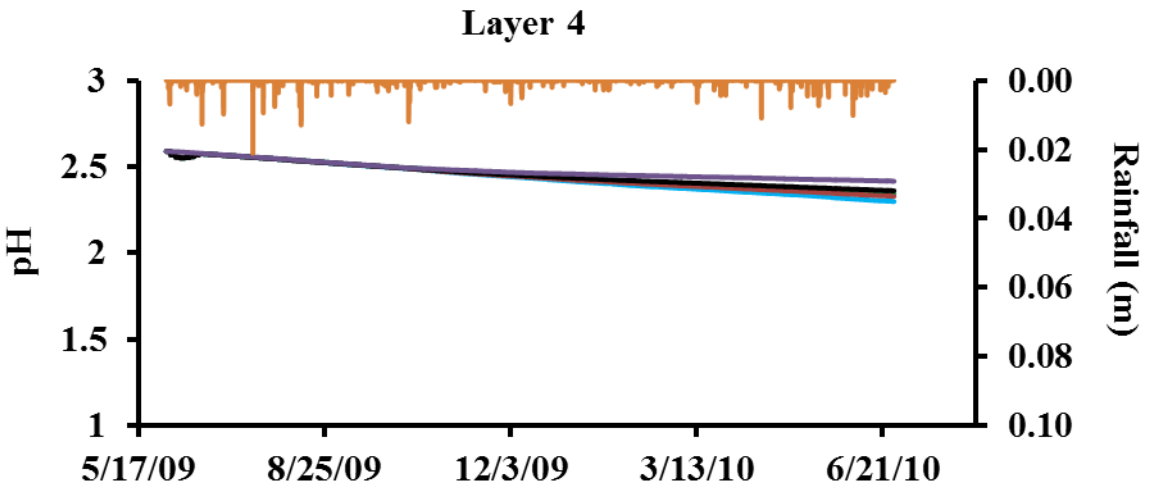
Layer 4
pH
Rainfall (m)
3
2.5
2
1.5
1
0.00
0.02
0.04
0.06
0.08
0.10
5/17/09
8/25/09
12/3/09
3/13/10
6/21/10

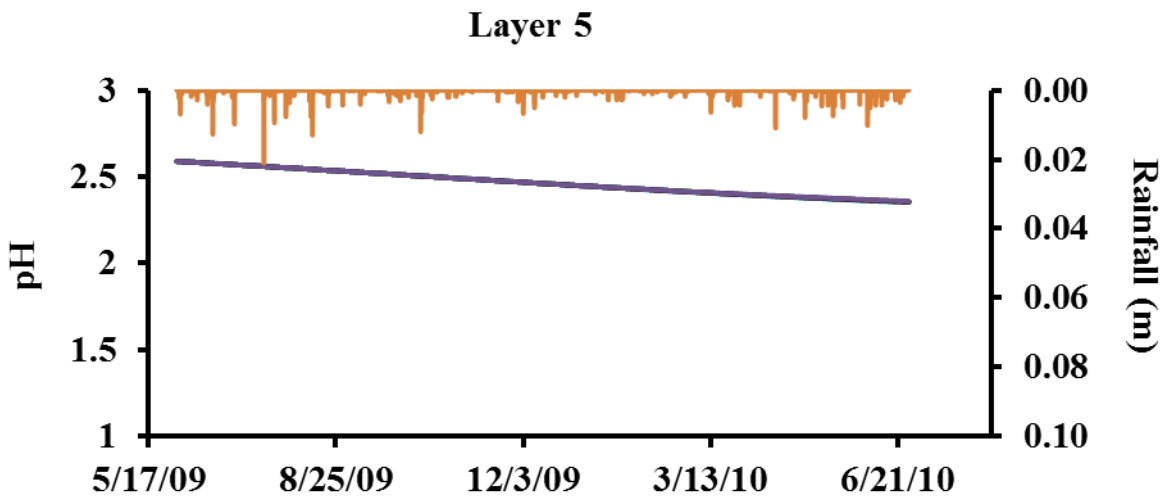

Figure 4.11 The simulations of pH for the four scenarios in the plot of 90% CR + 10% BR.

4.5.2 Long-term impact of remediation

What the effects of amended zone in a long-term period are on the amended zone and deeper non-amended zone remains to be solved in this section through conducting ten-year simulations with the soil properties in plot 2. The benchmark is still Scenario 0 (non-amended scenario) in section 4.5.1, that is to assume 100% CR in all the layers. The other scenario is 90% CR +10% BR within the top three layers. That is identical to Scenario 3 in section 4.5.1. The weather of 06/2009-06/2010 is repeated for ten years i.e. 06/2009-06/2019 so that HTGCM v2.0 is able to "predict" the outcomes in future for the scenarios of remediation and no remediation.

Figure 4.12 and Figure 4.13 show the concentrations profiles of SO_4 and Fe (total) between non-amended scenario and amended scenario for initial, 3th, 5th and 10th year. It is obvious that the profiles of SO_4 and Fe (total) dramatically decrease in the amended scenario (blue curves) compared to the non-amended scenario (red curves) from the beginning to the 10th

year. The difference between the two scenarios for the concentrations of SO_4 at the bottom layer is ~30 kg/m^3 and Fe (total) is ~ 10 kg/m^3. Such a significant impact of the amended zone on the bottom non-amended layer is not obviously indicated by the short-term simulation in Chapter 2.0 . This is not obvious for total aluminum in Figure 4.14 as the decrease is 0.8 kg/m^3 and the decrease of total calcium is only 0.02 kg/m^3 in Figure 4.15.

Also, in 3th, 5th and 10th years, the concentration profiles of SO_4 and total Fe in the non-amended scenario (i.e. CR) show a wave-shape profile that migrates from the upper layer to the bottom layer in the non-amended scenario. The concentrations of SO_4 and total Fe are accumulating in the deeper layer. The pattern of wave migration is similar to the other related research [*Gerke et al.,* 1998]. The same phenomenon occurs in the profile of total aluminum. However, the concentrations of total aluminum are low and the wave-shape profile is not as obvious as for SO_4 and total Fe. Regarding the concentrations of total calcium, they are also too low in CR and the migration of total calcium in CR is difficult to be seen. Such a wave migration may be related to the pyrite oxidation front but more field experiments are needed to explain it.

Figure 4.16 shows the comparisons of pH between the non-amended scenario and the amended scenario for initial, 3th, 5th and 10th year. The pH value in the amended scenario is higher than the non-amended scenario within the upper layers. But in the deep non-amended zone such as in the bottom layer 5, i.e. below 6.32 m, the difference between the amended scenario and the non-amended scenario is very small in these 10 years. Therefore, the effects of remediation in the deep non-amended layer are found through the decrease of SO_4 and Fe (total), while the impact on pH is not distinct in such a deep layer for ten-year simulation.

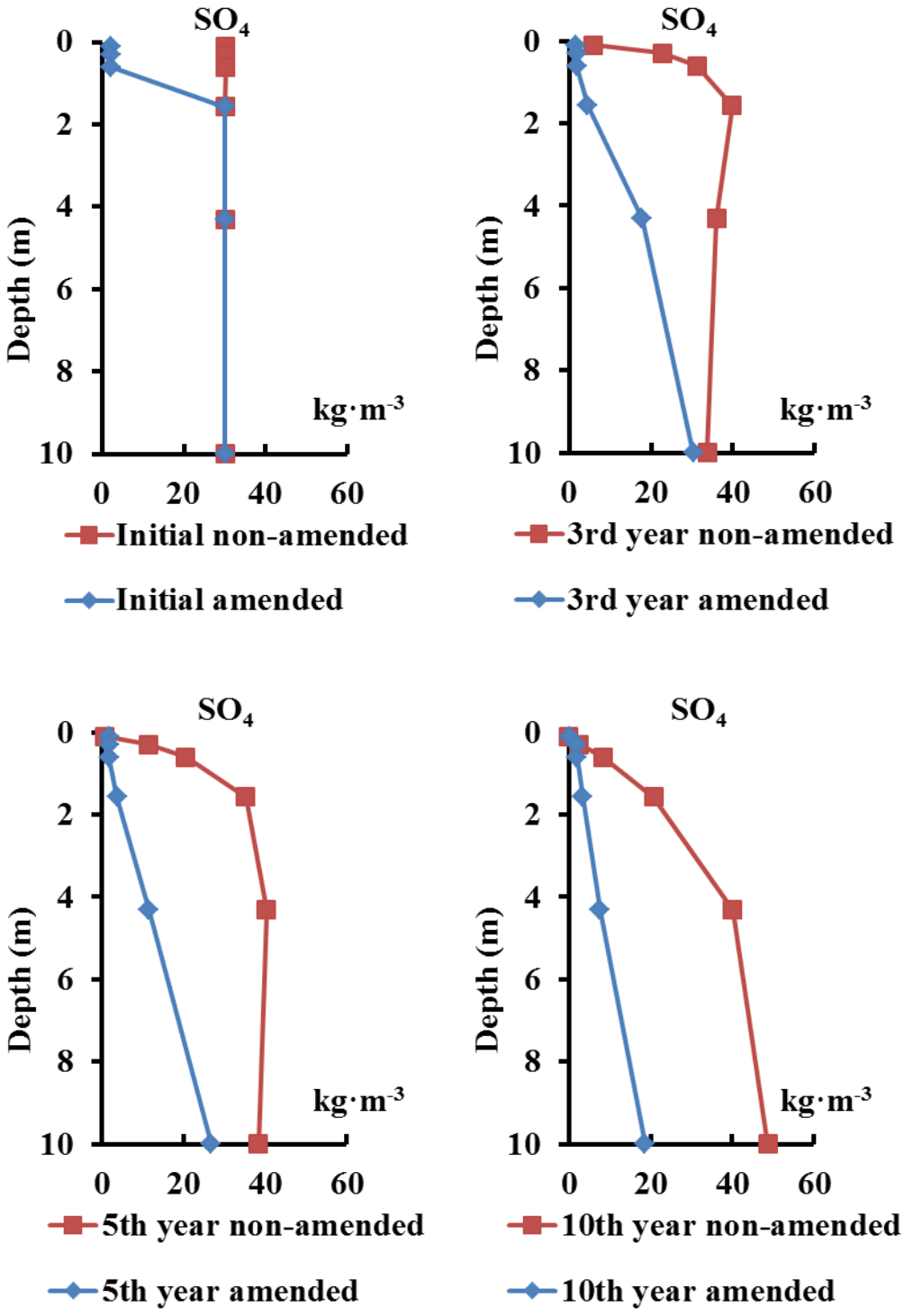

Figure 4.12 The comparisons of SO_4 between non-amended scenario and amended scenario for initial, 3th, 5th and 10th year.

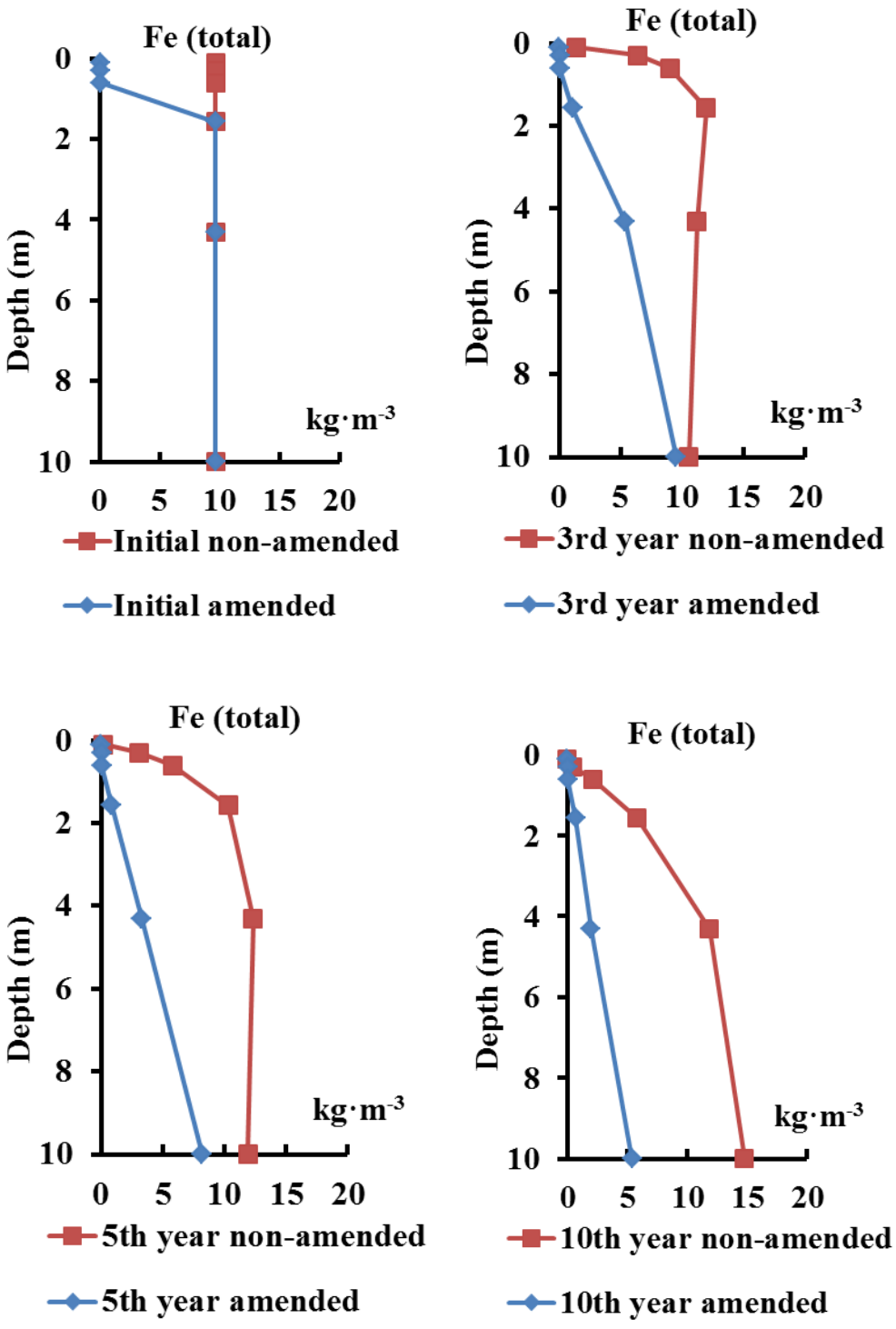

Figure 4.13 The comparisons of Fe (total) i.e. Fe(II) + Fe(III) between non-amended scenario and amended scenario for initial, 3th, 5th and 10th year.

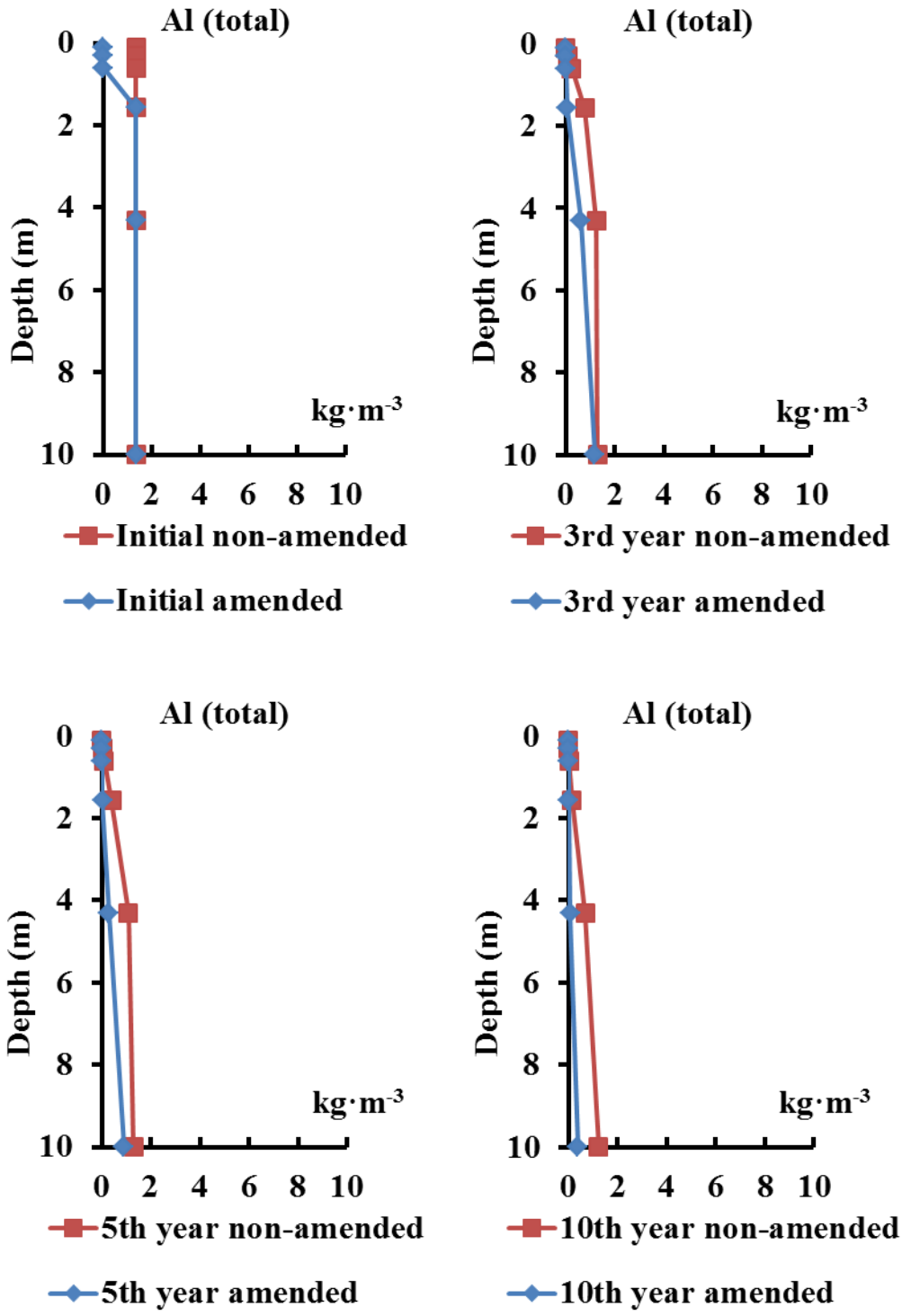

Figure 4.14 The comparisons of total aluminum between non-amended scenario and amended scenario for initial, 3th, 5th and 10th year.

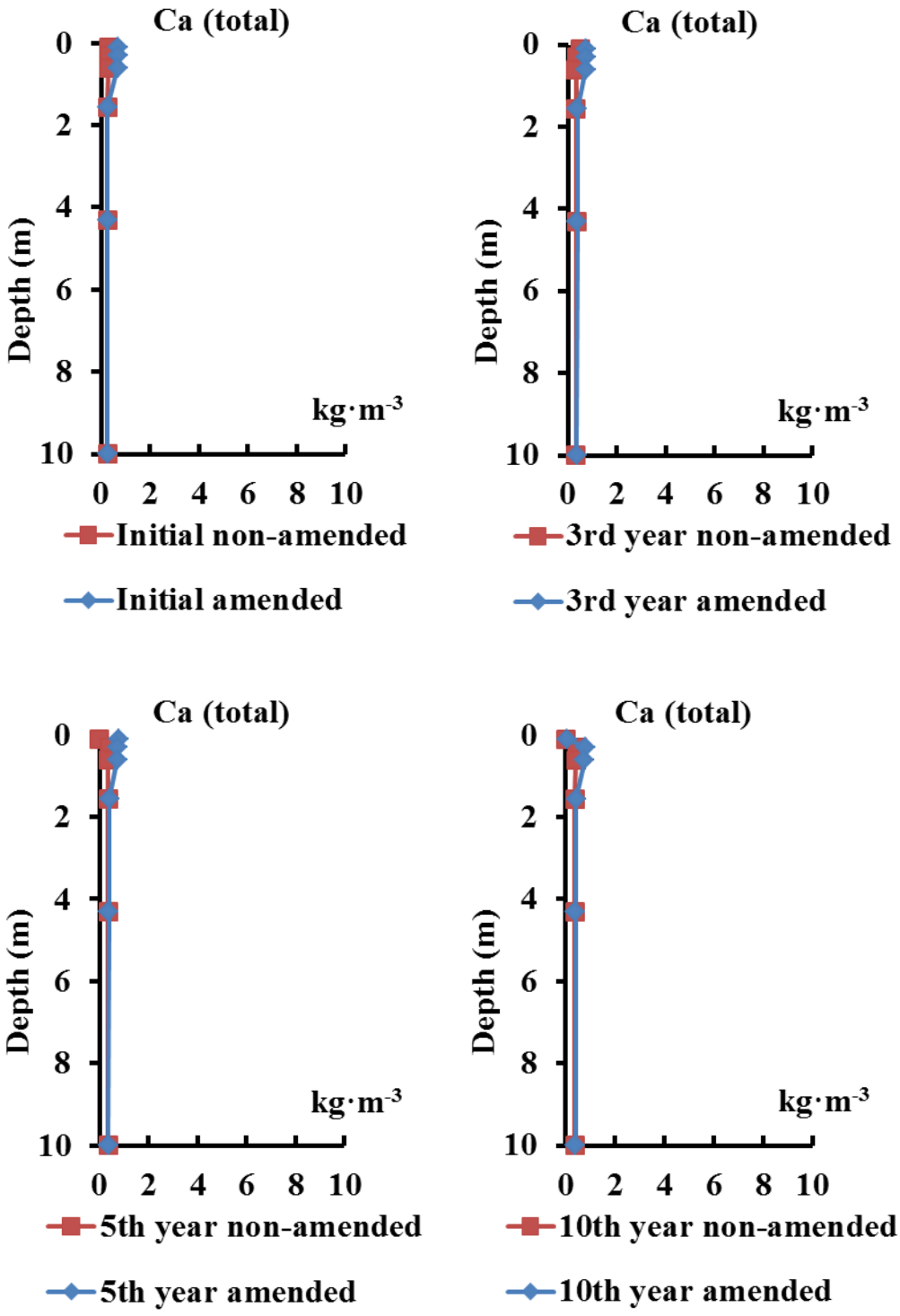

Figure 4.15 The comparisons of total calcium between non-amended scenario and amended scenario for initial, 3th, 5th and 10th year.

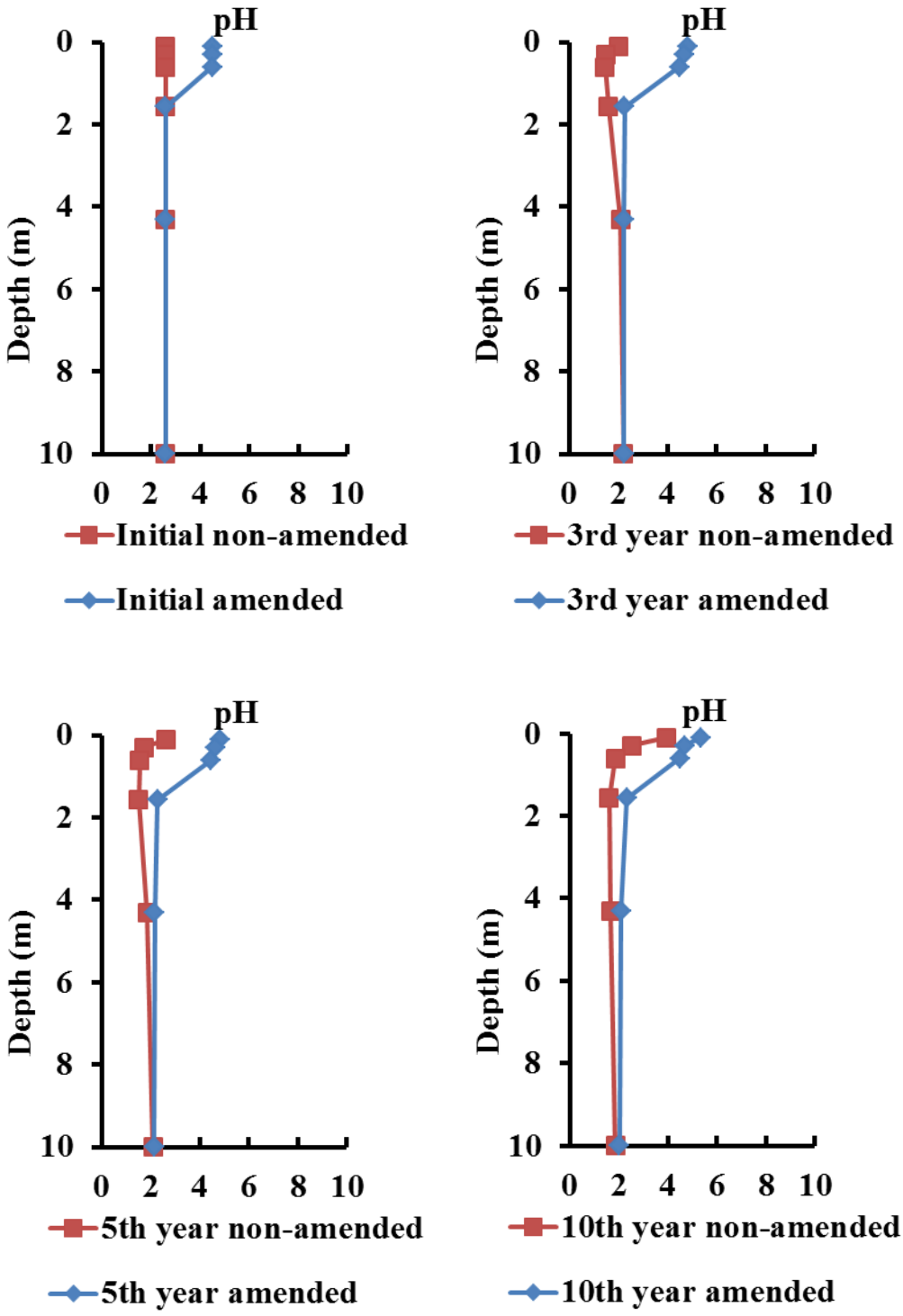

Figure 4.16 The comparisons of pH between non-amended scenario and amended scenario for initial, 3th, 5th and 10th year.

4.6 CONCLUSIONS

This chapter improves HTGCM to be a pH-dynamic model by coupling PHREEQC. Such a great improvement allows the model to be better applied in the real environment e.g. the CR plot and the remediated plot without the assumptions of the constant pH value. More chemicals and secondary minerals are included in the calculation, although pyrite oxidation is still the dominating reaction in the model. The simulation results lead to the following conclusions.

Firstly of all, the one-year simulation result in this chapter is similar to the results in section 2.4 and they all catch the pattern of observation. In this chapter, pH value is stable for one-year simulation in plot 1 and plot 2. It means that the assumption of the constant pH value in Chapter 2.0 is reasonable for the short-term period.

In the three-year result, the concentrations of SO_4 and total Fe are more seasonal in plot 1 compared to plot 2. The remediation impact of plot 2 shows lower concentrations of SO_4, Fe (total) and total aluminum at 61 cm. Also pH is enhanced to be less acidic in plot 2. But calcium is relatively stable.

An appropriate depth of amended zone is obtained based on the further sensitivity analysis in this chapter. That is 0.4 m amended zone may be a good choice if we want to neutralize the non-amended zone at the depth of 0.82~2.32 m. However, this conclusion may not be true if the mixture is not 90% CR + 10% BR since the sensitivity analysis was only conducted on this combination so far.

The long-term simulation attempts to show the effects of remediation in 10 years: (1) SO_4 and Fe (total) are significantly reduced at the bottom layer in the amended scenario compared to the non-amended scenario, the concentrations of total aluminum are less reduced and the concentrations of total calcium are too low for its changes to be seen; (2) the migration of wave-

shape profile of chemical concentrations are exiting for SO_4, Fe (total) and total aluminum in the non-amended scenario .i.e. 100% CR; (3) in the amended scenario, pH value is not enhanced much in the deep non-amended zone. All these conclusions from the long-term simulation are the initial outcomes which were obtained under the conditions of 10 years repeated forcing data and the reason for concentration migration has not been proved by laboratory experiment yet. Moreover, the long-term impact of the amended scenario on the deep non-amended layer has to been investigated further in the laboratory and field as well.

5.0 CONCLUSIONS AND FUTURE WORK

5.1 CONTRIBUTIONS

This study has built a hydro-thermal-geochemical model (HTGCM) [*Xu and Liang*, 2013; *Xu et al.*, 2013a; *Xu et al.*, 2013b] to investigate the environmental impacts of beneficial reuse of bauxite residue (BR) in coal-refuse (CR) piles. The main contributions and findings in the entire study are summarized as model development and simulation, field work and laboratory testing.

First of all the findings of the model development and simulation are listed from points (1) to (7):

(1) HGCM [*Xu et al.*, 2013a] is the version before HTGCM v1.0. It is developed from the basic framework of DHSVM [*Wigmosta et al.*, 1994]. Hydrological improvements in DHSVM e.g. including six soil layers, calculating infiltration with the slope impact and modifying free drainage boundary have been completed to satisfy with the deeply and hilly unsaturated zone in CR piles. The high resolution DEM 3×3 meters has been used in the model to deal with the complex terrain for the study site.

(2) The main functions e.g. shrinking-core module and oxygen transport module in PYROX [*Wunderly et al.*, 1996] have been programmed and coupled into the model, which allow the model to be able to calculate pyrite oxidation in a geochemical manner. Due to the functions of pyrite oxidation in PYROX and the simulation of water cycle in DHSVM, the new

model is able to mimic the mainly reactive transport in CR areas. Meanwhile the governing equation has been built into HGCM so that the liquid-phase concentrations can transport in the vertical direction of soil and the mass balance concept has been applied into the flow routing for the horizontal transport. The simulation results and the observations are consistent in showing that the concentrations of SO_4 and Fe (total) are significantly reduced in the remediated plots. Also in the remediated plots, the concentrations decrease not only in the amended zone but also in the non-amended zone. Moreover the thicker amended zone may decrease more the concentrations of SO_4 and Fe (total) at the some depth below it. Besides, pH values at 61 cm in the amended plots were observed to be higher than the coal-refuse plot.

(3) A thermal transport module has been developed into HTGCM v1.0, which includes not only the heat from the natural environment e.g. solar radiation but also the heat from the chemical and biological oxidation. Importantly, it is able to calculate the soil temperature in each layer, which DHSVM is unable to do so far. The model has been calibrated and validated in the remediated plot i.e. 90% CR + 10% BR. The soil moisture and soil temperature in this plot captured the patterns of observation very well. The analysis for the new parameters in the thermal module provide a few significant information about the sensitivity of heat parameters for soil moisture and soil temperature, which gives suggestions for future users.

(4) In addition, the impact of vegetation on soil temperature decreases with the soil depth. Below the vegetation-impact depth, the effect of vegetation on soil temperature is almost gone. But, this depth is dependent on plant's properties e.g. root depth. To date, the role of vegetation is mainly discussed as an aspect of soil temperature, which may pave the way to assess the heat pollutant in CR areas. Given that the role of plants affecting temperature is important, the

interaction between plant growth and chemical activities is another important topic that needs further research in order to see a broad view for the role of vegetation in the remediated area.

(5) In HTGCM v2.0, PHREEQC [*Parkhurst et al.*, 1980; *Parkhurst*, 1995; *Parkhurst and Appelo*, 1999] has been coupled into the model and it allows the model to calculate not only SO_4 and Fe (total) but also include total calcium, total aluminum, pH and many other chemicals. It is a hydro-thermal-geochemical model with dynamic pH values and more initial solutions and solid compositions have been encompassed compared to the basic model. Although the input data require more information in this sophisticated model, it is better to represent the pH-dynamic environment in the field instead of making assumptions of constant pH for each plot.

(6) Comparing the HGCM with HTGCM v2.0, the one-year results from HTGCM v2.0 convince us that the assumption of constant pH in the basic modeling development is reasonable for the short-time period. But it may not be true for the long-term simulation. The sensitivity analysis shows that 0.4m of 90% CR + 10% BR may be good to neutralize the non-amended zone within 0.82~2.32m. However, it may be changed by different compositions of CR and BR.

(7) Long-term simulation indicates that the effects of the amended zone will influence the concentrations of SO_4 and Fe (total) in the deep non-amended zone significantly in 10 years. The concentrations of total aluminum in the deep non-amended zone are also reduced by the above remediation but not as obviously as SO_4 and Fe (total). The concentrations of total calcium are much lower than the other three elements and the variation is very small in the non-amended zone. The pH value in the amended zone has been enhanced to be less acidic, but in the deep non-amended zone it is not improved as obviously as the above amended zone. The long–term modeling results also show that the concentrations of SO_4, Fe (total) and total aluminum migrate

in the CR pile, which has been documented by other related work. However, it is just an initial result for such a long term period and it needs the long-term experiment to verify this outcome.

The contributions in the field work are including from points (8) to (9):

(8) The soil moisture sensors had been installed in 2010 in the study site and the soil temperature sensors were installed in 2012. The soil moisture and soil temperature data have been downloaded frequently. The site boundary was measured by GPS equipment. The lysimeters were installed in 2009 by our collaborators who provided the chemical concentrations and pH in the field for us.

(9) We purchased our solar radiation sensor and installed it into a weather station nearby. Some of the solar radiation data were from NOAA National Solar Radiation Data Base before we installed the radiation sensor. All the other weather information in this research were from the weather station.

Finally, the work of the laboratory testing is summarized as (10):

(10) Different soil samples have been collected from the field and they have been used to determine the soil properties for the model. The chemical components were obtained based on the laboratory measurements and the stoichiometry calculation. The chemical species (e.g. ferric precipitate) was found and the chemical measurements were completed with the help of our collaborators in the environmental group.

Overall, this study provides a scientific approach to investigate the environmental impacts of bauxite residue in the coal-refuse pile at Mather, PA. Numerous simulations, field work and laboratory tests have been completed. To date, the combination of 90% CR and 10% BR in this study site has proven advantageous to neutralize the acidic water within a certain depth and reduce the chemical concentrations of SO_4, Fe (total) and total aluminum in both

amended zone and non-amended zone. However, there is still further work needed on this remediation protocol before it is spread to the entire CR area or other similar areas.

5.2 FUTURE WORK

The future work is suggested to be as follows, including both modeling developments and experiments.

Two main improvements are needed for the modeling development:

(1) Vegetation plays an important role in remediation. It not only affects the soil temperature, but also may change the flow direction, stabilize the solid precipitates and accelerate pyrite oxidation [*Johnson and Hallberg*, 2005]. In order to assess the effects of vegetation further, it is recommended to develop a biological module into HTGCM v2.0 to deal with the interaction between the plant growth and the bio-geo-chemical environment around it. Meanwhile, the model has to be tested at the watershed scale with all the new modules in the future.

(2) Underground mine fires occur around the world and they may not only bring air pollutant, but also could also change the soil temperature and the oxidation rate. To date, this process has not been considered in HTGCM v2.0 yet and more work may be needed to improve the module of thermal transport.

The potential experiments may have to be conducted in the future:

(3) The processes of armoring and precipitation could change the soil porosities e.g. soil porosity and hydraulic conductivity, which is one of the ways of reducing the reactive surface of

pyrite and prevent penetration of oxygen and water from air into the soil. However, more laboratory experiments are needed to prove this hypothesis.

(4) The best composition of CR and BR in the mixture is yet unknown, although the current design i.e. 90% CR + 10% BR in the field has shown the ability to neutralize the acidic water and lower the concentrations of SO_4, Fe (total) and Al (total) in the CR area. Thus, more laboratory experiments are suggested to be conducted to investigate the optimum composition in the future. The model would also be able to predict the chemical concentrations for this best composition from the laboratory to the field.

(5) The long-term simulation shows the migration of chemical concentrations e.g. SO_4 and Fe (total) in the CR profile, which may be relevant to the pyrite oxidation front. Thus, a down-scaling experiment is suggested to investigate this relation. Meanwhile, it has to verify if the significant decrease of SO_4 and Fe (total) can be shown in the non-amended zone in the amended scenario as the long-term modeling results already indicated.

(6) The International Aluminum Institute have pointed out that heavy metals and radioactive materials are quite low in BR and they have proved that adverse health effects from BR are unlikely to happen [*International Aluminium Institute*, 2010]. Also the safety report of BR from the source area does not show high concentrations of heavy metals or radioactive materials. Even so, one still needs to be careful to do the experimental detection in order to make sure it is safe to use BR for the entire site and other similar sites in the future.

APPENDIX A

MODEL SETUP AND OUTPUT

The model is designed for the three stages: basic framework HGCM (couple DHSVM v3.0 with the module of pyrite oxidation and advection-dispersion transport) [*Xu et al.*, 2013a], middle level HTGCM v1.0 (add thermal module) [*Xu and Liang*, 2013] and sophisticated level HTGCM v2.0 (couple middle level model with PHREEQC) [*Xu et al.*, 2013b] . In this appendix, it describes the model setup for the each stage.

A.1 HGCM

A.1.1 HGCM setup

The Distributed Hydrology Soil Vegetation Model [*Wigmosta et al.*, 1994] version 3.0 (i.e., DHSVM v3.0) is the basic hydrological framework during the entire modeling development. In this stage, the basic level model HGCM incorporates DHSVM v3.0 with the processes of pyrite oxidation and advection-dispersion transport. Therefore, most of the input files of this stage are designed based on the format of DHSVM v3.0. The input folders for DHSVM v3.0 are

classified: ArcGIS maps, meteorological data, model state data and configuration information provided by the DHSVM website [*The Land Surface Hydrology Research Group University of Washington*]. Thus, this section only emphasizes on the new input data in the improved model.

In the ArcGIS maps folder, a new mask map was added to distinguish coal-refuse (CR) and non-CR region. The cell marked as 1 represents CR area. If marked as 0, the cell is non-CR area. In CR region, the model calculates the pyrite oxidation, while outside the region the module of pyrite oxidation will not serve in the model. No matter inside or outside CR region, all the cells are able to address the one dimensional advection-dispersion transport and the two dimensional flow routing. This design saves the computer memory and also reduces the time of calculation, because the chemical-related functions in non-CR region are inactive and the parameters would not be given memory in this area. This characteristic is inherited by the other two modeling stages. This map has to be converted from text format into binary format as the map of modeling mask (control modeling area) in DHSVM v3.0 before running the model. The command of format conversion can be executed as follows:

$ ./myconvert ascii char CoalMap.txt ../arcinfo/ CoalMap.bin row_number column_number

In this command, myconvert is an executable file in the directory of program in DHSVM, which needs to be compiled firstly based on the manual of DHSVM. CoalMap.txt is the CR map in ASCII format, CoalMap.bin is the CR Map in binary format, row_number and column_number are the total number of rows and columns in the entire map.

The meteorology folder includes the time series of air temperature (℃), wind speed (m/s), humidity (%), short wave radiation (Watts/m^2), long wave radiation (Watts/m^2), soil temperature (℃) in each layer and rainfall (m). This is the input format when the option of

Sensible Heat Flux is turned on. This file indicates that in the basic stage of model development, the soil temperature should be known when the model calculates sensible heat flux. It will not work if soil temperature is not provided.

In the model state folder, a few files were added to initialize the chemical concentrations and parameters of pyrite oxidation and chemical transport:

- Oxygen_con.txt: initializes oxygen concentration in pore space. The value in every line represents the oxygen concentration in one layer and the unit is kg/m^3.
- Old_rc.txt: gives radius of mineral particle for every layer and the unit is meter.
- Chemical_proportion.txt: represents the proportion of total sulfur (negative divalence for oxidation) and total Fe (i.e. Fe(II) + Fe(III)) in solid and the unit is kg/kg.
- Concentration.txt: initializes the concentrations of total sulfur (the main sulfur specie here is sulfate) and total Fe (kg/m^3) in the moisture within every layer.
- Transport_parameter.txt: gives the parameters of advection-dispersion for sulfate and Fe species at a constant temperature. These parameters are including: number of chemical elements, name of chemical elements, solute/insoluble index, diffusion coefficients and the temperature-dependent rate for the diffusion coefficients.

In the configuration file, it saves the path of all the input files and the parameters of soil and vegetation. Also the paths of all the maps e.g. the modeling mask and the CR map have to be provided in this file. The options of sediment and road routing are turned off.

A.1.2 HGCM output

Based on the design of DHSVM v3.0, the output format is divided into pixel and image. Here, the pixels are the points in the study plots where the moisture sensors and lysimeters were installed.

In the basic stage of model development, the model is not only able to export all the variables in DHSVM v3.0 e.g. soil moisture, discharge, evaporation, percolation etc., but also gives the new variables, for instance, the concentrations of SO_4 and Fe (total) in liquid, oxygen concentration in pore space and radius of mineral particle. These variables are owned in all the soil layers in every cell.

A.2 HTGCM V1.0

A.2.1 HTGCM v1.0 setup

In this middle level stage of the model development, the heat module is designed to calculate soil temperature, biological oxidation heat and chemical oxidation heat. In this stage, the model not only keeps the same input files as the first stage, but also includes more information in order to satisfy with the requirement of energy cycle calculation.

In the ArcGIS folder, all the maps remain the same as the first stage. However, the sources of heat from pyrite oxidation and solar radiation are utilized to calculate the soil temperature inside CR region, while outside CR area the soil temperature would be only affected by the solar radiation without the consideration of oxidation.

In the meteorological file, the soil temperature is not required in this stage. This is a great advantage when there is no observed soil temperature provided. The model can skip to read the soil temperature data even though the soil temperature is provided in the meteorology file.

In the model-state folder, a file heat_par.txt is added to store the heat parameters, for example the heat production coefficients for the two pyrite oxidation processes (chemical and biological processes) and the heat decay coefficients for the two processes.

In the configuration file, most of the settings are the same as the first stage. The option of sensible heat flux must be turned on to calculate soil temperature.

A.2.2 HTGCM v1.0 output

In this stage, the output not only includes all the variables in HGCM, but also has the results of soil temperature, heat from chemical oxidation and biological oxidation.

A.3 HTGCM V2.0

A.3.1 HTGCM v2.0 setup

HTGCM v2.0 not only has all the features of HGCM and HTGCM v1.0, but also calculates more chemical elements and solid components.

In the ArcGIS folder, another map was introduced into the model to control the boundary of PHREEQC region. The cell marked as 1 means PHREEQC area and the capabilities of PHREEQC are active, on the opposite, the cells are given 0 and PHREEQC is turned off. It can

reduce the computational resources significantly if this map constrains a small PHREEQC region. The users will not waste too much memory or time to calculate the chemical processes in the area that are not necessarily considered. This map also has to be converted into binary file and the data format is also converted from ASCII to character string, which are similar to the CR map mentioned in the first stage. The following command shows how to convert the file:

$ ./myconvert ascii char phreeqcMap.txt ../arcinfo/phreeqcMap.bin row_number column_number

In the meteorology file, no modification has to be made in it. The model is able to calculate soil temperature as the middle-level development.

In the model-state folder, more chemical solutions and solid compositions were added into the model. For instance, calcium, aluminum, sodium, magnesium, potassium, silicon, phosphorus, chlorine and manganese are considered in Chapter 4.0 . Following lists the modification in this folder:

- The new files C_P1.txt and C_P2.txt are created in this stage to replace the file of Concention.txt to initialize the new chemical elements and solid components for plot 1 and plot 2. The file format is compatible to the input of PHREEQC. Here is an example of C_P1.txt for plot 1.

  SOLTUION 1-3

Temp	23
pH	2.2
units	ppm
density	1
S(6)	5880 as SO4

Fe	1200
Ca	430
Na	200
Mg	65
K	7.6
Si	177.9 as SiO2
P	15
Al	280
Cl	100
Mn	8.9
-water	1 # kg

SOLUTION 4-6

temp	10.0
pH	2.4
units	ppm
density	1
Fe(3)	5500
S(6)	22800 as SO4
Ca	460
Na	365
Mg	65
K	4.8
Si	186.4 as SiO2

P 52

Al 2000

Cl 100

Mn 39

-water 1 # kg

END

EQUILIBRIUM_PHASES 1-3

Quartz 1.5 130

Gypsum -0.04 0.75

Calcite -12 1.4

EQUILIBRIUM_PHASES 4-6

Quartz 1.76 130

Gypsum 0.15 0.75

Calcite -12 1.4

REACTION 1-3

K-mica 0.65

Kaolinite 0.35

0.0000015 moles

REACTION 4-6

K-mica 0.65

Kaolinite 0.35

0.0000015 moles

SELECTED_OUTPUT

-reset false

USER_PUNCH

-Heading charge H O S Fe Ca Na Mg K Si P Al Cl Mn pH

10 PUNCH charge_balance

20 PUNCH TOTMOLE("H"),TOTMOLE("O"),TOTMOLE("S") , TOTMOLE("Fe"), TOTMOLE("Ca")

30 PUNCH TOTMOLE("Na") , TOTMOLE("Mg"),TOTMOLE("K"),TOTMOLE("Si"), TOTMOLE("P"), TOTMOLE("Al")

40 PUNCH TOTMOLE("Cl"), TOTMOLE("Mn"), -LA("H+")

END

The explanations of SOLUTION, EQUILIBRIUM_PHASES, REACTION and SELECTED_OUTPUT can be found in the manual of PHREEQC.

- Extend transport_parameter.txt: the transport parameters are given to all the new chemical elements.
- Database: a database was created into this folder i.e. phreeqc.dat that includes a number of mineral reactions and the reactive rates. It was the database of PHREEQC, which was downloaded from the USGS website. However, it is not adequate to deal with all the minerals such as Dicalcium silicate and Gehlenite. Therefore, this database was enlarged by the other databases. For instance, there are a few additional databases provided in the package of the Windows version of PHREEQC such as llnl.dat, which includes of the above two mineral reactions.

In the configuration file, the paths of the modeling mask map, the CR map and the PHREEQC map should all be set into the file.

Moreover, the library of the latest version of IPhreeqc i.e. v3.0.6-7757 was included into the "makefile" in model. Following shows how to generate the library from IPhreeqc and how to compile the model:

- Download IPhreeqc package "iphreeqc-3.0.6-7757.tar.gz" from USGS website [*USGS PHREEQC*].
- Decompress the above file by the command:

  $ tar xvzf iphreeqc-3.0.6-7757.tar.gz
- Go to the directory of iphreeqc-3.0.6-7757, create a new folder "build" under this directory with the command:

  $ mkdir build
- Configure and compile IPhreeqc:

  $ cd build

  $ ../configure --prefix=$HOME

  $ make

  $ make check (all tests should pass)

  $ make install (generate the static library of IPhreeqc)
- Add the path of library and the head files into the "makefile" in HTGCM v2.0

  LIBS = -lm -L/home /iphreeqc-3.0.6-7757/build/src/.libs –liphreeqc

  CFLAGS = -g -I/home /iphreeqc-3.0.3-7671/src
- Go to HTGCM v2.0 directory and compile the codes:

  $ cd

  $ cd HTGCM v2.0/dhsvm_srcw/

  $ make

A.3.2 HTGCM v2.0 output

The output includes the concentrations of SO_4, Fe (total), Ca (total), Al (total), Na (total), Mg (total), K (total), Si (total), P (total), Cl (total), Mn (total) and pH. Certainly, soil temperature, oxidation heat and all the outputs from DHSVM can be exported from this model.

APPENDIX B

THE BOUNDARY OF STUDY PLOTS

Table B. 1 The raw data of the study plots boundary based on the projected coordinate system of NAD83 UTM ZONE 17N.

Name	Grid Northing (m)	Grid Easting (m)
1	4420552.524	579207.836
2	4420555.984	579211.01
3	4420559.201	579214.367
4	4420562.778	579217.698
5	4420566.113	579221.234
6	4420569.61	579225.019
7	4420572.898	579228.897
8	4420576.013	579232.65
9	4420578.477	579236.831
10	4420582.225	579240.361
11	4420585.108	579244.634
12	4420587.662	579249.156
13	4420590.917	579253.175
14	4420593.632	579257.338
15	4420596.661	579261.122
16	4420599.713	579264.527
17	4420602.507	579268.082
18	4420605.484	579271.996
19	4420608.35	579275.546
20	4420611.158	579279.36
21	4420614.513	579282.895

Table B.1 (Continued)

Name	Grid Northing (m)	Grid Easting (m)
22	4420616.998	579286.539
23	4420618.222	579287.875
24	4420619.894	579287.781
25	4420623.003	579285.379
26	4420625.945	579283.011
27	4420628.96	579281.138
28	4420631.656	579278.624
29	4420633.7	579276.085
30	4420636.051	579273.779
31	4420638.393	579271.027
32	4420641.069	579268.482
33	4420643.413	579265.635
34	4420645.224	579263.154
35	4420645.706	579261.479
36	4420645.202	579259.594
37	4420644.323	579258.07
38	4420642.776	579258.207
39	4420640.57	579255.332
40	4420638.401	579253.215
41	4420636.059	579251.432
42	4420634.898	579249.215
43	4420632.221	579246.454
44	4420628.413	579242.866
45	4420625.169	579239.049
46	4420622.396	579236.272
47	4420620.535	579234.935
48	4420617.941	579233.482
49	4420615.063	579232.331
50	4420612.662	579230.323
51	4420610.325	579228.377
52	4420608.148	579224.925
53	4420606.123	579221.618
54	4420603.243	579218.296
55	4420600.396	579215.053
56	4420597.447	579211.735
57	4420595.152	579208.206

Table B.1 (Continued)

ID	Grid Northing (m)	Grid Easting (m)
58	4420593.013	579204.444
59	4420590.217	579199.918
60	4420587.617	579194.947
61	4420583.806	579188.657
62	4420580.578	579183.661
63	4420578.427	579180.224
64	4420577.352	579177.633
65	4420575.029	579173.193
66	4420573.093	579171.607
67	4420572.404	579169.202
68	4420570.865	579165.318
69	4420568.722	579161.022
70	4420566.073	579156.462
71	4420564.488	579152.269
72	4420562.762	579149.752
73	4420559.829	579148.042
74	4420560.256	579144.943
75	4420558.517	579140.376
76	4420555.776	579135.522
77	4420553.18	579132.014
78	4420551.319	579128.995
79	4420547.962	579124.224
80	4420544.803	579118.6
81	4420542.411	579114.711
82	4420540.706	579110.158
83	4420536.291	579108.668
84	4420533.287	579109.764
85	4420528.663	579112.25
86	4420524.265	579114.748
87	4420520.519	579116.385
88	4420515.42	579116.761
89	4420513.154	579118.691
90	4420512.381	579124.196
91	4420510.857	579128.019
92	4420510.015	579132.453
93	4420510.946	579137.531

Table B.1 (Continued)

ID	Grid Northing (m)	Grid Easting (m)
94	4420512.699	579143.081
95	4420514.936	579148.8
96	4420517.418	579154.804
97	4420519.554	579160.648
98	4420521.924	579165.873
99	4420523.647	579171.332
100	4420525.875	579176.969
101	4420528.191	579182.684
102	4420530.374	579187.942
103	4420533	579192.05
104	4420537.421	579195.471
105	4420541.923	579198.898
106	4420545.423	579202.127

BIBLIOGRAPHY

Allison, J. D., D. S. Brown, and K. J. Novo-Gradac (1991), MINTEQA2/PRODEFA2, a geochemical assessment model for environmental systems :Version 3.0 User's Manual*Rep.*, Environmental Research Laboratory, Office of Research and Development, U. S. Environmental Protection Agency, Athens, Georgia,U.S.A.

Beamish, B. B., M. A. Barakat, and J. D. St George (2000), Adiabatic testing procedures for determining the self-heating propensity of coal and sample ageing effects, *Thermochim Acta*, *362*(1-2), 79-87.

Bicknell, B. R., J. C. Imhoff, J. L. Kittle Jr., T. H. Jobes, and A. S. Donigian Jr. (2001), Hydrological Simulation Program ‐ FORTRAN, Version 12: User's Manual, *Mountain View, Cal.: Aqua Terra Consultants.*

Charlton, S. R., C. L. Macklin, and D. L. Parkhurst (1997), PHREEQCI—A graphical user interface for the geochemical computer program PHREEQC*Rep.*, U.S. GEOLOGICAL SURVEY, Lakewood, CO.

Charlton, S. R., and D. L. Parkhurst (2011), Modules based on the geochemical model PHREEQC for use in scripting and programming languages, *Comput Geosci-Uk*, *37*(10), 1653-1663.

Chen, C., J. Herr, and L. Ziemelis (1998), Watershed Analysis Risk Management Framework-A Decision Support System for Watershed Approach and TMDL Calculation. Documentation Report TR110809, *Electric Power Research Institute, Palo Alto, California*.

Chen, L., and M. H. Young (2006), Green-Ampt infiltration model for sloping surfaces, *Water Resour Res*, *42*(7), W07420. doi: 10.1029/2005WR004468.

Cherkauer, K. A., and D. P. Lettenmaier (1999), Hydrologic effects of frozen soils in the upper Mississippi River basin, *J Geophys Res-Atmos*, *104*(D16), 19599-19610.

Coulson , S., I. D. Hodkinson, A. Strathdee, J. S. Bale, W. Block, M. R. Worland, and N. R. Webb (1993), Simalated climate change: the interaction between vegetation type and microhabitat temperatures at Ny Alesund, Svalbard, *Polar Biology*, *1993*(13), 67-70.

da Silva, J. C., E. do Amaral Vargas, and O. Sracek (2009), Modeling multiphase reactive transport in a waste rock pile with convective oxygen supply, *Vadose Zone J*, *8*(4), 1038-1050.

Davis, G. B., and A. I. M. Ritchie (1986), A model of oxidation in pyritic mine wastes .1. equations and approximate solution, *Appl Math Model*, *10*(5), 314-322.

DeNicola, D. M., and M. G. Stapleton (2002), Impact of acid mine drainage on benthic communities in streams: the relative roles of substratum vs. aqueous effects, *Environ Pollut*, *119*(3), 303-315.

Deutsch, W. J. (1997), *Groundwater Geochemistry: fundamentals and applications to contamination*, CRC Press LLC, Florida.

Elberling, B., R. V. Nicholson, and D. J. David (1993), Field-evaluation of sulfide oxidation rates, *Nord Hydrol*, *24*(5), 323-338.

Elberling, B., R. V. Nicholson, and J. M. Scharer (1994), A combined kinetic and diffusion model for pyrite oxidation in tailings: a change in controls with time, *J Hydrol*, *157*(1–4), 47-60. doi: 10.1016/0022-1694(94)90098-1.

Gerke, H. H., J. W. Molson, and E. O. Frind (1998), Modelling the effect of chemical heterogeneity on acidification and solute leaching in overburden mine spoils, *J Hydrol*, *209*(1-4), 166-185.

Gieré, R., and P. Stille (2004), *Energy, waste and the environment: a geochemical perspective*, Geological Society of America.

Herr, J. W., C. W. Chen, R. A. Goldstein, R. Herd, and J. M. Brown (2003), Modeling acid mine drainage on a watershed scale for TMDL calculations[1], *J Am Water Resour As*, *39*(No. 2).

Hollesen, J., B. Elberling, and P. E. Jansson (2011), Modelling temperature-dependent heat production over decades in High Arctic coal waste rock piles, *Cold Regions Science and Technology*, *65*(2011), 258-268.

International Aluminium Institute (2010), IAI-Background-paper.

Jacques, D., J. Šimůnek, D. Mallants, and M. T. van Genuchten (2006), Operator-splitting errors in coupled reactive transport codes for transient variably saturated flow and contaminant transport in layered soil profiles, *J Contam Hydrol*, *88*(3), 197-218.

Jacques, D., J. Šimůnek, D. Mallants, and M. T. van Genuchten (2008), Modeling coupled hydrologic and chemical processes: Long-term uranium transport following phosphorus fertilization, *Vadose Zone J*, *7*(2), 698-711.

Jansson, P. E., and L. Karlberg (2004), Coupled heat and mass transfer model for soil-plant-atmosphere systems*Rep.*, Royal Institute of Technology, Dept of Civil and Environmental Engineering, Stockholm.

Johnson, D. B., and K. B. Hallberg (2005), Acid mine drainage remediation options: a review, *The Science of the total environment*, *338*(1-2), 3-14. doi: 10.1016/j.scitotenv.2004.09.002.

Kawakami, K., J. Sato, K. Kusunoki, K. Kusakabe, and S. Morooka (1988), Kinetic-Study of Oxidation of Pyrite Slurry by Ferric-Chloride, *Ind Eng Chem Res*, *27*(4), 571-576.

Lamers, L. P., H. B. Tomassen, and J. G. Roelofs (1998), Sulfate-induced eutrophication and phytotoxicity in freshwater wetlands, *Environ Sci Technol*, *32*(2), 199-205.

Lefebvre, R. (1994), Characterization and numerical modeling of acid mine drainage in waste rock dump.(In French.), *Ph.D. thesis. Univ. Laval, Quebec, Canada.*

Leung, L. R., M. S. Wigmosta, S. J. Ghan, D. J. Epstein, and L. W. Vail (1995), A Physically-Based Mountain Watershed Model Driven by a Regional Climate Model.

Leung, L. R., and M. S. Wigmosta (2007), POTENTIAL CLIMATE CHANGE IMPACTS ON MOUNTAIN WATERSHEDS IN THE PACIFIC NORTHWEST1, *JAWRA Journal of the American Water Resources Association*, *35*(6), 1463-1471.

Liang, X., D. P. Lettenmaier, E. F. Wood, and S. J. Burges (1994), A Simple Hydrologically Based Model of Land-Surface Water and Energy Fluxes for General-Circulation Models, *J Geophys Res-Atmos*, *99*(D7), 14415-14428.

Mayer, K. U., E. O. Frind, and D. W. Blowes (2002), Multicomponent reactive transport modeling in variably saturated porous media using a generalized formulation for kinetically controlled reactions, *Water Resour Res*, *38*(9), 1174.

Molson, J., O. Fala, M. Aubertin, and B. Bussière (2005), Numerical simulations of pyrite oxidation and acid mine drainage in unsaturated waste rock piles, *J Contam Hydrol*, *78*(4), 343-371.

Molson, J. W., E. O. Frind, M. Aubertin, and D. Blowes (2004), POLYMIN: A Reactive Mass Transport and Sulphide Oxidation Model, User Guide, *Ecole Polytechnique, Montreal.*

Neitsch, S. L., J. G. Arnold, J. R. Kiniry, J. R. Williams, and K. W. King (2002), Soil and Water Assessment Tool: Theoretical documentation, Version 2000, *Temple, Tex.: Blackland Research Center and USDA - ARS Grassland Soil and Water Research Laboratory Investigation*.

Neufeld, R. D. (1990), COAL REFUSE TO ENERGY, paper presented at The environmental challenge of the 1990s: proceedings of the International Conference on Pollution Prevention, Clean Technologies and Clean Products, Washington, DC, June 10-13, 1990, The Laboratory.

Nicholson, R. V., R. W. Gillham, and E. J. Reardon (1988), Pyrite Oxidation in Carbonate-Buffered Solution .1. Experimental Kinetics, *Geochim Cosmochim Ac*, *52*(5), 1077-1085.

Nordstrom, D. K. (1982), Aqueous pyrite oxidation and the consequent formation of secondary iron minerals, in *Kittrick, J.A., Fanning, D.F. Hossner, L.R., (Eds.), Acid sulfate weathering*, edited, pp. 37-56, Soil Science Society of America Press, Madison, WI.

Ohio State University Research Foundation (1971), Acid mine drainage formation and abatement *Rep.*

Parkhurst, D., and C. Appelo (2013), Description of Input and Examples for PHREEQC Version 3—A Computer Program for Speciation, Batch-Reaction, One-Dimensional Transport, and Inverse Geochemical Calculations, *Modeling Techniques*, *6*.

Parkhurst, D. L., D. C. Th orstenson, and L. N. Plummer (1980), PHREEQE: A computer program for geochemical calculations.*Rep.*, 80-96 pp, USGS, Lakewood, Colorado.

Parkhurst, D. L. (1995), User's guide to PHREEQC: A computer program for speciation,reaction-path, advective transport, and inverse geochemical calculations.*Rep.*, 95-4227 pp, USGS, Lakewood, Colorado.

Parkhurst, D. L., and C. A. J. Appelo (1999), User's guide to PHREEQC (version 2)--A computer program for speciation, batch-reaction, one-dimensional transport, and inverse geochemical calculations:U.S. Geological Survey. Water-Resources Investigations Report*Rep.*, 99-4259, 4312 pp, Denver, Colorado.

Philip, J. R. (1991), Hillslope infiltration:planar slopes, *Water Resour Res*, *27*(1), 109-117. doi: 10.1029/90WR01704.

Pruess, K. (1991), TOUGH2: A general-purpose numerical simulator for multiphase fluid and heat transfer., *LBL-29400. Lawrence Berkeley Laboratory,Berkeley, CA.*

Schoonon, M., A. Elesetinow, M. Borda, and D. Strongin (2000), Effect of temperature and illumination on pyrite oxidation between pH2 and 6, *Geochemical Transnsactions*, *4*.

Silva, J. C. (2004), Modeling and numerical simulation of multiphase transport in porous media with thermo-chemical interactions (In Portuguese), *Ph.D. thesis . Catholic Univ. of Rio de Janeiro, Brazil.*

Šimůnek, J., and D. L. Suarez (1993), Modeling of Carbon-Dioxide Transport and Production in Soil .1. Model Development, *Water Resour Res*, *29*(2), 487-497.

Šimůnek, J., K. Huang, and M. T. Van Genuchten (1998), The HYDRUS code for simulating the one-dimensional movement of water, heat, and multiple solutes in variably-saturated media,Version 6.0, Research Report No. 144, U.S. Salinity Laboratory, USDA, ARS,*Rep.*, Riverside, California.

Šimůnek, J., M. Sejna, and M. T. van Genuchten (1999), The Hydrus-2D software package for simulating two-dimensional movement of water, heat, and multiple solutes in variably saturated media. Version 2.0 /GWMC-TPS - 53*Rep.*, 251 pp.

Šimůnek, J., M. T. van Genuchten, and M. Sejna (2008), Development and applications of the HYDRUS and STANMOD software packages and related codes, *Vadose Zone J*, *7*(2), 587-600.

Stange, C. F. (2007), A novel approach to combine response functions in ecological process modelling, *Ecol Model*, *204*, 547-552.

Stumm, W., and J. J. Morgan (1981), *Aquatic Chemistry:An Introduction Emphasizing Chemical Equilibria in Natural Waters*, John Wiley & Sons, New York.

The Land Surface Hydrology Research Group University of Washington Available from: http://www.hydro.washington.edu/Lettenmaier/Models/DHSVM/documentation.shtml.

Truesdell, A. H., and B. F. Jones (1973), *WATEQ, a computer program for calculating chemical equilibria of natural waters*, US Department of the Interior, Geological Survey.

USGS PHREEQC Available from: http://wwwbrr.cr.usgs.gov/projects/GWC_coupled/phreeqc/.

Waichler, S. R. (2000), Simulation of vegetation and hydrology for climate change analysis of a mountain watershed.

Walter, A. L., E. O. Frind, D. W. Blowes, C. J. Ptacek, and J. W. Molson (1994), Modeling of multicomponent reactive transport in groundwater .1. Model development and evaluation, *Water Resour Res*, *30*(11), 3137-3148.

Wigmosta, M. S., L. W. Vail, and D. P. Lettenmaier (1994), A distributed hydrology-vegetation model for complex terrain, *Water Resour Res*, *30*(6), 1665-1679. doi: 10.1029/94WR00436.

Wigmosta, M. S., and D. P. Lettenmaier (1999), A comparison of simplified methods for routing topographically driven subsurface flow, *Water Resour Res*, *35*(1), 255-264. doi: 10.1029/1998WR900017.

Williamson, M. A., and J. D. Rimstidt (1994), The kinetics and electrochemical rate-determining step of aqueous pyrite oxidation, *Geochim Cosmochim Ac*, *58*(24), 5443-5454.

Wunderly, M. D., D. W. Blowes, E. O. Frind, and C. J. Ptacek (1996), Sulfide mineral oxidation and subsequent reactive transport of oxidation products in mine tailings impoundments: A numerical model, *Water Resour Res*, *32*(10), 3173-3187. doi: 10.1029/96WR02105.

Xu, T., S. P. White, K. Pruess, and G. H. Brimhall (2000), Modeling of pyrite oxidation in saturated and unsaturated subsurface flow systems, *Transport in Porous Media*, *39*, 25–56.

Xu, Y., X. Liang, T.W. Davis, J. Patterson, J. K. Fu, and P. Koranchie-Boah (2011), An assessment of the long-term environmental impacts of reusing alkaline clay on coal refuse piles with a dynamic solute transport model at a watershed scale, *American Geophysical Union Fall meeting*.

Xu, Y., and X. Liang (2013), Assessment of the soil temperature in the remediated coal-refuse region by a hydro-thermal-geochemical model, *in preparation for submission to Water Resources Research*.

Xu, Y., X. Liang, T. Davis, J. Nichols, J. K. Fu, and P. Koranchie-Boah (2013a), An assessment of environmental impacts of bauxite residue in acidic coal-refuse piles, *submitted to Water Resources Research*

Xu, Y., X. Liang, H. Deng, Y. Wen, and J. Nichols (2013b), Development of a hydro-thermal-geochemical model for the investigation of remediation in coal-refuse region, *in preparation for submission to Water Resources Research*.

Zhang, Y., C. S. Li, C. C. Trettin, H. Li, and G. Sun (2002), An integrated model of soil, hydrology, and vegetation for carbon dynamics in wetland ecosystems, *Global Biogeochem Cy*, *16*(4). doi: Doi 10.1029/2001GB001838.

Zhao, R., Y. Zhang, L. Fang, X. Liu, and Q. Zhang (1980), The Xinanjiang model, *Hydrological Forecasting Proceedings Oxford Symposium, IASH*, *129*, 351-356.

Zhao, R. (1992), The Xinanjiang model applied in China, *J Hydrol*, *135*(1), 371-381.

Zhao, R., X. Liu, and V. Singh (1995), The Xinanjiang model, *Computer models of watershed hydrology.*, 215-232.

Ziemkiewicz, P. F., J. G. Skousen, D. L. Brant, P. L. Sterner, and R. J. Lovett (1997), Acid mine drainage treatment with armored limestone in open limestone channels, *Journal of Environtal Quality*, *24*(4), 1017-1024.